ARCHIEF

Hy A

**Hydrodynamics
Section**

A Model Testing Technique and Method of Analysis for the Prediction of Steering and Manoeuvring Qualities of Surface Vessels

BY

J. STRØM-TEJSEN

and

M. S. CHISLETT

Hy-7

HYDRO- OG AERODYNAMISK LABORATORIUM

is a self-supporting institution, established to carry out experiments for industry and to conduct research in the fields of Hydro- and Aerodynamics. According to its by-laws, confirmed by His Majesty the King of Denmark, it is governed by a council of eleven members, six of which are elected by the Danish Government and by research organizations, and five by the shipbuilding industry.

Research reports are published in English in two series: **Series Hy** (blue) from the Hydrodynamics Section and **Series A** (green) from the Aerodynamics Section.

The reports are on sale through the Danish Technical Press at the prices stated below. Research institutions within the fields of Hydro- and Aerodynamics and public technical libraries may, however, as a rule obtain the reports free of charge on application to the Laboratory.

The views expressed in the reports are those of the individual authors.

Series Hy:

No.:	Author:	Title:	Price: D. Kr.
Hy-1	PROHASKA, C. W.	Analysis of Ship Model Experiments and Prediction of Ship Performance (Second printing)	5,00
Hy-2	PROHASKA, C. W.	Trial Trip Analysis for Six Sister Ships	6,00
Hy-3	ŠILOVIĆ, V.	A Five Hole Spherical Pitot Tube for Three Dimensional Wake Measurements	6,00
Hy-4	STRØM-TEJSEN, J.	The HyA ALGOL-Programme for Analysis of Open Water Propeller Test	6,00
Hy-5	ABKOWITZ, M. A.	Lectures on Ship Hydrodynamics — Steering and Manoeuvrability	20,00
Hy-6	CHISLETT, M. S., and STRØM-TEJSEN, J.	Planar Motion Mechanism Tests and Full-Scale Steering and Manoeuvring Predictions for a MARINER Class Vessel	12,00
Hy-7	STRØM-TEJSEN, J., and CHISLETT, M. S.	A Model Testing Technique and Method of Analysis for the Prediction of Steering and Manoeuvring Qualities of Surface Vessels	12,00
Hy-8	CHISLETT, M. S., and BJÖRHEDEN, O.	Influence of Ship Speed on the Effectiveness of a Lateral-Thrust Unit	12,00

Series A:

No.:	Author:	Title:	Price: D. Kr.
A-1	TEJLGÅRD JENSEN, A.	An Experimental Analysis of a Pebble Bed Heat Exchanger for a Small Hypersonic Wind Tunnel	5,00

H Y D R O - O G   A E R O D Y N A M I S K

L A B O R A T O R I U M

Lyngby - Denmark

A Model Testing Technique and
Method of Analysis for the Prediction of
Steering and Manoeuvring Qualities
of Surface Vessels

by

J. Strøm-Tejsen[1] and M. S. Chislett[2]

TABLE OF CONTENTS

LIST OF FIGURES

LIST OF FIGURES (Cont.)

LIST OF FIGURES (Cont.)

LIST OF TABLES

ABSTRACT

A semi-theoretical method of investigating steering and manoeuvring qualities of surface-vessels is described. A general mathematical model, consisting of non-linear equations of motion for a body free to move in the horizontal plane, is used as a basis. The hydrodynamic coefficients of the equations are obtained by carrying out captive-model experiments for each particular vessel, after which any desired manoeuvre can be predicted with the aid of a computer.

The hydrodynamic coefficients are determined using a Planar-Motion Mechanism System to test 6 m. (20 ft.) wax models in a conventional towing tank. Details of the design, construction and use of this mechanism are given, together with a description of the methods used to analyse the measured forces. The convenient manner in which non-linear and cross-coupling coefficients, necessary for the accurate prediction of radical manoeuvres, can be obtained with a Planar-Motion Mechanism technique is described.

Short mention is made of the influence of frequency and tank-interference effects on the measured hydrodynamic forces, and it is shown that troublesome resonant standing-wave conditions can be avoided.

INTRODUCTION

There is no completely analytical method available at this time for predicting the steering and manoeuvring characteristics of ships. Due to this lack of theoretical methods, experimental techniques using free-running models have been employed by model basins for many years. Of more recent development is a semi-theoretical technique which utilizes the experimental results of captive-model tests in conjunction with the equations of motion expanded to include significant non-linear terms. The captive model tests may be experiments using either a rotating arm or a Planar-Motion Mechanism, and the predictions of manoeuvring characteristics are obtained from a solution of the equations of motion by means of either a digital or an analogue computer.

A semi-theoretical technique of this kind has been adopted at the Hydro- and Aerodynamics Laboratory (HyA) for investigating steering

and manoeuvring qualities of ships and is dealt with in this paper.
The HyA-method utilizes a Planar-Motion Mechanism system for experi-
mental measurement of the hydrodynamic coefficients in the equations
of motion, and uses the HyA-GIER digital computer for the numerical
solution of the equations. Before launching into technical details,
however, it is relevant to consider briefly the reasons which make such
an approach desirable.

Free-running model tests constitute the simplest and most direct
means of assessing the behaviour of a given ship design during the exe-
cution of a particular manoeuvre. The tests are made by simulating
full-scale conditions as closely as possible. The disadvantages of
free-running model tests are firstly that they can only be conducted
with difficulty in a conventional long narrow towing tank and preferably
require a large manoeuvring basin. Secondly, whereas free-running tests
provide information enabling engineering decisions to be made as to
the suitability or otherwise of a given design, the reasons for the
observed performance are not apparent from the test results. The
tests are unsatisfactory in that little insight is gained into the
hydrodynamic phenomena involved, and a rational basis for improvements
in design is difficult to establish. Finally, even when large facilities
are available for making free-running model tests, certain scaling
problems are difficult to avoid. It is, for instance, difficult to
obtain the correct conditions of propeller loading corresponding to
the ship propulsion point. When making captive-model tests this is
very simply achieved by applying a towing force via the rigid connection
to the carriage.

The semi-theoretical thechnique employing captive-model tests
in combination with a mathematical model is a more analytical and poten-
tially more powerful approach, which overcomes these disadvantages.
If a Planar-Motion Mechanism is employed for the execution of the captive
model tests the disadvantages of the free-running tests mentioned above
are eliminated and scale effects in general are reduced because of the
large models which can conveniently be used. If a rotating arm is
utilized for the captive model experiments, the disadvantage that a
special manoeuvring basin is necessary is not eliminated. Furthermore,
because of the small size of most rotating arm facilities, scale effects
are likely to be troublesome.

The equations of motion, which constitute the mathematical model
of the situation under investigation, must closely represent the real

physical occurrences and be capable of yielding results with an accuracy
at least as good as those obtainable from free-running model tests.
The ease with which this can be done depends largely on the degree of
complexity of the situation considered. Course stability characteristics
involving motions only deviating infinitesimally from zero are thus
more amenable to simulation by these means than are for example the
interaction effects between two ships passing in a shallow canal. The
difficulty in handling the more complex situations arises not, however,
as a result of the mathematical model, which even in a very general
case is almost ideally suited to computer solution, but rather in the
determination of the hydrodynamic coefficients of the equations of
motion.

Although some of the hydrodynamic coefficients can be approxi-
mated theoretically, the only reliable way at this time of obtaining
values with the accuracy needed for quantitative simulation is to
conduct captive model tests. This state of affairs has the merit of
great flexibility. As theory progresses, more and more coefficients
will be obtainable by calculation and fewer experiments will be
necessary. In the meantime, the orderly experimental approach ne-
cessitated by the structure of the mathematical model is conducive
to systematic and progressive collation of data, itself tending to
make testing redundant and to stimulate the creation of useful theore-
tical concepts.

MATHEMATICAL MODEL

The mathematical model at present in use at HyA for simulation
of steering and manoeuvring characteristics of surface ships is based
on the general equations of motion of a rigid body moving in the hori-
zontal plane. The detailed derivation of these equations in terms of
the now commonly accepted notation [1, 2] employed in steering and
manoeuvrability work is given by Abkowitz [3]. For a body having
freedom in surge, sway, and yaw, but restricted in heave, pitch and
roll[*], the equations, developed for a coordinate system fixed in the
symmetry plane of the body, are:

$$X = m(\dot{u} - rv - x_G r^2)$$
$$Y = m(\dot{v} + ru + x_G \dot{r}) \tag{1}$$
$$N = I_z \dot{r} + m x_G (\dot{v} + ru),$$

where terms on the right-hand side describe mass and inertial responses, and the left-hand side expresses the external hydrodynamic forces and moments acting on the body (see Figure 1).

Direction of Motion of
Origin of Axis System.
Velocity, U.
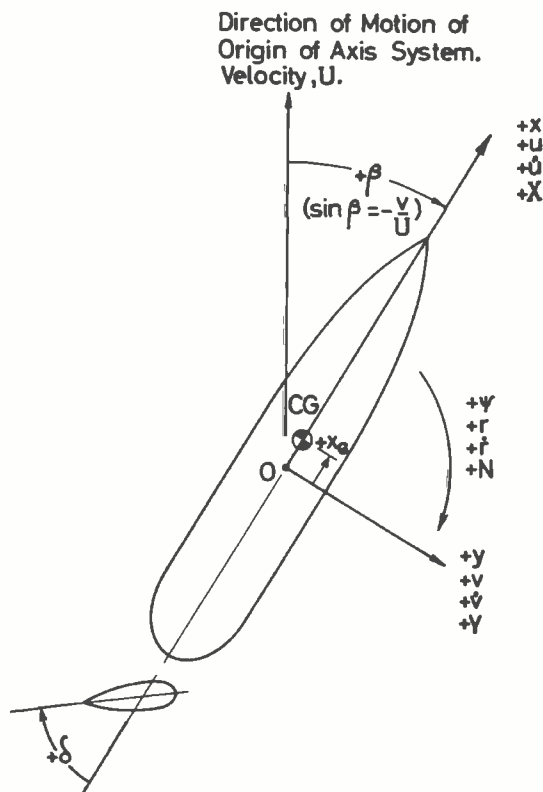
Figure 1

Diagrammatic Definition of Motion, Orientation and Force Parameters in Terms of Body-Axis Co-Ordinates.

The hydrodynamic forces and moments are functions of body geometry, motions and orientation. For a given body with a single control surface, moving in unrestricted water, they may be expressed as the general functions:

$$\left.\begin{array}{c} X \\ Y \\ N \end{array}\right\} = f(\dot{u}, \dot{v}, \dot{r}, u, v, r, \delta) \tag{2}$$

which must be defined, before simulation studies can be carried out.

*Rolling and heel have been neglected in the present model since they are felt to have little influence on the prediction of steering and manoeuvring characteristics, with the possible exception of fast warships, which heel appreciably in turns.

The functions describing the hydrodynamic forces and moments have been developed into a useful form for analysis purposes with the aid of a Taylor expansion of the functions. If the Taylor expansion is limited to the first order terms, the linearized equations are obtained [3, 4]. The present stage of development, which enables realistic simulations of ship manoeuvres to be made, is based largely on a third order Taylor expansion of the functions. Introducing the assumptions that:

1. Forces and moments have appropriate port and starboard symmetry except for a constant force and moment caused by the propeller,

and 2. There are no second- or higher-order acceleration terms, and that cross-coupling between acceleration and velocity parameters is negligible,

the validity of which has been verified, for instance, by the measurements reported in [5], the third order Taylor expansion reduces to the following expressions:

$$X = X_{\dot{u}}\dot{u} + X_{*} + X_{u}\Delta u + \frac{1}{2}X_{uu}\Delta u^2 + \frac{1}{6}X_{uuu}\Delta u^3 \tag{3}$$
$$+ \frac{1}{2}X_{vv}v^2 + \frac{1}{2}X_{rr}r^2 + \frac{1}{2}X_{\delta\delta}\delta^2 + \frac{1}{2}X_{vvu}v^2\Delta u + \frac{1}{2}X_{rru}r^2\Delta u + \frac{1}{2}X_{\delta\delta u}\delta^2\Delta u$$
$$+ X_{vr}vr + X_{v\delta}v\delta + X_{r\delta}r\delta + X_{vru}vr\Delta u + X_{v\delta u}v\delta\Delta u + X_{r\delta u}r\delta\Delta u$$

$$Y = Y_{\dot{v}}\dot{v} + Y_{\dot{r}}\dot{r} + Y_{*} + Y_{*u}\Delta u + Y_{*uu}\Delta u^2 \tag{4}$$
$$+ Y_{v}v + \frac{1}{6}Y_{vvv}v^3 + \frac{1}{2}Y_{vrr}vr^2 + \frac{1}{2}Y_{v\delta\delta}v\delta^2 + Y_{vu}v\Delta u + \frac{1}{2}Y_{vuu}v\Delta u^2$$
$$+ Y_{r}r + \frac{1}{6}Y_{rrr}r^3 + \frac{1}{2}Y_{rvv}rv^2 + \frac{1}{2}Y_{r\delta\delta}r\delta^2 + Y_{ru}r\Delta u + \frac{1}{2}Y_{ruu}r\Delta u^2$$
$$+ Y_{\delta}\delta + \frac{1}{6}Y_{\delta\delta\delta}\delta^3 + \frac{1}{2}Y_{\delta vv}\delta v^2 + \frac{1}{2}Y_{\delta rr}\delta r^2 + Y_{\delta u}\delta\Delta u + \frac{1}{2}Y_{\delta uu}\delta\Delta u^2$$
$$+ Y_{vr\delta}vr\delta$$

The corresponding expression for N is obtained by replacing Y by N in Equation (4).

Equating the hydrodynamic forces and moments based on Equations (3) to (4), with mass and inertial responses, Equation (1), then the non-linear mathematical model finally becomes [4]:

$$X\text{-Equation: } (m-X_{\dot{u}})\dot{u} = f_1(u,v,r,\delta)$$

$$Y\text{-Equation: } (m-Y_{\dot{v}})\dot{v} + (mx_G-Y_{\dot{r}})\dot{r} = f_2(u,v,r,\delta) \quad\quad (5)$$

$$N\text{-Equation: } (mx_G-N_{\dot{v}})\dot{v} + (I_z-N_{\dot{r}})\dot{r} = f_3(u,v,r,\delta)$$

where

$$f_1(u,v,r,\delta) = X_* + X_u\Delta u + X_{uu}\Delta u^2 + X_{uuu}\Delta u^3 +$$

$$X_{vv}v^2 + (X_{rr}+mx_G)r^2 + X_{\delta\delta}\delta^2 + X_{vvu}v^2\Delta u + X_{rru}r^2\Delta u + X_{\delta\delta u}\delta^2\Delta u +$$

$$(X_{vv}+m)vr + X_{v\delta}v\delta + X_{r\delta}r\delta + X_{vru}vr\Delta u + X_{v\delta u}v\delta\Delta u + X_{r\delta u}r\delta\Delta u$$

$$f_2(u,v,r,\delta) = Y_* + Y_{*u}\Delta u + Y_{*uu}\Delta u^2 + Y_{vr\delta}vr\delta +$$

$$Y_v v \quad\quad + Y_{vvv}v^3 + Y_{vrr}vr^2 + Y_{v\delta\delta}v\delta^2 + Y_{vu}v\Delta u + Y_{vuu}v\Delta u^2 +$$

$$(Y_r-mu)r \quad + Y_{rrr}r^3 + Y_{rvv}rv^2 + Y_{r\delta\delta}r\delta^2 + Y_{ru}r\Delta u + Y_{ruu}r\Delta u^2 +$$

$$Y_\delta\delta \quad\quad + Y_{\delta\delta\delta}\delta^3 + Y_{\delta vv}\delta v^2 + Y_{\delta rr}\delta r^2 + Y_{\delta u}\delta\Delta u + Y_{\delta uu}\delta\Delta u^2 + Y_{\delta\delta\delta u}\delta^3\Delta u$$

$$f_3(u,v,r,\delta) = N_* + N_{*u}\Delta u + N_{*uu}\Delta u^2 + N_{vr\delta}vr\delta +$$

$$N_v v \quad\quad + N_{vvv}v^3 + N_{vrr}vr^2 + N_{v\delta\delta}v\delta^2 + N_{vu}v\Delta u + N_{vuu}v\Delta u^2 +$$

$$(N_r-mx_Gu)r + N_{rrr}r^3 + N_{rvv}rv^2 + N_{r\delta\delta}r\delta^2 + N_{ru}r\Delta u + N_{ruu}r\Delta u^2 +$$

$$N_\delta\delta \quad\quad + N_{\delta\delta\delta}\delta^3 + N_{\delta vv}\delta v^2 + N_{\delta rr}\delta r^2 + N_{\delta u}\delta\Delta u + N_{\delta uu}\delta\Delta u^2 + N_{\delta\delta\delta u}\delta^3\Delta u$$

The factorials, $\frac{1}{2}$ and $\frac{1}{6}$, have been dropped as they unnecessarily complicate the book-keeping, and the fourth order terms, $Y_{\delta\delta\delta u}$ and $N_{\delta\delta\delta u}$, have been introduced in order to obtain sufficient flexibility of expression for the influence of speed on rudder action.

Experience has shown that several of the hydrodynamic coefficients or derivatives contained in the above mathematical model are negligibly small. In particular, the coefficients which give the changes of the non-dimensional coefficients Y_*, Y_v, Y_r, N_*, N_v, N_r, X_{vv}, X_{rr}, X_{vr}, $X_{v\delta}$, and $X_{r\delta}$, with speed, are small, as will be discussed later.

It is not suggested that the above mathematical model represents the ultimate in sophistication. It is felt, however, that further significant elaboration will not be justified before advances are made in theoretical or experimental methods of defining the pertinent hydrodynamic coefficients. The next logical step is perhaps to include freedom in roll, which might be necessary for simulation of radical manoeuvres of fast warships, which heel appreciably in high speed turns. Additional terms would of course also be necessary, if it was desired to simulate more complex situations.

The solution of the mathematical model using a digital computer is described in detail in [4].

GENERAL CONSIDERATIONS ON TESTING PROCEDURES

It is seen that the mathematical model, Equations (5), is comprised of numerous coefficients such as Y_{vvv}, N_r, $X_{\delta\delta}$ etc.. These coefficients in general depend on the particular geometry and design of a ship, and they must be known with reasonable accuracy before manoeuvres can be simulated by solving the mathematical model with the aid of a computer.

Ideally, numerical values for the coefficients would be evaluated by theoretical means, but although some of the hydrodynamic coefficients can be calculated approximately, the only reliable way at this time of obtaining values with the accuracy needed for simulations is to conduct captive model tests.

In a captive model test, the model is forced to perform precisely controlled movements, one or two of the different motion and rudder parameters being assigned values simultaneously. The resulting hydrodynamic forces and moments acting on the model are measured as functions of the parameters and the coefficients are subsequently obtained from these measurements. The expressions for the hydrodynamic forces and moments, Equations (5), may be considered having been developed on the basis of a superposition process, the accuracy of which is progressively improved by successive inclusion of "cross-coupling" terms expressing deviations from simple superposition. Similarly, in the execution of the captive model tests, parameters are first explored one at a time, all other parameters being zero. The resulting forces and moments can then be expressed by coefficients which are

functions of the single parameter. The next step in the captive model tests is to vary two parameters simultaneously, and if the resulting forces and moments differ from the superimposed results of the individually measured values, then the difference is expressed as a two-variable function of the parameters, and the coefficient representing the "cross-coupling" effect can be determined. Whereas, it is possible to generate three or more parameters simultaneously and so obtain cross-coupling terms in more than two variables, such terms have been found to be less than the accuracy of measurement. It is perhaps interesting in this connection to consider a free-sailing ship as a special case of captive model testing in which the ultimate stage of superposition has been reached. The totals of forces and moments acting can be inferred from the accelerations, and compared with model data expressed as one- and two-variable functions. This is done in effect when full-scale trajectories are compared with simulations based on model results.

The range of motion and rudder parameters explored during testing should, in principle, cover the range of subsequent simulation. Surge, sway- and yaw-accelerations, speed loss, drift angle, yaw velocity and rudder angle should therefore be varied systematically up to the values corresponding to maximum-rudder manoeuvres for the free-sailing ship.

Captive model tests in which measurements are made of hydrodynamic forces and moments resulting from drift angle, from rudder angle, and from combinations of drift and rudder angles, can be conducted with relatively simple equipment in a conventional towing tank.

Many methods have been used to measure forces and moments due to angular velocity, amongst them being such devices as curved models, curved-flow channels and freely decaying oscillators. All of these systems have major disadvantages, being either inaccurate or unwieldy or both. The use of a rotating arm in a circular tank is at present by far the most widely used approach and is furthermore a most satisfactory means of obtaining cross-coupling terms in angular velocity and drift angle, and angular velocity and rudder angle. The disadvantages of a rotating arm, apart from its high capital costs, are that it is not practicably possible to measure acceleration derivatives, and that it is not well suited to the generation of small angular velocities.

The Planar-Motion Mechanism system conceived and developed by Gertler and Goodman [6,7], provides a means of conducting captive model tests in which angular and straight line motion can be imposed on a model in a conventional towing tank. Developed as a technique for submerged body research, the original mechanism generated motions of the body in the vertical plane. For application to surface ships, a Planar-Motion Mechanism must operate in the horizontal plane, and the following description of the HyA Planar-Motion Mechanism system is consequently given in terms of sway and yaw motions.

A Planar-Motion Mechanism can be used in two different modes of operation, designated "static" and "dynamic". In the static mode, the model is constrained to travel along a straight path at constant velocity, and the mechanism is used to set discrete drift angles. Figure 2 schematically represents the three main types of tests made

Static Drift Angle Test

Fig. 2a

Static Rudder Angle Test

Fig. 2b
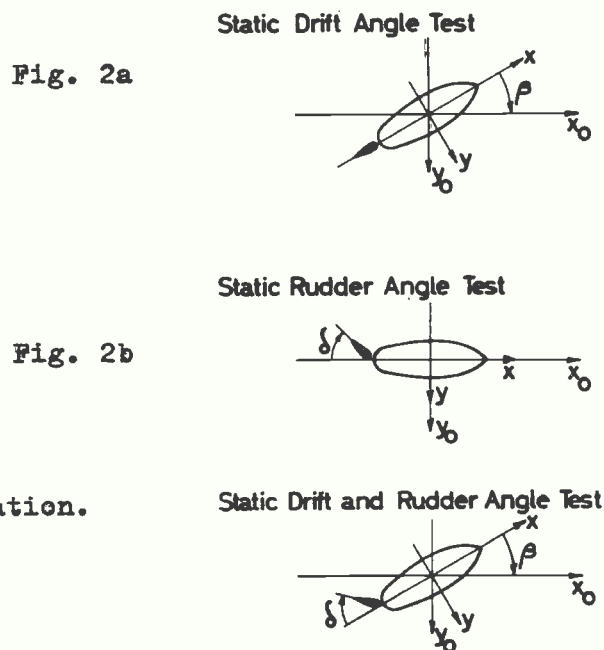
Figure 2

Various Examples of Tests
Executed in Static Mode
of Planar Motion Mechanism Operation.

Static Drift and Rudder Angle Test

in the static mode. Forces and moments resulting from drift angle (Figure 2a), rudder angle (Figure 2b) and from combinations of drift and rudder angles are measured in these tests.

The unique feature of the Planar-Motion Mechanism is its ability to generate oscillatory motions which are produced in the dynamic mode of its operation. Sinusoidal motions are imposed on the model with sway and yaw phased in such a way as to produce conditions of "pure-sway" and "pure-yaw". In the "pure-sway-test", the bow and stern are oscillated in-phase, and pure side-velocity and acceleration result, as shown schematically in Figure 3.

Pure Sway Test
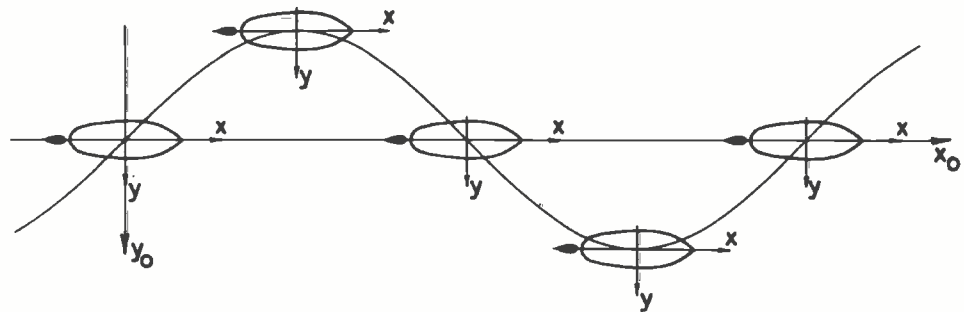
Figure 3

Pure Sway Test Executed in Dynamic Mode of
Planar-Motion Mechanism Operation.

Pure Yaw Test
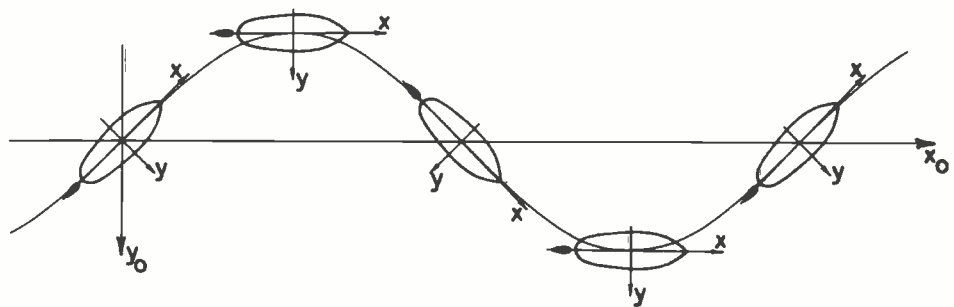
Yaw and Drift Angle Test
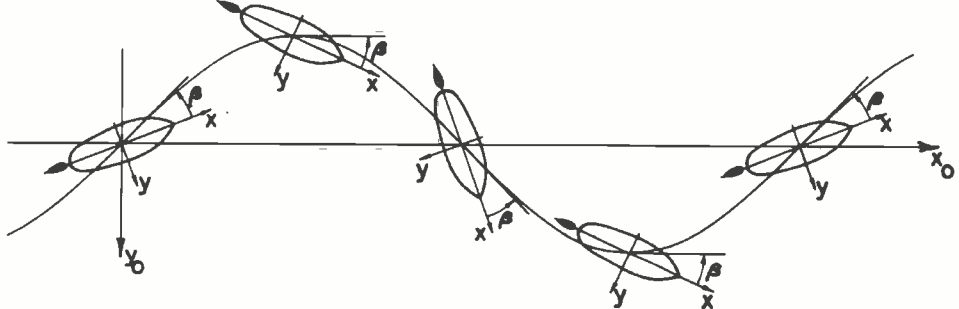
Yaw and Rudder Angle Test
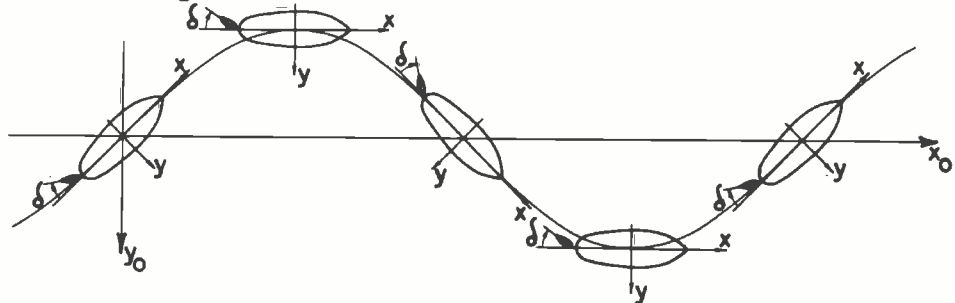
Figure 4

Various Examples of Yaw Tests Executed in Dynamic Mode
of Planar-Motion Mechanism Operation.

In the "pure-yaw-test" bow and stern are oscillated with phase-angle chosen such that pure angular-velocity and acceleration result. Various examples of this type of test are shown in Figure 4, the two developments of the "pure-yaw-test", i.e. the "yaw-and-drift-angle-test", and the "yaw-and-rudder-angle-test", constitute a means of measuring cross-coupling terms in the equations of motion.

As a means of experimentally measuring acceleration as well as angular velocity, drift angle, and rudder angle derivatives, the Planar-Motion Mechanism system constitutes an almost ideal method of obtaining all the linear terms needed for course stability studies [6,7]. The same basic approach can be extended to measurement of non-linear and cross-coupling terms in angular velocity, thus enabling all of the terms in the above non-linear mathematical model, Equations (5), to be measured.

The principles of motion generation for operation of the Planar-Motion Mechanism in the dynamic mode, a description of the HyA Planar-Motion Mechanism, and associated force measurement and analysis procedures are given in detail in the following sections.

PLANAR-MOTION MECHANISM - PRINCIPLES OF MOTION GENERATION

The difficulty of generating a yaw velocity in a conventional tank is due to the fact that if a constant angular velocity is maintained for more than a short length of time, while travelling at the necessary speed, a collision with one of the side-walls will result. Use of a Planar-Motion Mechanism overcomes this problem by forcing the model to travel with alternately port and starboard yaw velocities. This results in an S-shaped path which in rough terms may be considered as being built up of segments of the circular path travelled by a model under a rotating arm. (Figure 5). To be more precise, a Planar-Motion Mechanism generates a sinusoidal trajectory and the angular velocity is thus constantly varying, but the rotating arm comparison is none the less valid because the variation is so slow that quasi-steady conditions are obtained.

A continuously varying yaw velocity is necessarily accompanied by a continuously varying yaw acceleration to which the same quasi-steady conditions apply.

Reference to Figure 5 shows that if the model is to move with

a "pure yaw" motion, i.e. with zero drift angle, then it must at all
times move along the tangent to its path. In terms of the body-axis
system fixed in the model (Figure 1), this means that the side-velocity,
v, must be zero, or the total velocity vector, U, of the origin, 0, of
the axis system, must lie along the model centre-line. It can be seen

TOWING TANK   ROTATING ARM
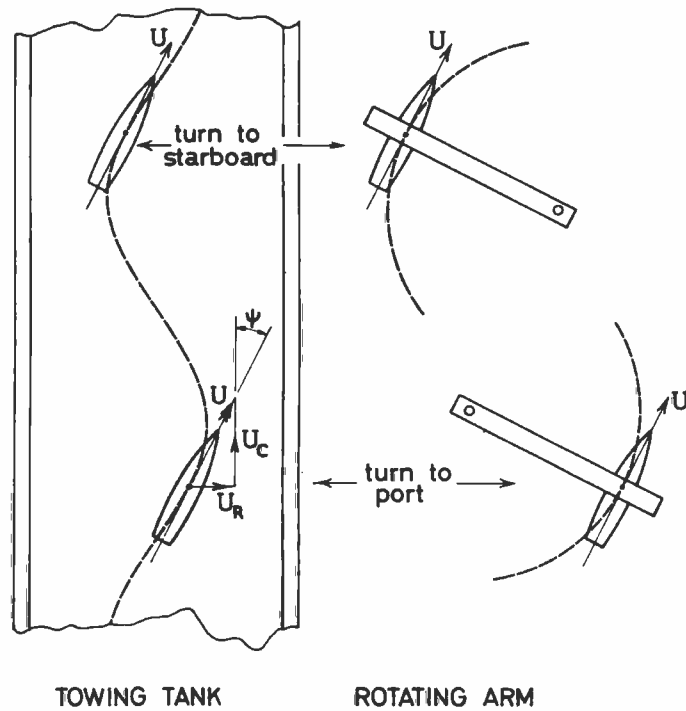
Figure 5

Comparison of Pure Yawing Motion Generated with
a Planar-Motion Mechanism and a Rotating Arm.

that for a model moving down the tank with carriage speed, U_C, this
is achieved by moving the model perpendicularly to the carriage centre-
line with a relative velocity, U_R. The magnitude of this velocity is
given by

$$\tan \psi = \frac{U_R}{U_C} \, , \tag{6}$$

where ψ is the angular displacement from the tank centre-line. Thus
the generation of an angular motion and linear motion <u>relative to the
carriage</u> results in a pure angular motion of the model <u>relative to the
water.</u>

A practical realization of this requirement as adopted in the
HyA Planar-Motion Mechanism is diagrammatically illustrated in Figure 6.
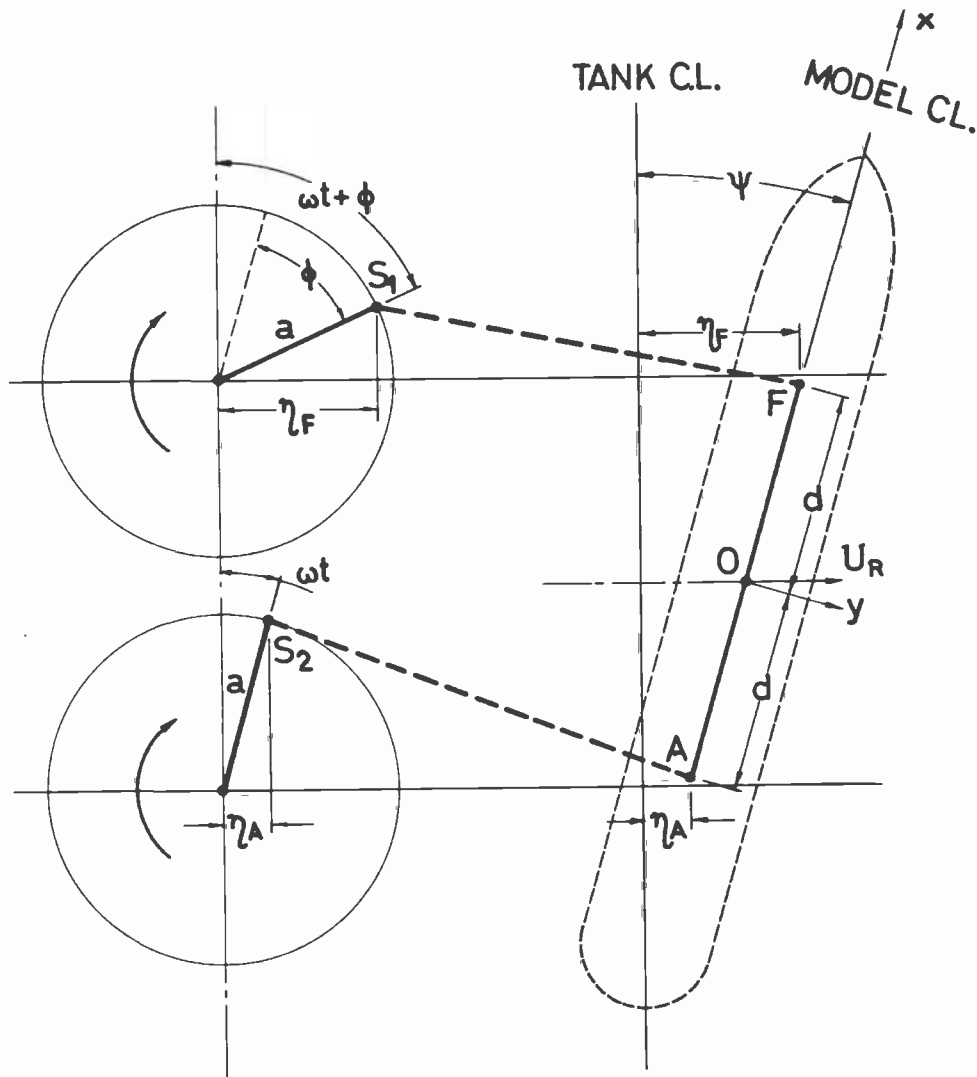
Figure 6

Diagrammatic Representation of Motions
Generated by a Planar-Motion Mechanism.

The arrangement consists of two scotch-yokes connected by a rigid
shaft. Rotation of the shaft results in periodic movement perpendi-
cular to the carriage centre-line of two points, F and A, fixed in the
model. By variation of the phase angle, ϕ , between the forward and
aft scotch-yokes, various combinations of angular velocity and movement
perpendicular to the carriage centre-line are obtained. The phase
angle, resulting in the fulfilment of the conditions for pure angular
motion of the model relative to the water, is found as follows.

Let

η_F, η_A = lateral displacements relative to carriage centre-line of points F and A fixed in model.

d = distance of points F and A from origin, O, of body-axis system fixed in model.

a = amplitude of scotch-yokes and of lateral displacement of points F and A.

ϕ = phase angle by which forward scotch-yoke leads aft.

ω = rate of rotation of shaft connecting scotch-yokes.

ψ = angular displacement of model centre-line relative to tank centre-line.

t = time.

Then

$$\eta_F = a \sin(\omega t + \phi)$$

$$\eta_A = a \sin \omega t$$

$$U_R = \frac{d}{dt}\left(\frac{\eta_F + \eta_A}{2}\right) = a\omega \cos\frac{\phi}{2} \cos\left(\omega t + \frac{\phi}{2}\right)$$

Also

$$\sin \psi = \frac{\eta_F - \eta_A}{2d} = \frac{a}{d} \sin\frac{\phi}{2} \cos\left(\omega t + \frac{\phi}{2}\right) \tag{7}$$

Substituting for $\sin \psi$ and U_R in Equation (6)

$$\frac{1}{\cos \psi} \frac{a}{d} \sin\frac{\phi}{2} \cos\left(\omega t + \frac{\phi}{2}\right) = \frac{a\omega}{U_C} \cos\frac{\phi}{2} \cos\left(\omega t + \frac{\phi}{2}\right)$$

$$\tan\frac{\phi}{2} = \frac{\omega d}{U_C} \cos \psi \tag{8}$$

Since ψ is small, we make the approximation $\cos \psi = 1$, giving:

$$\tan\frac{\phi}{2} = \frac{\omega d}{U_C} \tag{9}$$

Thus the phase-angle, ϕ, is not a cyclic quantity since it only depends on frequency of oscillation and carriage speed, the distance d being fixed in the model.

The present HyA Planar-Motion Mechanism has maximum amplitude, a, at the scotch-yokes of 100 mm and the distance, d, is 1050 mm, giving a maximum possible value of 5.46 degrees for ψ , when the error in the approximation cos ψ = 1 is less than 0.5 per cent. This value is only obtained at zero speed when the phase-angle between the scotch-yokes is 180 degrees. In a normal operating condition, the maximum value of ψ is reduced by the factor sin $\frac{\phi}{2}$ to approximately half this value, when the error is 0.1 per cent. While these considerations give a good indication that the error involved is negligible, the only rigorous way of checking this is to analyse the "contaminating" cyclic motions and corresponding impure forces, by carrying through the exact calculation. This has been done in another connection and has shown that the error is indeed negligible.

Accepting that a phase angle between the forward and aft scotch-yokes given by Equation (9) results in pure angular motion of the model relative to the water, the expressions for the model's angular velocity and angular acceleration are obtained by differentiating Equation (7) with respect to time.

$$\text{Angular displacement, } \psi \;=\; \frac{a}{d} \sin \frac{\phi}{2} \cos \left(\omega t + \frac{\phi}{2} \right) \tag{7}$$

$$\text{Angular velocity, } \quad r \;=\; -\frac{a\omega}{d} \sin \frac{\phi}{2} \sin \left(\omega t + \frac{\phi}{2} \right) \tag{10}$$

$$\text{Angular acceleration, } \dot{r} \;=\; -\frac{a\omega^2}{d} \sin \frac{\phi}{2} \cos \left(\omega t + \frac{\phi}{2} \right) \tag{11}$$

It is seen that angular velocity and angular acceleration are out-of-phase with each other.

Similarly, when the scotch-yokes are in-phase ($\phi = 0$), the model centre-line is always parallel to that of the tank and carriage, and the model experiences pure swaying motions. In terms of body-axis parameters, lateral displacement, velocity and acceleration are then given by:

$$\text{Sway displacement, } \quad y \;=\; a \sin \omega t \tag{12}$$

$$\text{Sway velocity, } \quad v \;=\; a\omega \cos \omega t \tag{13}$$

$$\text{Sway acceleration, } \quad \dot{v} \;=\; - a \omega^2 \sin \omega t \tag{14}$$

To summarize, hydrodynamically pure yawing or swaying motions can be generated by setting the phase angle between forward and aft scotch-yokes to an appropriate value. In both cases, the velocity and

acceleration are 90 degrees out of phase with each other.

A constant drift angle or rudder angle can easily be superimposed on the pure yaw motion as shown in Figure 4. Non-zero drift angle is obtained by changing the lengths of the arms shown symbolically in Figure 6 as S_1F and S_2A. This has the effect of adding a sizeable constant component, β, to the small cyclic value of ψ resulting from yawing motion. The phase-angle is then found from Equation (9) by substituting d cos β for d and similarly d is replaced by d cos β in Equations (7), (10) and (11).

DESCRIPTION OF THE HyA PLANAR-MOTION MECHANISM

Mechanical Structure

The HyA Planar-Motion Mechanism is in many ways similar to instruments previously reported [6, 7, 9, 10]. It is not felt necessary for this reason to describe the structure or design of the mechanism in detail, and the following is limited to a general outline of the main structural arrangement and of some novel features.

The HyA towing tank facility measures 240 x 12 x 6 metres in length, width and depth respectively, [8], enabling resistance and propulsion experiments to be performed with 6-7 metre models without encountering serious blockage effects. When designing the Planar-Motion Mechanism it was considered important that the large, accurate, wax models used for resistance and propulsion work should also be used for Planar-Motion Mechanism tests. This enabled the wide experience available regarding these models to be utilized and was also advantageous from an economic point of view. The conventional wax models have been found to be sufficiently robust when re-inforced by the addition of two transverse wooden bulkheads, and one or two laminates of glass-fibre on the inside surface (see, for example, Figure 8).

In order to obtain acceleration and damping of the same order of magnitude, and to reduce the likelihood of frequency problems while still enabling sizeable yaw velocities to be generated, the HyA Planar-Motion Mechanism was designed for lower frequencies and larger amplitudes of oscillation than the mechanism of Gertler and Goodman [6,7]. This proved to be a fortunate decision, as frequency problems caused by reflection of surface-waves from the tank walls arose at lower frequencies than expected.
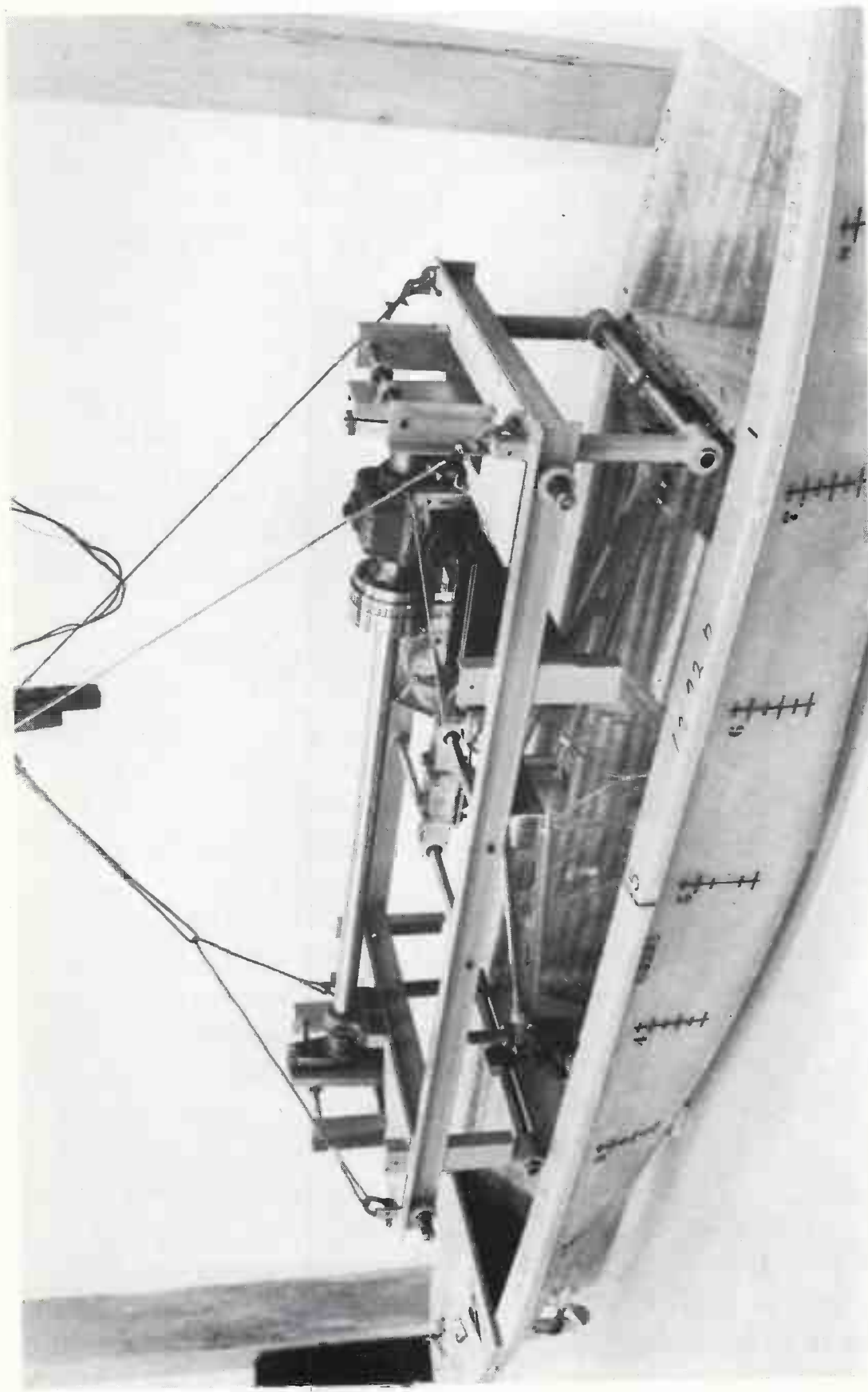
Figure 7

The HyA Planar-Motion Mechanism Shown Suspended over
a 6 m. (20 ft.) Wax Model for Photographic Purposes.

A general impression of the layout of the mechanism is given in Figures 7 and 8. It is contained in a flat frame of welded-up angle sections which is in itself flexible in torsion, but very stiff when in use, by virtue of being solidly clamped to the strong working-section of the carriage.

The solid main shaft is driven via a 1:50 MOSS worm-and-wheel reduction gearbox and a 1:2 POWER-GRIP "timing" belt-drive by a $2\frac{1}{2}$ hp THRIGE synchronous electric motor.

Both worm-and-wheel reduction gearbox and belt-drive are designed and manufactured to allow a chatter- and vibration-free angular motion even under the most rapidly changing load conditions. Current is supplied to the motor by a Ward Leonard system installed on the carriage, enabling revolutions to be continuously varied from 2 to 40 rpm. By these means a predetermined revolution value can be maintained within fine limits, independent of loading.

The uniform rotary motion of the main shaft is converted to periodic translatory motion in the horizontal plane by means of a scotch-yoke attached to each end (Figure 9). The amplitudes of the scotch-yokes can be continuously varied from 0 to 100 mm and the settings are indicated with an accuracy of 0.1 mm by small built-in mechanical digital counters. No appreciable wear has occurred in the brass-to-steel block and slider systems after several hundred hours of operation.

The translatory motion at each scotch-yoke is transmitted to the model by a rectangular cross-frame and two links. The upper arm of each cross-frame is supported by four axial bearings which also permit the frames to swing forward and aft. Constant drift angles can be introduced by sliding the short link on each lower arm and clamping it (see Figure 8), when it effectively becomes part of the cross-frame. The links are connected to axial and rotary bearings at each end of a longitudinal beam on the model centre-line. The beam is restrained at its centre point to prevent cyclic longitudinal movements of the model, and it maintains the links at a constant distance from the centre of the mechanism during all types of oscillatory motions. The beam together with the force gauges is mounted in the model in the workshop prior to being transported out to the carriage and connected up with the rest of the mechanism. This facilitates accurate positioning of the beam, symmetrically around the origin of the model's body axes, as well as permitting model and mechanism to be transported and attached
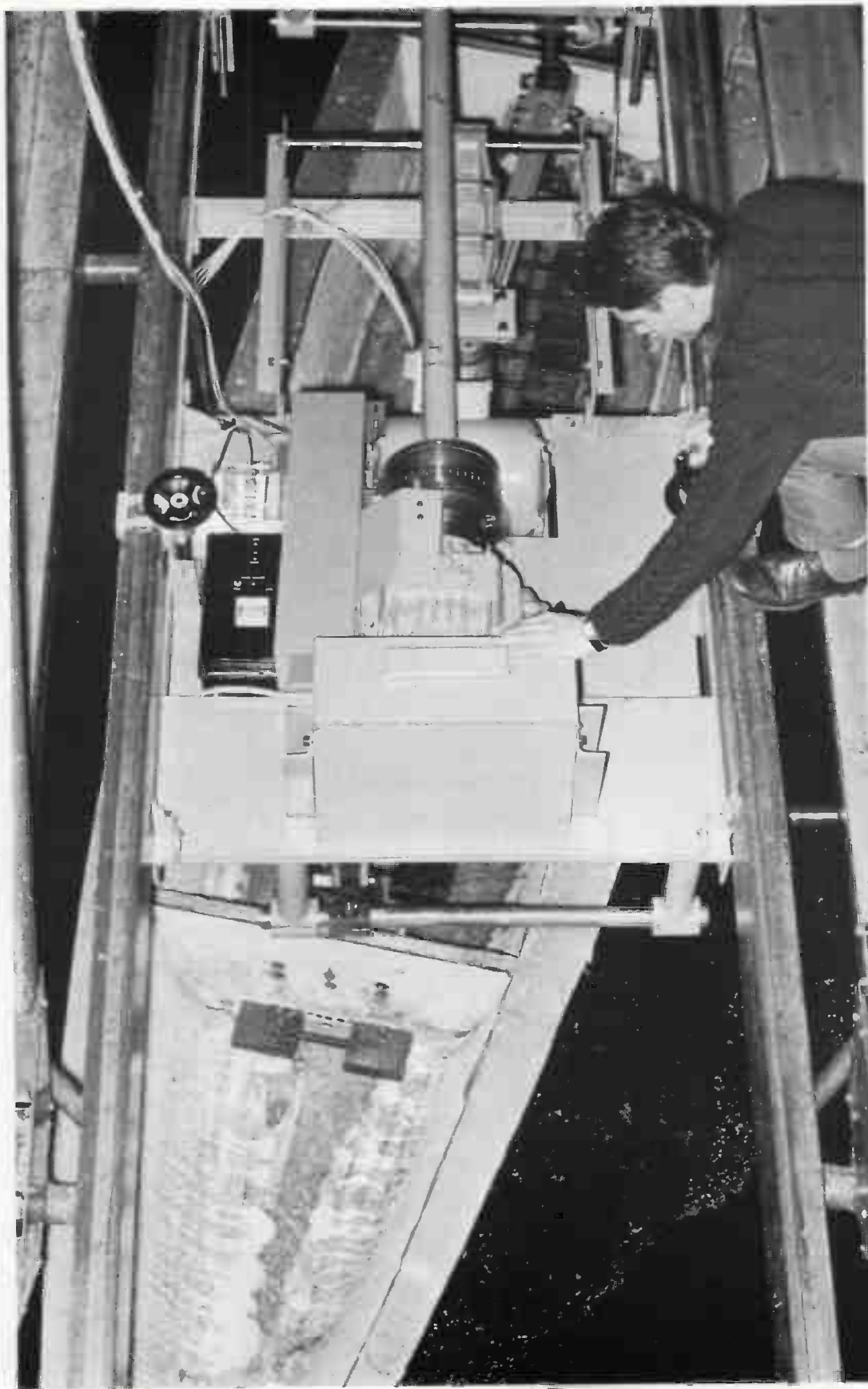
Figure 8

The HyA Planar-Motion Mechanism Mounted
on the Towing Carriage During Testing.
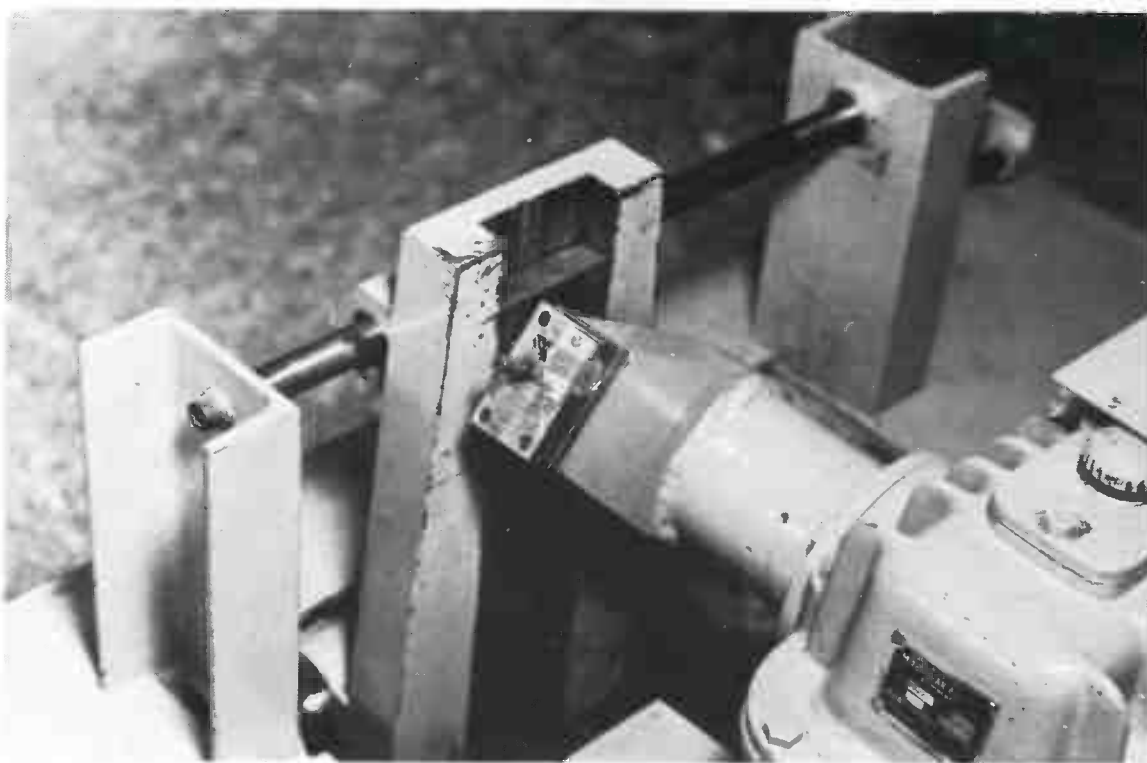
Figure 9

Variable Amplitude Scotch Yoke.
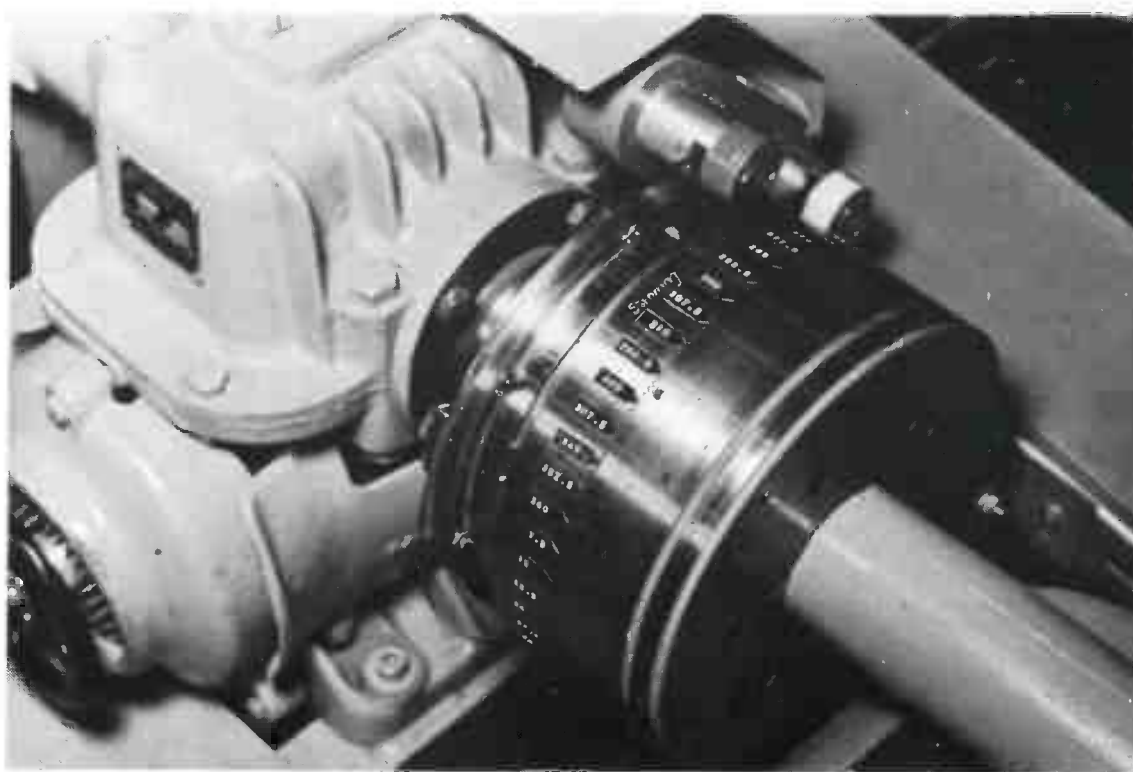
Figure 10

Electro-Magnetic Phase-Angle Coupling
and Synchronous Switch Arrangement.

to the carriage in a simple and convenient manner.

A STROMAG electro-magnetic tooth-coupling in the main-shaft permits the phase-angle between forward and aft scotch-yokes to be precisely set in descrete intervals of 1.5 degrees (Figure 10). Also mounted on the coupling is the synchronous switch that controls the integrator circuits used in conjunction with the force-measurement system. The switch consists of a perspex ring having four black lines spaced at 90 degree intervals. As the shaft rotates, the black lines interrupt light beams shining on two photo-cells, giving rise to two trains of electrical impulses. The perspex ring can be rotated relative to the main shaft and locked so as to give impulses at positions of zero and maximum yaw or sway displacement. This is accomplished by rotating the ring through half of the phase-angle between the scotch-yokes.

A mechanical micro-switch, giving one impulse per revolution of the main shaft, is used for identification purposes.

Dynamometry and Recording Instrumentation

Two modular force-gauges are attached to each end of the centre-beam (Figure 11). The physical proportions of the gauges are such that they are only flexible in one direction and they are orientated to pick up either side-force, Y, or longitudinal force, X. Gimbals, also seen in Figure 11, bolted to wooden bulkheads ensure that the model behaves as a "simply supported" beam. The model hull, force-gauges and centre-beam form a closed loop, eliminating any errors due to friction. Total X- and Y-forces and N-moment acting on the model are obtained from the gauge forces as follows,

$$X = X_F + X_A$$
$$Y = Y_F + Y_A \tag{15}$$
$$N = (Y_F - Y_A) \cdot l$$

where the subscripts F and A denote forces measured at forward and aft gauges, and l is the distance from origin to gimbal axis (1150 mm).

The electrical signals from the two X-gauges pass through DISA control units, are electrically summed and then recorded on a 10-inch-span PHILIPS pen-recorder. The control units are used to adjust sensitivity and zero position and also contain accurate reference (span-check) signals, which can conveniently be regarded as equivalent to

known forces at the gauges. When calibrated together with the gauges, these reference signals enable widely differing sensitivities to be used.

The signals from the Y-gauges are processed in one of two alternative ways dependent on the nature of the test. If the Planar-Motion Mechanism is being used in the static mode, i.e. if only constant forces resulting from drift and/or rudder angles are to be measured, then the gauge signals are passed via control-units to pen recorders in exactly the same manner as the X-forces, except that the signals from forward and aft gauges are recorded individually and not summed. When the mechanism is used in its "dynamic" mode, and periodic forces
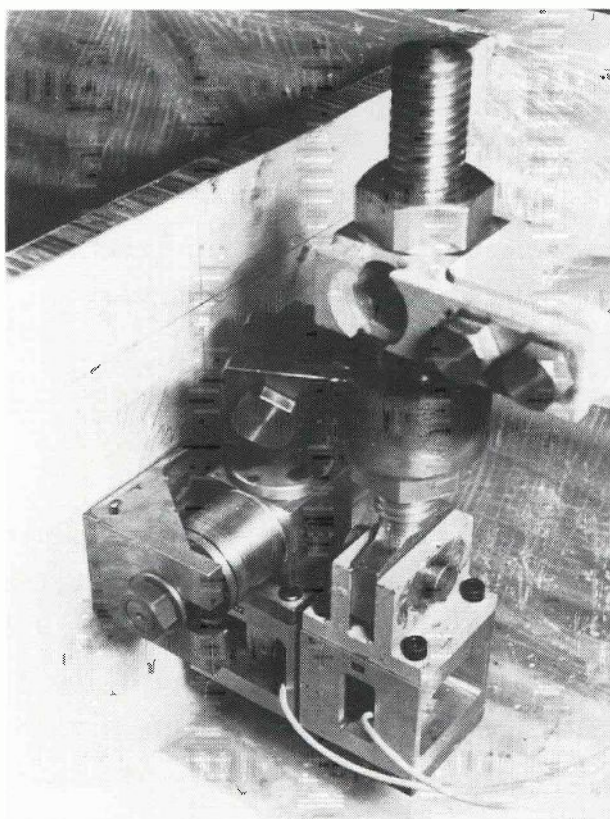
Figure 11

X- and Y-Force Gauges and Two-Degree-Freedom
Gimbal Attached to Bulkhead in Model.

are acting at the gauges, the signals are integrated before being recorded on the pen-recorders. The principles of the force integration are discussed in detail in the following section.

INTEGRATION OF PERIODIC FORCES

Basic Principles

The periodic forces acting at the Y-gauges in "pure sway" and "pure yaw" tests are composed of velocity-dependent and acceleration-dependent components. Assuming in the following, in order to simplify the discussion, that the periodic forces are directly proportional to the motions, and that there is no interaction between velocity-dependent and acceleration-dependent forces, then the cyclic forces, like the generated velocities and accelerations, will be of sine and cosine form. Each Y-gauge thus simultaneously senses a sine-wave force and a cosine-wave force, almost certainly of different amplitude, but necessarily of the same frequency, having the form:

$$\text{Gauge Force} = a_1 \sin \omega t + a_2 \cos \omega t$$

where a_1 and a_2 are constants in time.

If such a gauge-force is recorded directly on a pen-recorder, the record will be a sinusiodal curve of amplitude a_3 given by:

$$a_1 \sin \omega t + a_2 \cos \omega t = a_3 \sin (\omega t + e)$$

$$\text{where} \qquad a_1 = a_3 \cos e$$
$$\text{and} \qquad a_2 = a_3 \sin e$$

It is possible to measure a_3 and e from a paper record and so obtain a_1 and a_2, but the authors can say from experience that this is not a practicable solution, if only because of the difficulty of coping with the great quantities of paper records involved.

In the method chosen for the HyA Planar-Motion Mechanism the force-signal is integrated electrically, with periodic reversals of polarity as illustrated in Figure 12. It is seen that if polarity is reversed after half a period, then the sine component is measured and the cosine component eliminated. If polarity is reversed after one quarter and three quarters of a period, then the sine component is eliminated and the cosine component measured. Figure 12 also shows that if a constant force component is included to give the more general expression:

$$\text{Gauge Force} = a_0 + a_1 \sin \omega t + a_2 \cos \omega t$$
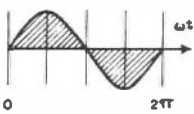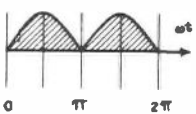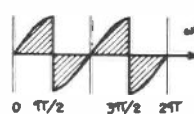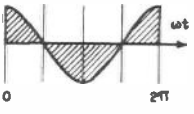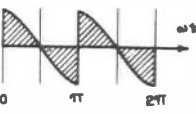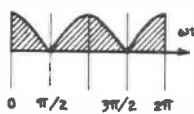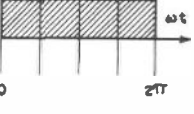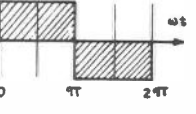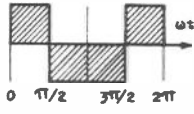
	PROGRAMME		
FUNCTION	**CONST.** Integration over one period with no change of polarity. (Sin & Cos eliminated, Const. measured).	**OSCIL.** Integration over one period with change of polarity after $\omega t = \pi$ (Cos & Const. eliminated, Sin measured).	**OSCIL.** Integration over one period with changes of polarity after $\omega t = \pi/2$ and $\omega t = 3\pi/2$ (Sin & Const. eliminated, Cos measured).
SINE	$\int_0^{2\pi} a\sin\omega t \, d(\omega t) = 0$	$\int_0^{\pi} a\sin\omega t \, d(\omega t) - \int_{\pi}^{2\pi} a\sin\omega t \, d(\omega t) = 4a$	$\int_0^{\pi/2} a\sin\omega t \, d(\omega t) - \int_{\pi/2}^{3\pi/2} a\sin\omega t \, d(\omega t) + \int_{3\pi/2}^{2\pi} a\sin\omega t \, d(\omega t) = 0$
COSINE	$\int_0^{2\pi} a\cos\omega t \, d(\omega t) = 0$	$\int_0^{\pi} a\cos\omega t \, d(\omega t) - \int_{\pi}^{2\pi} a\cos\omega t \, d(\omega t) = 0$	$\int_0^{\pi/2} a\cos\omega t \, d(\omega t) - \int_{\pi/2}^{3\pi/2} a\cos\omega t \, d(\omega t) + \int_{3\pi/2}^{2\pi} a\cos\omega t \, d(\omega t) = 4a$
CONSTANT	$\int_0^{2\pi} a \, d(\omega t) = 2\pi a$	$\int_0^{\pi} a \, d(\omega t) - \int_{\pi}^{2\pi} a \, d(\omega t) = 0$	$\int_0^{\pi/2} a \, d(\omega t) - \int_{\pi/2}^{3\pi/2} a \, d(\omega t) + \int_{3\pi/2}^{2\pi} a \, d(\omega t) = 0$

Figure 12

Integration with Periodic Polarity Reversals.

then either a_0, a_1 or a_2 may be obtained by suitable polarity reversal. A constant force signal will, for example, result when a constant rudder or drift angle is superimposed on pure yaw motion, or from imperfect gauge zero-adjustment.

These simple concepts form the basis used in the HyA Planar-Motion Mechanism system for the measurement of periodic forces.

Integration Programmes

The integration of the force signals is, in practice, controlled by programming circuits contained in a processing unit (Figure 13) designed for this particular purpose. The same programming circuits simultaneously control two parallel and identical measuring channels, used in conjunction with the forward and aft Y-gauges.

The circuits are built up from flip-flops, pulse-shapers, relays, etc., shown in the circuit diagram, Figure 14. The operations
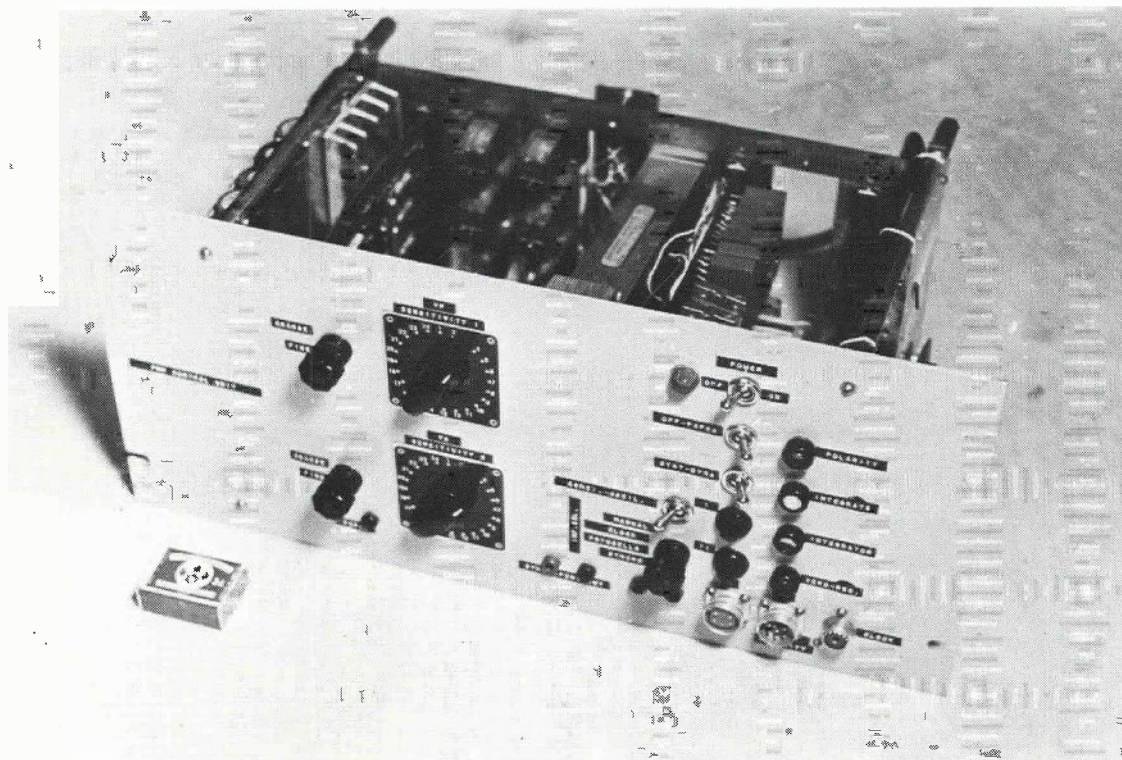
Figure 13
Processing Unit.

controlled by the programmes consist of reversing the polarity of the
signals fed to integrator-condensers, controlling the limits of inte-
gration, activating the output and recording mechanisms, and resetting
the condensers after each integration period.

The operations are activated by electrical impulses fed alter-
nately to Input 1 and Input 2 of the processing unit. The trains of
impulses are generated by the two photo-cells of the synchronous
switch mounted on the shaft-coupling. Four impulses are generated
by each photo-cell during each revolution of the mechanism. Impulses
can also be generated by a miniature synchronous motor in conjunction
with an analogous photo-cell arrangement, or by means of manually
operated push-buttons. The mini-synchronous motor is positioned in-
side the processing unit and is used for integration of span-check
signals after each measuring run and for calibration. The push-buttons
are mainly used for checking and adjusting purposes, but are also
useful for special tests needing long integration-times.

Integration can be made using either of two different pro-
grammes, designated OSCIL and CONST, the sequence of events of which
is shown in Table 1 and Figure 15. The only difference between the
two programmes is that the polarity of a signal integrated by means
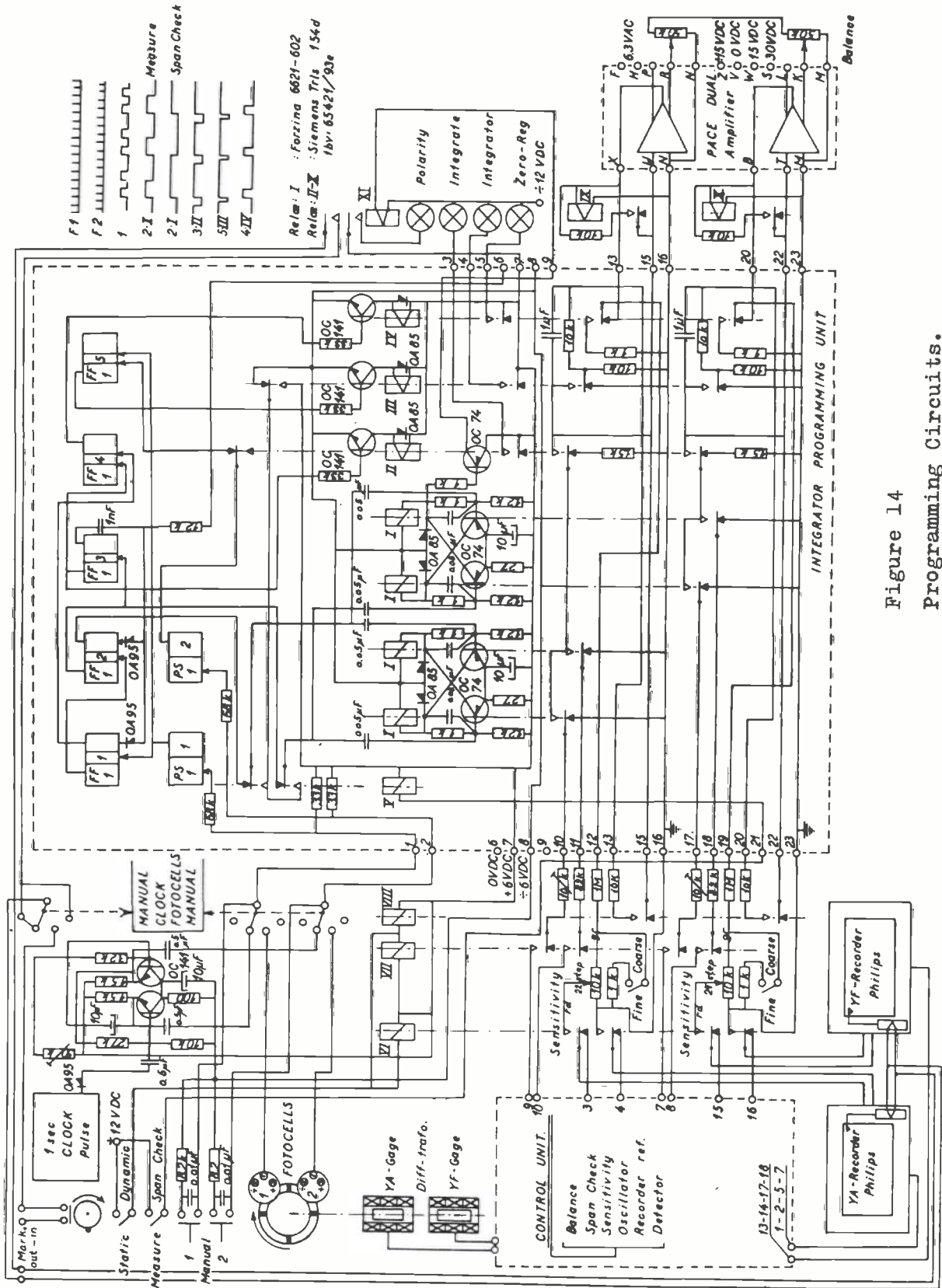
Figure 14
Programming Circuits.

Number of Impulses received		OSCIL. PROGRAMME	CONST. PROGRAMME
Input 1	Input 2		
0	0	Zero Condition (condensers at zero)	Zero Condition (condensers at zero)
1	0	Pens switched OFF Integration begins Polarity changed	Pens switched OFF Integration begins
1	1	-	-
2	1	Pens switched ON	Pens switched ON
2	2	-	-
3	2	Polarity Changed	-
3	3	-	-
4	3	-	-
4	4	-	-
5	4	Integration ends	Integration ends Polarity changed
5	5	Condensers reset to zero	Condensers reset to zero

Table 1

Sequence of Events Controlled
by Programming Circuits.

of the OSCIL programme is negative for the first half and positive for
the second half of an integration period, whereas the polarity of a
signal integrated by means of the CONST programme is the same during
a whole integration period. In both cases, the integration period
corresponds to one complete revolution of the mechanism, and hence to
one period of the force-signal. The complete programmes, however,
utilize one and a quarter periods, resulting in the start of each inte-
gration period occurring $\frac{\pi}{2}$ later than the one preceding it. This
facilitates alternate elimination of sine and cosine force-components,
when using the OSCIL programme. Subsequent integrations of, for in-
stance, the sine component will furthermore have opposite polarity

Input 1

Input 2

Polarity { OSCIL.
changes { CONST.

Integration period

Hold Condition

Condensers resetting

Pens switched OFF

Example of a
constant signal
integrated using
the CONST.
programme.
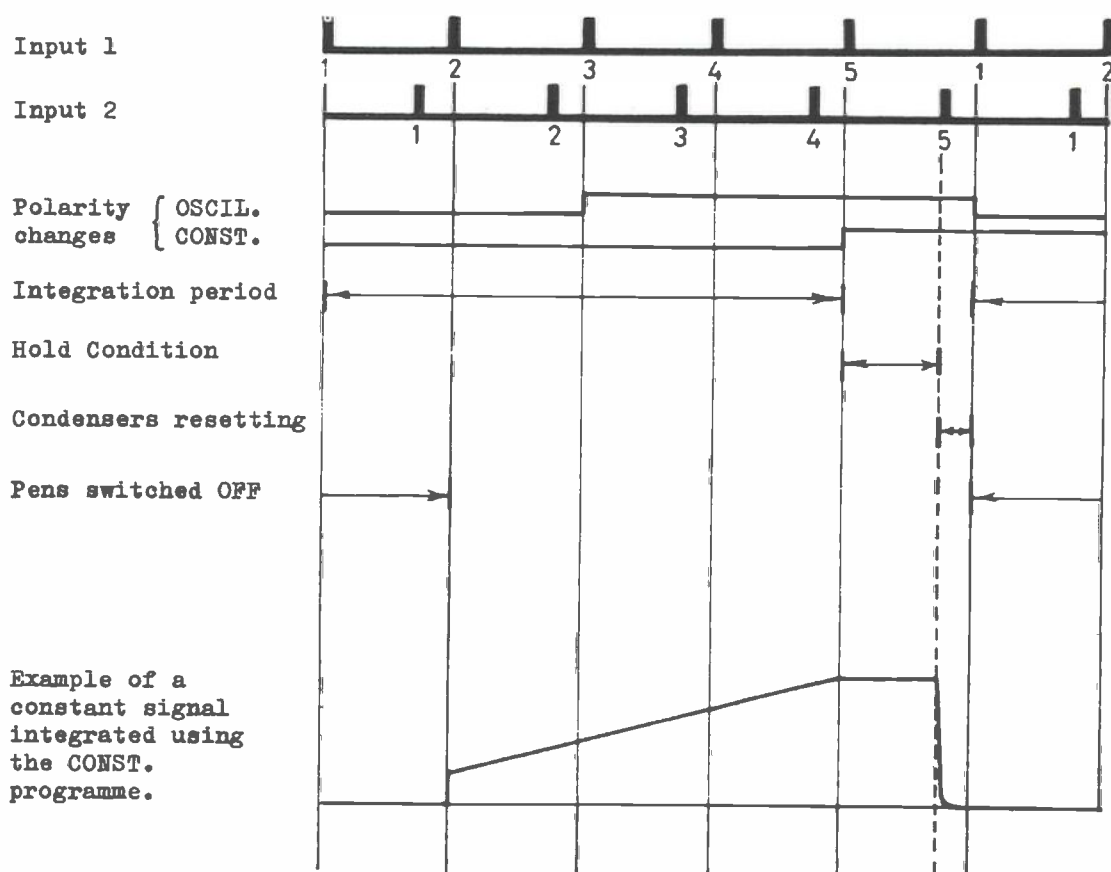
Figure 15

Sequence of Events Controlled by
Programming Circuits.

sequences enabling any differences in positive and negative integration
rates to be averaged out.

The duration of the hold period, in which the desired final
value is recorded, is governed by the time-lag between the impulses fed
to Input 1 and Input 2 of the unit.

Integration of Forces in Pure-Yaw Tests

Periodic forces resulting from "pure-yaw" motions are processed
by the OSCIL programme. Figure 16 shows that the angular velocity of
the origin of the body axes is OUT-of-phase, and angular acceleration
is IN-phase (but of opposite sign) with angular displacement. It is
therefore convenient to use displacement as a reference, and the syn-
chronous switch is consequently adjusted to give impulses to Input 1
at positions of zero, maximum and minimum angular displacement, i.e.

at $\omega t + \frac{\phi}{2} = 0, \frac{\pi}{2}, \pi, \frac{3}{2}\pi, 2\pi$ etc. This is accomplished by rotating the synchronous switch to a position half way between the angular displacement of the forward and aft scotch-yokes, i.e. if the forward yoke leads the aft by a phase angle ϕ, the synchronous switch has a phase angle of $\frac{\phi}{2}$.

In the first integration period shown in Figure 16, it is seen that because the polarity is reversed at $\omega t + \frac{\phi}{2} = \pi$, the cosine and any constant component are eliminated and the sine component is measured. The integrated value is designated OUT $\oplus$. The designation OUT is used to indicate that the measured force is OUT-of-phase with angular displacement. $\oplus$ indicates that the force corresponds to positive yaw velocity, as the effective yaw velocity has been positive throughout the whole of the integration period.

The next quarter revolution of the mechanism is used for the hold-condition, activating the recording and output mechanism, and to discharge the condenser. As a result, the second integration period starts at $\omega t + \frac{\phi}{2} = \frac{\pi}{2}$, and not at $\omega t + \frac{\phi}{2} = 0$ as did the first. The polarity is reversed half way through the integrating period, now corresponding to $\omega t + \frac{\phi}{2} = \frac{3}{2}\pi$, and in this case the sine and any constant components are eliminated, and the cosine component is measured. The final integrated value is designated IN $\ominus$, as the measured force is IN-phase with the angular displacement, and corresponds to negative acceleration.

In a similar way the third and fourth integration periods measure forces corresponding to negative velocity and positive acceleration, and are designated OUT $\ominus$ and IN $\oplus$ respectively. The fifth integration period is the same as the first after which the cycle is repeated.

Characteristic features of forces recorded during "pure-yaw" tests are illustrated in the typical records at the bottom right of Figure 16. A margin-pen, activated by the mechanical micro-switch once per revolution of the main shaft, is used to identify the different force components and is shown symbolically on the top of the forward scotch-yoke. It is seen, for example, that an IN $\oplus$ record is characterized by margin-pen marks $(90 - \frac{\phi}{2})$ after the start and stop of the integration period.

The forward and aft IN $\oplus$ and IN $\ominus$ forces are of the same order of magnitude but of opposite sign. This is natural as mass and submerged lateral-area are distributed nearly symmetrical about
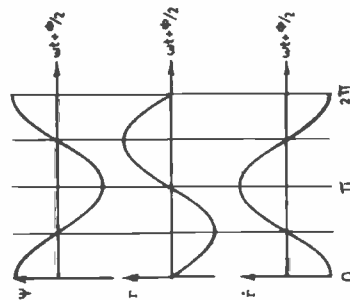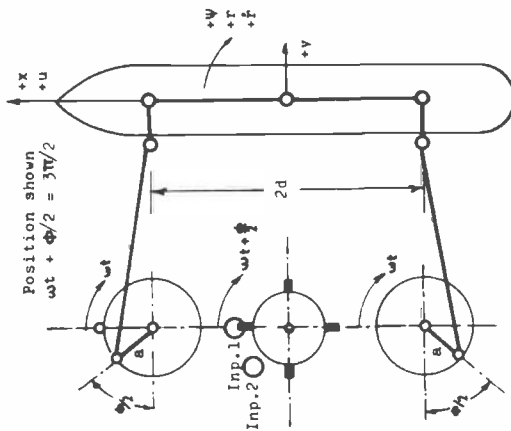
Figure 16

Yaw Test Analysis.
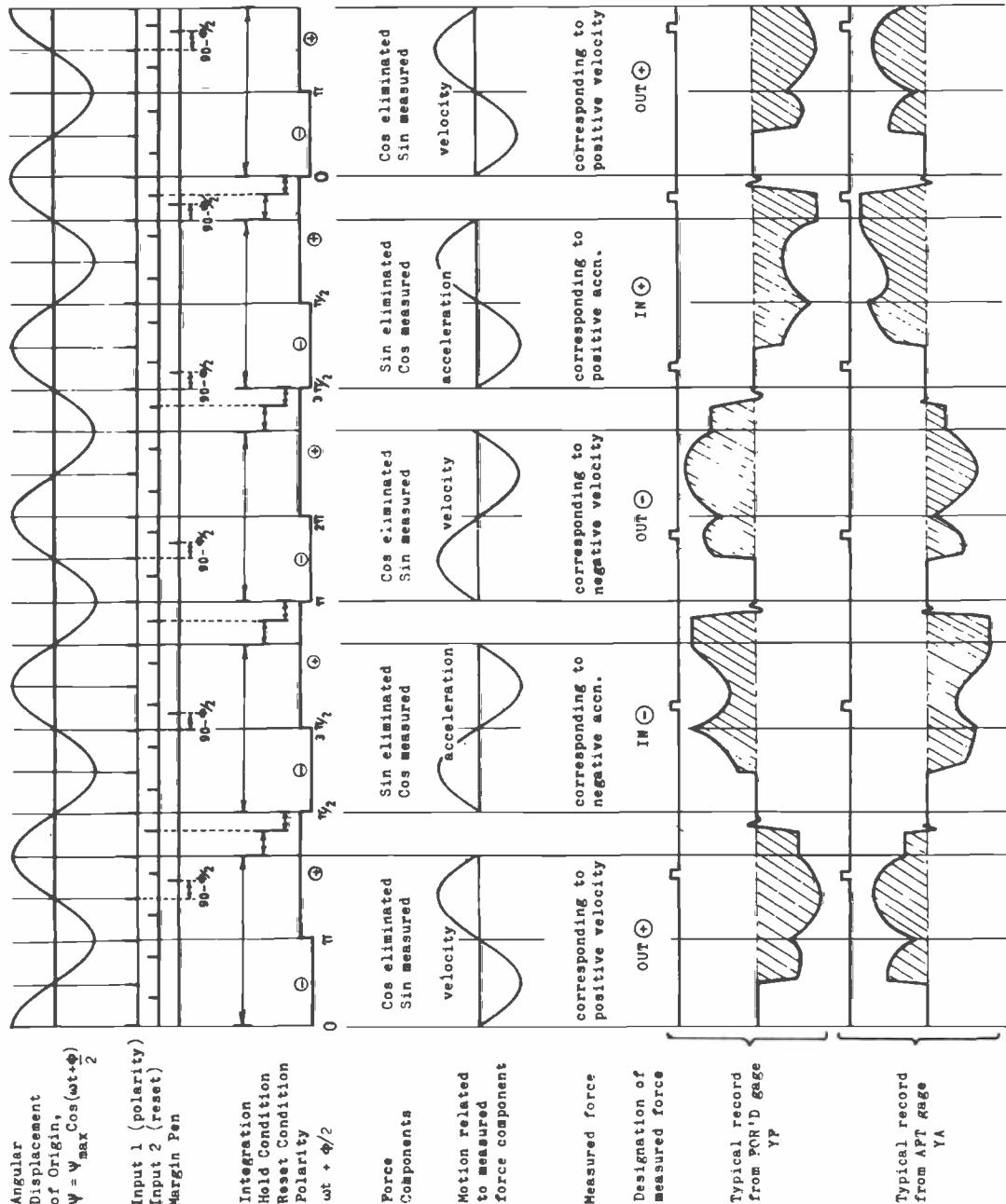
the origin, and because yaw acceleration causes the forebody to swing to port while the afterbody swings to starboard, and vice versa.

The forward and aft OUT ⊕ (and OUT ⊖) forces are of the same order of magnitude but of opposite sign, the aft force being positive. The centrifugal effect of the ship's mass acts in the same direction at both forward and aft gauges, adding to the hydrodynamic force at the forward gauge and reducing the effect of the hydrodynamic force at the aft gauge. The forward gauge-force is therefore usually of greater absolute magnitude than the aft. For ships with pronounced rake of keel, however, the hydrodynamic force aft is greater than that forward and the measured forces become of almost equal absolute magnitude.

Acceleration-dependent forces are usually of greater absolute magnitude than those dependent on velocity. The relative proportions of the two change with frequency of oscillation and model speed, however, and, for low frequencies or high speeds, the velocity-dependent forces can be the largest.

By adding and subtracting the forward and aft IN and OUT components according to Equations (15), side forces and turning moments are obtained as functions of yaw acceleration and yaw velocity. When these values are faired, the slopes of the fairing lines at the origin give the terms $(Y_{\dot{r}}-mx_G)$, $(N_{\dot{r}}-I_z)$, (Y_r-mu) and (N_r-mx_Gu). These terms contain the effects of known model mass and inertia, which may be eliminated, leaving the hydrodynamic terms, $Y_{\dot{r}}$, $N_{\dot{r}}$, Y_r and N_r. Ship mass and inertia values can then be re-introduced. This ability to account for differences in mass and inertia between model and ship is convenient as it permits the model to be constructed without paying any regard to its inertia. Model displacement is usually kept to the scaled ship value and ballast is adjusted until the correct trim is obtained.

Integration of Forces in Pure-Sway Tests

The forces measured in "pure-sway" tests are treated in a manner exactly analogous to the "pure-yaw" tests described above. As seen in Figure 17, the forces are integrated with sign reversals related to lateral instead of angular displacement. The synchronous switch is thus adjusted to give impulses to Input 1 at positions of zero, maximum
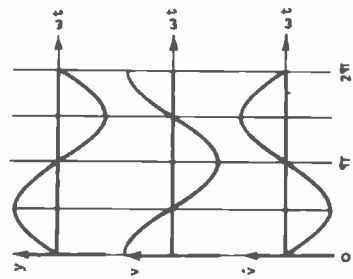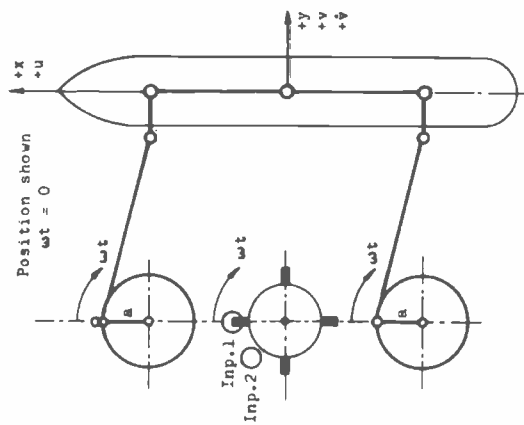
Figure 17

Sway Test Analysis.
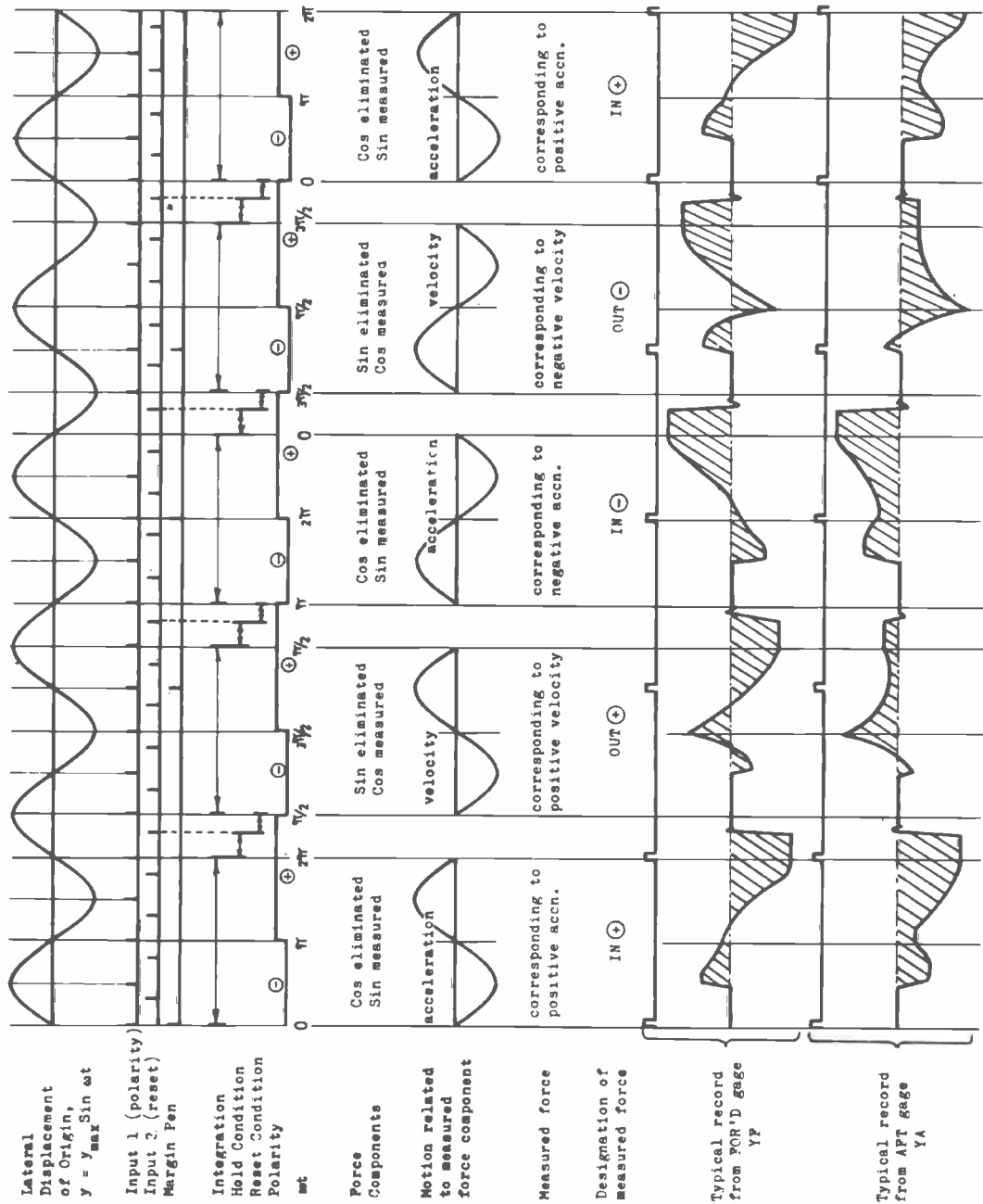
and minimum sway displacement. The measured forces are again desig-
nated IN and OUT to indicate IN-phase or OUT-of-phase relationships
with sway displacement.

Typical records of forces measured at the forward and aft
gauges, shown in the bottom right of Figure 17, are explained in simi-
lar manner to the results of "pure-yaw" tests. Forward and aft IN $\oplus$
forces are in this case of the same sign because forebody and afterbody
accelerate simultaneously to port or to starboard. Forward and aft
OUT $\oplus$ forces, resulting from positive sway-velocity (or negative
drift-angle) are largely functions of lift, due to circulation built
up around the hull, which acts at approximately the quarter-chord
point, i.e. close to the forward Y-gauge for a 6 m. model.

Addition and subtraction of the IN-phase force-components
according to Equations (15) gives the side force and turning moment
due to sway-acceleration. The slopes of straight lines used to fair
these data give the terms $(Y_{\dot{v}}-m)$ and $(N_{\dot{v}}-mx_G)$, again including the
effects of the model mass, the elimination of which results in the hydro-
dynamic derivatives $Y_{\dot{v}}$ and $N_{\dot{v}}$.

OUT-of-phase force-components resulting from sway-velocity or
drift-angle are generally to some extent frequency and/or amplitude-
dependent and are discarded in favour of results obtained from tests
made with steady drift-angles in the static mode.

Integration and Interpretation of Non-Linear Forces

It has been assumed in the foregoing that the periodic forces
measured in "pure-yaw" and "pure-sway" tests are proportional to the
motions. This is, however, not a necessary condition for the use of
the integration technique described, but was rather introduced in order
to simplify the discussion. When the forces are related to the motions
in a non-linear fashion, the same principles can be used to obtain the
non-linear hydrodynamic coefficients.

Suppose for instance, that for a particular hull, the hydro-
dynamic force or moment resulting from yaw velocity is of the character
shown in Figure 18a. When an oscillator technique is used to generate
the yaw velocity, the force-response at a particular instant is basically
the same as in the steady state provided frequency of oscillation is
sufficiently low. If the sinusoidal angular velocity is of small am-

Fig. 18a
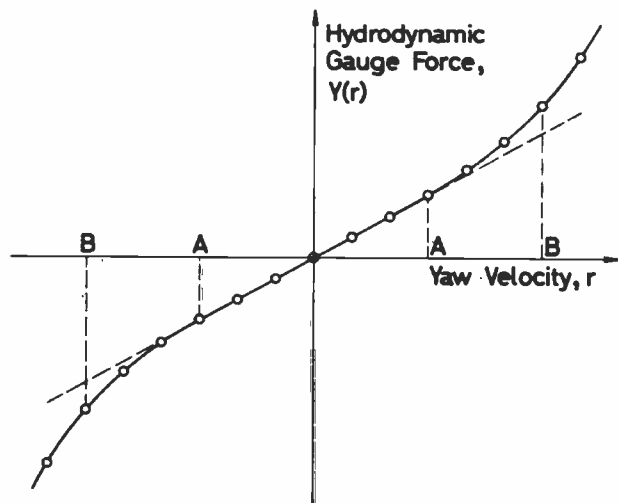
Figure 18

Non-Linear Force Response
to Steady-State Yawing
Motion and to Sinusoidal
Yawing Motion.

Fig. 18b
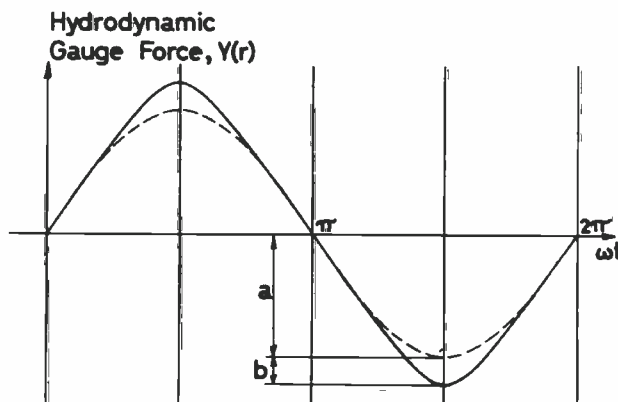
plitude, the forces are proportional to the motion and are also sinu-
soidal. This is the case within the range of linear force-response
A-A. Tests made within this area provide the linear terms Y_r and N_r
as discussed above. It is, however, desirable to explore the full range
of yaw velocities that a vessel can experience, and this will probably
extend into the non-linear area indicated by B-B. If an oscillatory
test is made in which a sinusoidal angular velocity of this amplitude
is impressed on the model, the force-response will be of sinusoidal
character within the region of lesser yaw velocities, A-A, but pro-
gressively deviate from sinusoidal in the regions A-B resulting in a
gauge force of the character illustrated in Figure 18b.

A curve of the character shown in Figure 18a can be expressed
with good accuracy by a linear and a cubic term:

$$Y(r) = Y_r r + Y_{rrr} r^3$$

Since the yaw velocity impressed on the model is sinusoidal,
described by

$$r = r_{max} \sin \omega t$$
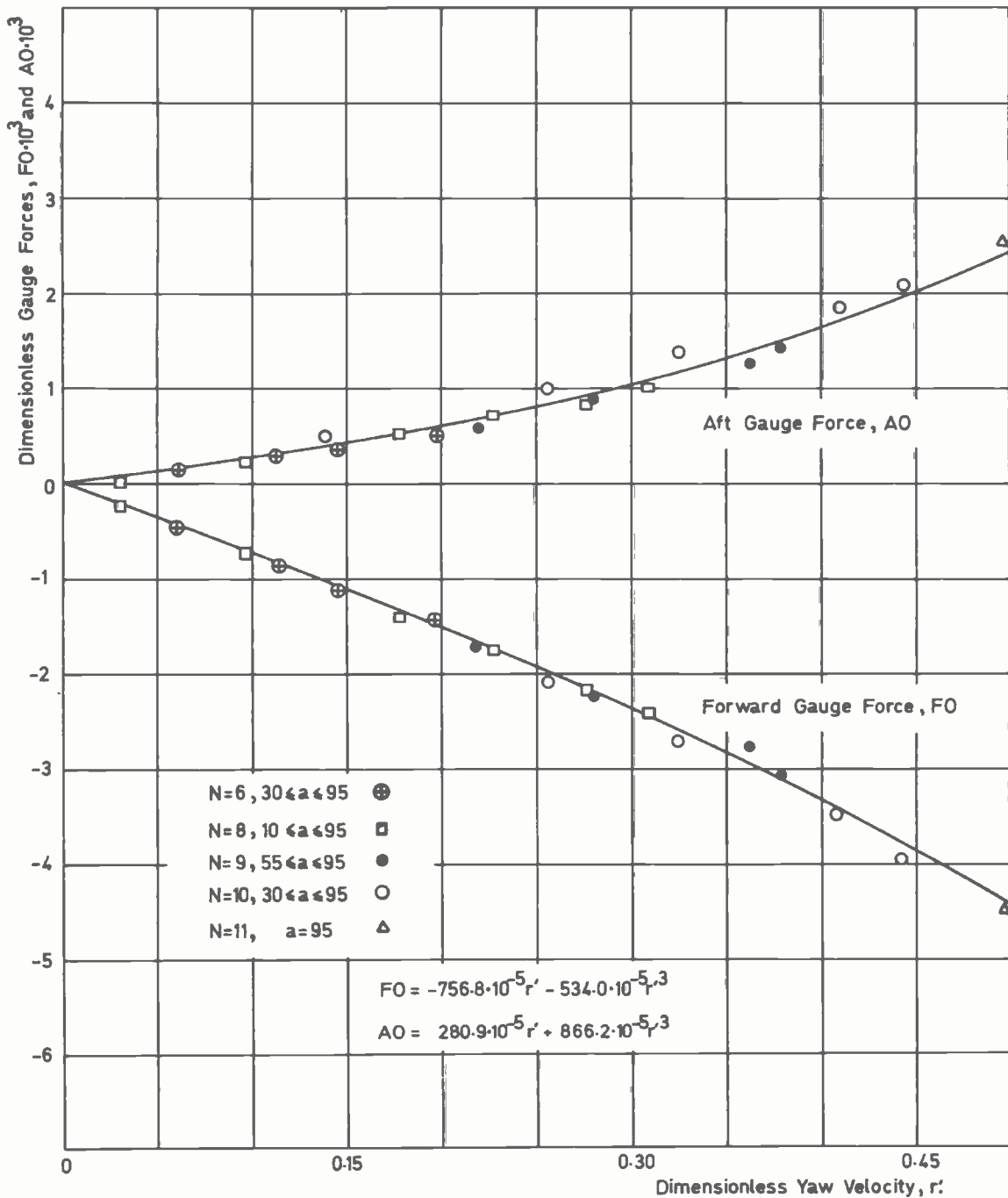
Figure 19

Pure Yaw Results Measured with the HyA Planar-Motion Mechanism,
Transverse (Y) Gauge Forces as Functions of Yaw Velocity.

it follows that the cyclic forces experienced by the force gauges
(Figure 18b) are expressed by:

$$Y(r) = Y_r \, r_{max} \, \sin \omega t + Y_{rrr} \, r_{max}^3 \, \sin^3 \omega t$$

or

$$Y(r) = a \sin \omega t + b \sin^3 \omega t$$

where a and b are constants in time. Integration over one period with
a change of polarity after half a period then gives:

$$\int_0^\pi Y(r) - \int_\pi^{2\pi} (Yr) = 4a + \frac{8}{3} b$$

i.e.

$$\frac{(\text{Integrated Value})}{4} = a + \frac{2}{3} b$$

$$= Y_r r_{max} + \frac{2}{3} Y_{rrr} r_{max}^3$$

The true cubic term, Y_{rrr}, corresponding to the steady-state
condition is thus one and a half times greater than the cubic term
obtained by fairing force-values which have been integrated over one
period of sinusoidal yaw-velocity.

Figure 19 shows an example of non-linear forces obtained in
this manner by means of the HyA Planar-Motion Mechanism. The integrated
forces have been obtained as a result of pure yawing motion forced on a
20-ft. model of the MARINER hull-form. The model, condition tested
and nomenclature are identical to that described in [5] , except that
the tests were made at a ship speed of 10 knots instead of 15 knots,
in order to facilitate the generation of large yaw-velocities. The mea-
sured forces have been faired with linear and cubic terms, the coeffi-
cients of the fairing polynomials being included in the figure. Steady-
state side-forces and turning moments can be obtained from the
gauge-forces according to Equations (15), the cubic terms having been
multiplied by $\frac{3}{2}$ as described above.

Integration and Interpretation of Cross-Coupling Terms in Yaw-and-Drift-Angle-Tests

Cross-coupling effects due to simultaneous yaw-velocity and
drift-angle are expressed in the mathematical model by the terms Y_{vrr},
N_{vrr}, Y_{rvv} and N_{rvv}. Similarly the cross-coupling due to yaw-velocity
and rudder-angle is expressed by $Y_{\delta rr}$, $N_{\delta rr}$, $Y_{r\delta\delta}$ and $N_{r\delta\delta}$. These
two sets of coefficients can be obtained from the "yaw-and-drift-angle"
and the "yaw-and-rudder-angle" tests respectively, outlined in Figure
4. As the same principles are used for measurement of both sets of
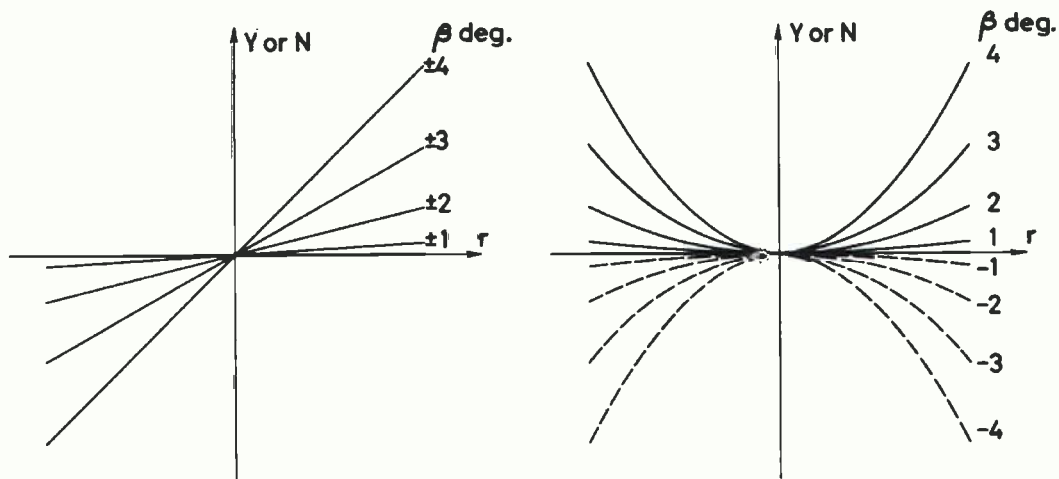
Figure 20

Diagrammatic Illustration of Cross-Coupling
Terms Y_{rvv}, N_{rvv}, Y_{vrr} and N_{vrr}.

terms, only the derivation of the cross-coupling between yaw-velocity
and drift-angle is described in the following.

The terms vrr and rvv, shown diagrammatically in Figure 20,
constitute a flexible means of expressing the experimental data, while
conforming to the port and starboard symmetry condition $f(r,v)$ =
$-f(-r,-v)$. The two terms have essentially the same character, as can
be seen by replotting on a base of v instead of r.

The side-force acting on a model in a "yaw-and-drift-angle"
test can be expressed on a time basis by:

$$Y(t) = Y_{\dot{r}}\dot{r}(t)+Y_r r(t)+Y_v v+Y_{rvv}r(t)v^2+Y_{vrr}vr(t)^2 \tag{16}$$

where v corresponds to drift-angle, held constant during each measuring
run, and $r(t)$ and $\dot{r}(t)$ are the sinusoidally varying yaw-velocity and
acceleration. Again, the corresponding expression for $N(t)$ is exact-
ly analogous.

The first three terms in Equation 16 are known from the "pure-
yaw" and "static-drift-angle" tests. The manner in which the last
two terms can be derived from the "yaw-and-drift-angle" test is shown
schematically in Figure 21

Figure 21a illustrates two characteristic situations, one for
positive (P) and the other for negative (N) yaw-velocity. It is again
helpful to relate the periodic forces, resulting from periodic motions
generated by the Planar-Motion Mechanism, to the corresponding steady-
state measurements shown in Figure 21b. The two sketches in Figure 21b

Fig. 21a
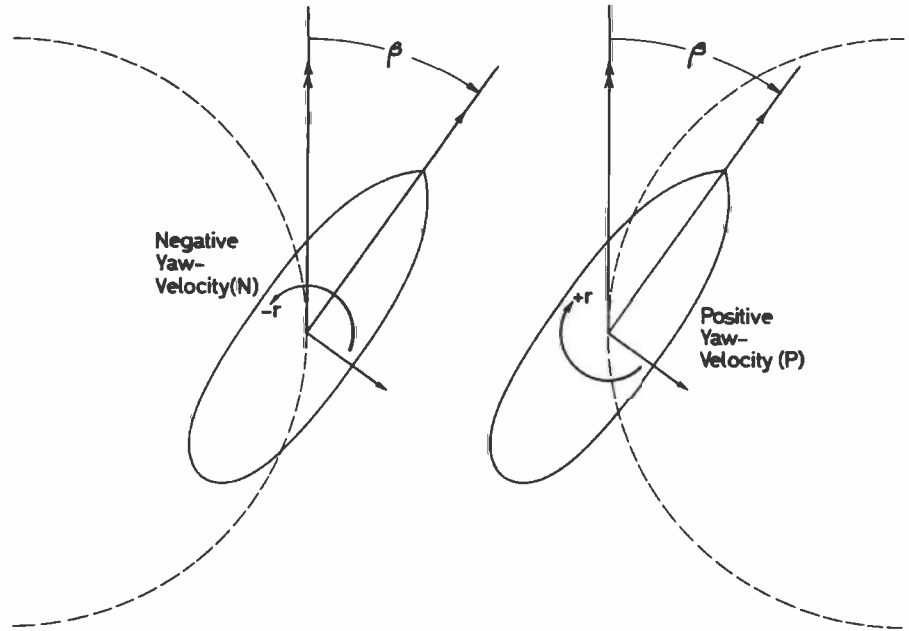
Fig. 21b
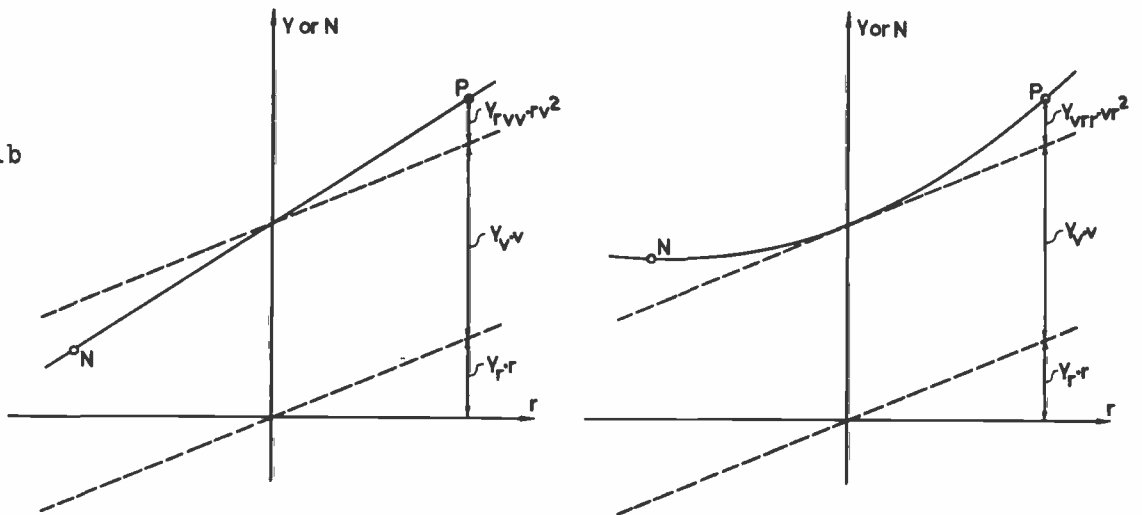
Fig. 21c
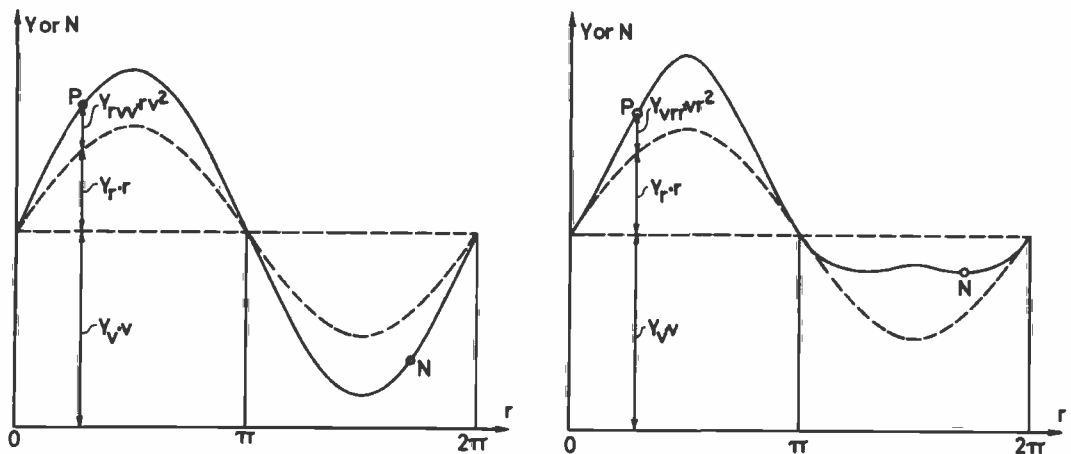
Figure 21

Generation, Interpretation and Measurement of Cross-Coupling
Effects in Yaw & Drift Angle Tests.

each diagrammatically illustrate one of the two terms rvv and vrr, assuming the other to be zero. The corresponding forces acting at the Y-gauges during one revolution of the mechanism are shown in the sketches in Figure 21c.

It is seen that using the OSCIL programme, the IN-phase measurements obtained from a "yaw-and-drift-angle" test correspond to $Y_{\dot{r}}\dot{r}(t)$, and the OUT-of-phase measurements correspond to $Y_r r(t)+Y_{rvv}r(t)v^2$, whereas the forces corresponding to the remaining two terms are eliminated. The component $Y_{rvv}r(t)v^2$ is then obtained by subtracting the known value corresponding to $Y_r r(t)$.

Similarly, use of the CONST programme gives measurements corresponding to $Y_v v + Y_{vrr}vr(t)^2$ and the component $Y_{vrr}vr(t)^2$ is obtained by subtracting the known value corresponding to $Y_v v$.

In practice, the rvv-term has been found to be of significant magnitude and the vrr-term to be small. The rvv-term is linear with r and so independent of the range of yaw-velocity, whereas the vrr-term, being second order in r, can only be measured if an adequate range is covered.

DESIGN OF EXPERIMENTAL PROGRAMME AND DETERMINATION OF HYDRODYNAMIC COEFFICIENTS

The complete experimental programme, which should be carried out in order to determine the hydrodynamic coefficients, would, in addition to the various Planar-Motion Mechanism tests illustrated in Figures 2 to 4, inclusive, consist of conventional open-water, resistance, and self-propulsion tests, and an experiment for determination of the model polar moment of inertia.

Two of the coefficients are furthermore obtained from numerical calculations, instead of experimentally. The added mass of the ship in surge acceleration, $X_{\dot{u}}$, is, for instance, normally assigned a value of -0.05 m based on theoretical considerations. Similarly, the ship moment of inertia, I_z, is computed on the basis of the longitudinal weight distribution of the full-scale ship.

Considerations in the design of the different tests, and the analysis of force measurements in the determination of the hydrodynamic coefficients are discussed in the following.

Design of Experimental Programme

The range of motion and rudder parameters explored during testing should, in principle, cover the range of subsequent simulation. Sway and yaw acceleration, speed loss, drift angle, yaw velocity and rudder angle should therefore be varied systematically up to the values corresponding to maximum-rudder manoeuvres for the free-sailing ship. Typical values for the range of motion parameters experienced by a cargo ship during the execution of a 35 degree rudder-angle turning circle and a 20-20 degree zig-zag manoeuvre are given in Table 2. Corresponding maximum values obtained with naval ships are often 1.5 to 2 times greater.

Table 2

Typical Range of Dimensionless Motion-Parameters
for a Cargo Ship.

Motion Parameter	35 Degree Turning Circle		20-20 Degree Zig-Zag
	Transition Period	Steady Turn	
u'		-0.6	-0.3
v'		± 0.16	± 0.13
r'		± 0.42	± 0.33
$\dot{u}'$	0.10		0.03
$\dot{v}'$	± 0.12		± 0.12
$\dot{r}'$	± 0.55		± 0.50

When testing with the HyA Planar-Motion Mechanism, the range of motion parameters a ship will encounter can be adequately covered with the exception of yaw velocity. In the static mode of operation, for example, drift-angle tests can be executed with drift angles up to ± 20 degrees corresponding to $v' = \pm 0.34$, which is comparable to the maximum sway-velocity experienced by naval ships. In the dynamic mode of operation, the range of motion parameters can be adjusted by varying the amplitude at the scotch yokes and the shaft revolutions. Adequate coverage of the desired range of yaw and sway accelerations can easily be obtained in these tests.

For the crucial yaw velocity, Figure 22 gives, for maximum amplitude, the relationship between non-dimensional yaw velocity and shaft revolutions as a function of model speed and model length. For example, in the case of a cargo ship model with a maximum non-dimensional yaw velocity, r' = 0.4, model length 6 metre and model speed 1.4 metre/sec, Figure 22 shows that shaft revolutions of 12 per minute would be adequate. Whereas this is well within the structural capability of the mechanism, experience has shown the practical limit of operation to be around 8 to 10 revolutions per minute.

This limitation is due to wave reflections from the basin walls, which for higher shaft revolutions interfere with the force measurements. As the problem is associated with a system of standing waves built up in the basin at certain frequences, it is in general independent of model speed and size.

With a maximum shaft r.p.m. of approximately 10, it is seen from Figure 22 that the HyA Planar-Motion Mechanism gives an acceptable coverage for 6 to 8 metre cargo ship models, whereas for naval ships, when smaller models would often be used, the desired range of yaw velocities can only be covered at lower speeds.

It would normally be desirable to cover the complete range as given in Table 2. In some circumstances it is possible, however, to economise on the number of captive-model experiments necessary for accurate simulation of a particular manoeuvre. For example, if interest is centred on the steady turning state corresponding to maximum rudder-angle, then acceleration terms are of minor importance and tests need only be made for one rudder angle, and for drift angles, yaw velocities and speeds covering a range centred about the estimated equilibrium state.

On the other hand, it should also be borne in mind that in order to obtain coefficients which truly represent the symmetry inherent in ship forms and reflected in the design of the mathematical model, it is necessary to plan the experiments accordingly. In particular, two-variable cross-coupling terms should preferably be obtained from measurements corresponding to a range of parameters in which at least one of the parameters is assigned both positive and negative values. The numerical values of the coefficients will then uniquely describe the steering and manoeuvring properties of the particular ship in question and can be used without reservation within the performance envelope corresponding to the ship's rudder action,
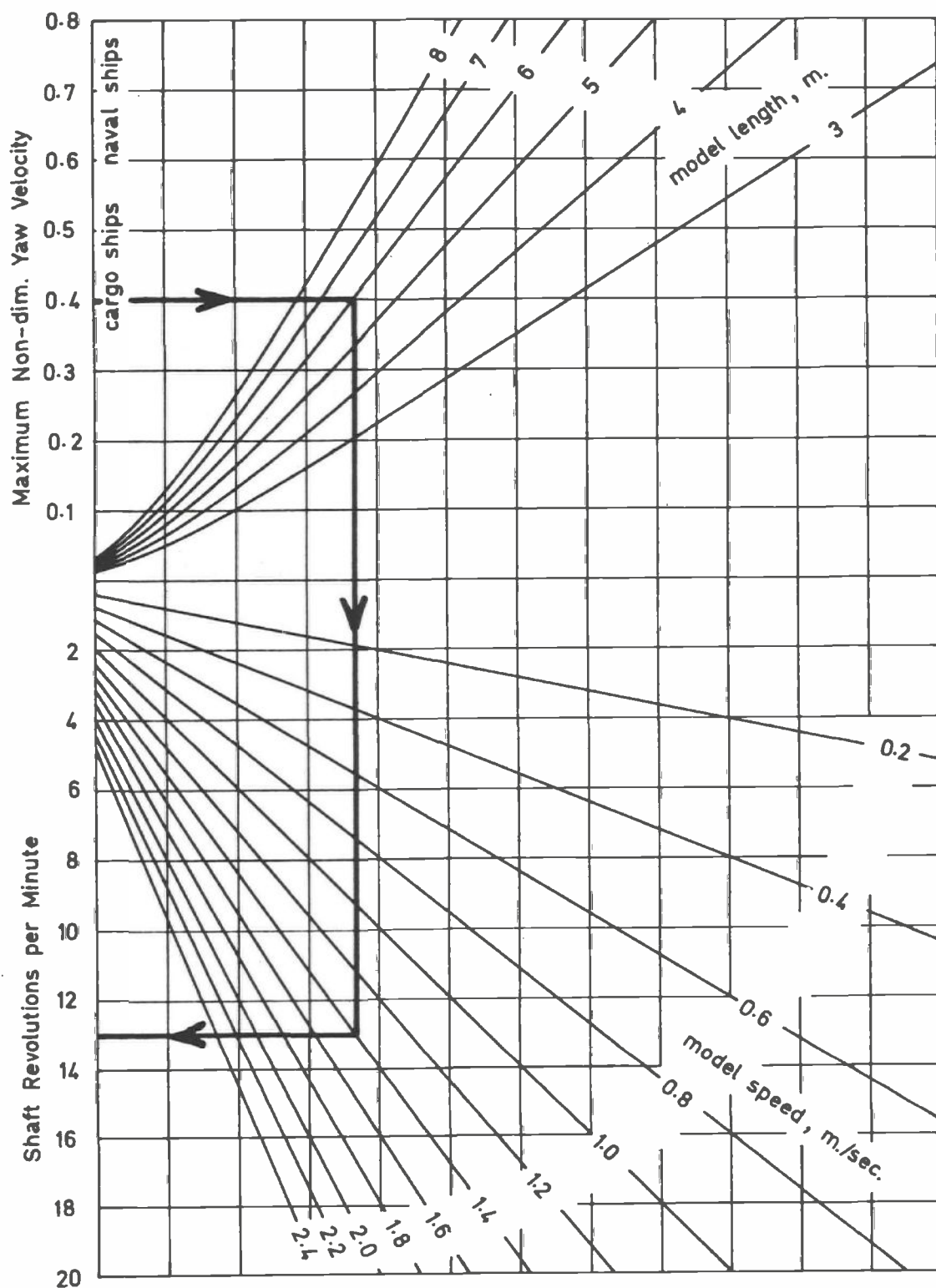
Figure 22

Relationship between Dimensionless Yaw Velocity and Shaft
Revolutions as Function of Model Speed and Model Size (for
100 mm. Amplitude at the Scotch Yokes).

instead of only being valid within a limited area.

In designing the experimental programme, emphasis should be placed on the more important terms. In general, the six linear velocity-dependent terms, Y_v, N_v, Y_r, Y_δ and N_δ , are predominant, while acceleration-dependent, higher-order and cross-coupling terms are of lesser influence (though many are far from negligible) in the accurate prediction of manoeuvres.

The larger hydrodynamic acceleration-dependent terms, $Y_{\dot{v}}$ and $N_{\dot{r}}$, are of the same order of magnitude as their related mass, m, and inertia, I_z, values, which effectively doubles their accuracy. Acceleration terms are, furthermore, only influential in transitional manoeuvres, having no influence during steady turning states.

Sufficient experimental measurements should be made to justify the use of least-squares fairing procedures. If too few points are used, the fairing expression may give a good fit, without truly representing the trend of the actual curves.

It is generally recognised that the propeller slipstream has a considerable influence on the characteristics of the rudder coefficients. In carrying out the model tests, it is consequently important to scale the slipstream as accurately as possible, for instance, by executing the tests for a propeller r.p.m. corresponding to the ship propulsion-point as opposed to that of the model. When a ship enters a manoeuvre its speed will reduce, and the propeller r.p.m. will consequently vary somewhat, the variation being dependent on the type of engine and the engine control-settings maintained during the manoeuvre. If it is simply assumed that constant propeller r.p.m. are maintained during the entire ship manoeuvre, the model tests carried out to measure the speed-dependent coefficients such as $Y_{\delta u}$, $Y_{\delta uu}$, etc. can simply be made with the model propeller r.p.m. maintained at the value corresponding to the initial speed of the ship. It is also possible, however, as will be discussed later, to compute the variations of propeller r.p.m., which occur as a ship reduces speed, and to obtain speed-dependent coefficients which correspond to specified machinery types and control-settings.

Analysis of Force Measurements

In the last stage of the testing procedure, the forces and moments measured in the course of the various Planar-Motion Mechanism

tests, are analysed to yield the different hydrodynamic coefficients. The analysis consists, in principle, of fairing the experimental data, using the mathematical model as the approximating function, and obtaining the hydrodynamic coefficients as those coefficients, which give the best fit to the measured values.

The results from a "static drift-angle" test would, for example, consist of measurements of X- and Y-forces and N-moment, as functions of drift angle and rudder angle. According to the mathematical model, these forces and moments are described by the expressions:

$$X = X_* + X_{vv}v^2 + X_{v\delta}v\delta + X_{\delta\delta}\delta^2$$

$$Y = Y_* + Y_v v + Y_{vvv}v^3 + Y_{v\delta\delta}v\delta^2 + Y_\delta \delta + Y_{\delta\delta\delta}\delta^3 + Y_{\delta vv}\delta v^2$$

$$N = N_* + N_v v + N_{vvv}v^3 + N_{v\delta\delta}v\delta^2 + N_\delta \delta + N_{\delta\delta\delta}\delta^3 + N_{\delta vv}\delta v^2$$

Hence, the hydrodynamic coefficients

$$X_*, \; X_{vv}, \; X_{v\delta}, \; X_{\delta\delta}$$

$$Y_*, \; Y_v, \; Y_{vvv}, \; Y_{v\delta\delta}, \; Y_\delta, \; Y_{\delta\delta\delta}, \; Y_{\delta vv}$$

$$N_*, \; N_v, \; N_{vvv}, \; N_{v\delta\delta}, \; N_\delta, \; N_{\delta\delta\delta}, \; N_{\delta vv}$$

are simply the coefficients of these expressions, when they are used as approximating functions in fairing the experimental measurements.

Figure 23 and Table 3 further illustrate the principle of the analysis. The figure shows results from a "static drift-angle" test carried out for the MARINER hull-form. The test was executed at 15 knots, and forces and moments were measured over the complete range of drift and rudder angles:

Drift Angles : β = -9.5, -7.5, -4.5, -2.0, -1.0, -0.5, 0.0
0.0, 0.5, 1.0, 2.0, 4.5, 7.0, 9.5 degrees.

Rudder Angles: δ = 0 to $\pm$40 degrees in steps of 10 degrees.

The experimental points are plotted in the figure as circles, whereas the solid curves show the expressions obtained from fairing the data.

Table 3 presents the corresponding output from the computer programme, used in the analysis. The experimental and faired values are indicated by "e" and "f", and the fairing polynomials are given at the bottom of the table.
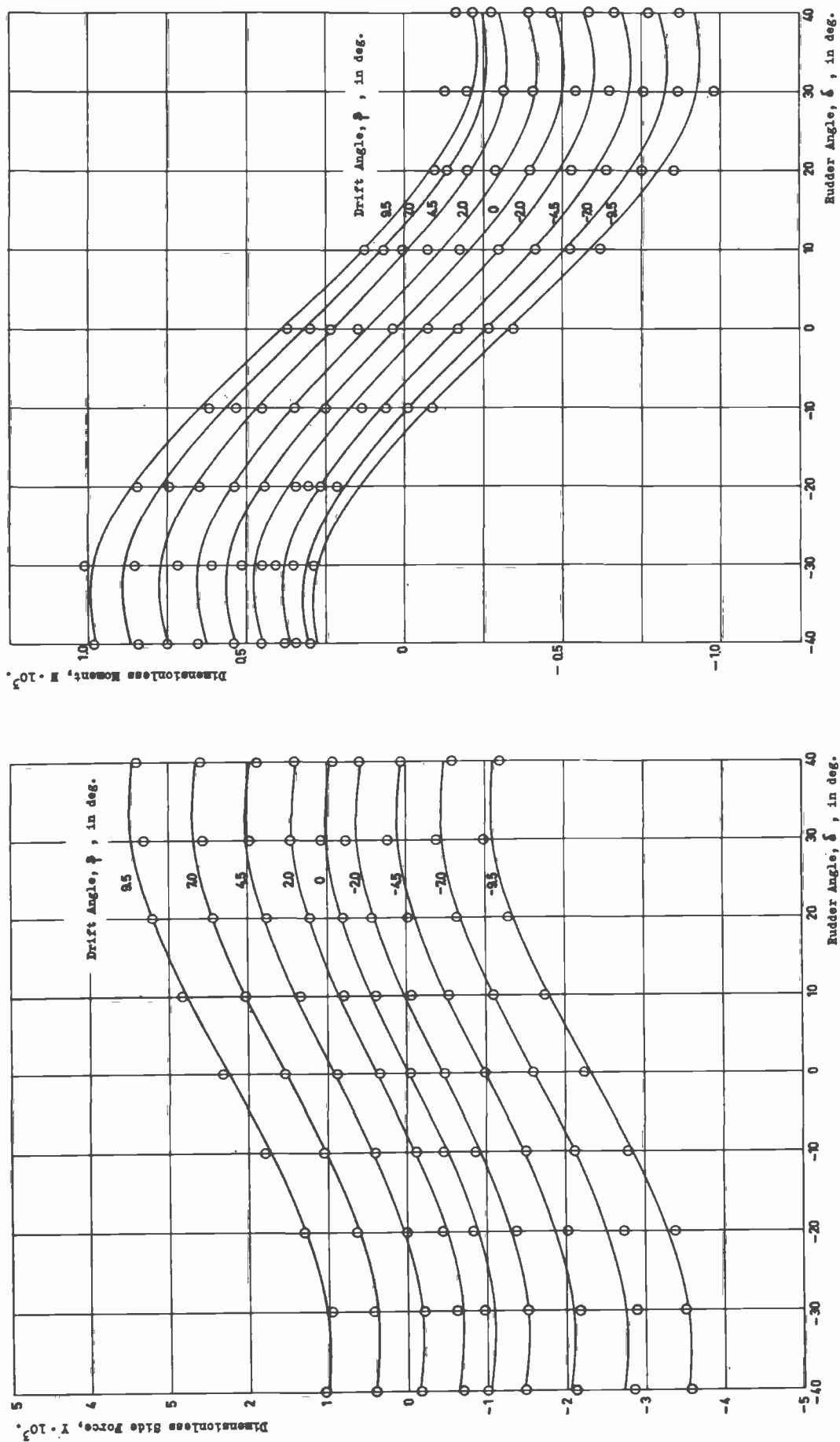
Figure 23

Example of Results from Static-Drift-Angle Test. Side Force
and Turning Moment as Functions of Drift Angle and Rudder Angle.

Non-dimensional Side Force, $YX_{B}3$

Drift Angle deg		Rudder Angle in deg.									rms
		-40.0	-30.0	-20.0	-10.0	0.0	10.0	20.0	30.0	40.0	
9.5	e	1.050	0.962	1.304	1.794	2.326	2.833	3.213	3.311	3.405	
	f	1.020	1.016	1.277	1.715	2.242	2.776	3.208	3.472	3.471	0.081
7.0	e	0.408	0.429	0.659	1.048	1.537	2.030	2.430	2.559	2.588	
	f	0.404	0.375	0.611	1.023	1.524	2.025	2.439	2.676	2.649	0.052
4.5	e	-0.151	-0.214	-0.003	0.396	0.878	1.340	1.759	1.970	1.876	
	f	-0.136	-0.183	0.036	0.430	0.913	1.396	1.792	2.011	1.965	0.049
2.0	e	-0.693	-0.618	-0.445	-0.117	0.343	0.791	1.216	1.457	1.402	
	f	-0.637	-0.693	-0.485	-0.101	0.372	0.845	1.250	1.438	1.382	0.044
1.0	e	-0.877	-0.847	-0.630	-0.251	0.131	0.540	0.981	1.214	1.176	
	f	-0.835	-0.893	-0.687	-0.304	0.167	0.638	1.021	1.227	1.169	0.053
0.5	e	-0.932	-0.922	-0.770	-0.391	0.040	0.470	0.873	1.156	1.046	
	f	-0.935	-0.994	-0.788	-0.405	0.065	0.536	0.918	1.124	1.065	0.042
0.0	e	-1.006	-0.972	-0.825	-0.457	-0.047	0.376	0.796	1.073	0.921	
	f	-1.036	-1.094	-0.889	-0.507	-0.036	0.434	0.816	1.022	0.965	0.062
-0.5	e	-1.098	-1.086	-0.947	-0.531	-0.132	0.307	0.749	1.067	0.902	
	f	-1.138	-1.196	-0.990	-0.608	-0.138	0.353	0.715	0.921	0.862	0.076
-1.0	e	-1.234	-1.196	-1.034	-0.651	-0.219	0.229	0.625	0.900	0.794	
	f	-1.241	-1.300	-1.093	-0.710	-0.239	0.232	0.614	0.821	0.762	0.057
-2.0	e	-1.484	-1.510	-1.369	-0.871	-0.476	-0.060	0.442	0.758	0.584	
	f	-1.455	-1.511	-1.302	-0.918	-0.445	0.088	0.413	0.621	0.564	0.067
-4.5	e	-2.123	-2.174	-2.016	-1.496	-0.988	-0.541	-0.024	0.236	0.057	
	f	-2.038	-2.083	-1.864	-1.469	-0.986	-0.503	-0.108	0.110	0.063	0.089
-7.0	e	-2.852	-2.885	-2.727	-2.123	-1.585	-1.096	-0.635	-0.386	-0.578	
	f	-2.722	-2.749	-2.511	-2.098	-1.597	-1.096	-0.683	-0.447	-0.476	0.111
-9.5	e	-3.572	-3.509	-3.480	-2.789	-2.235	-1.750	-1.284	-0.984	-1.182	
	f	-3.543	-3.544	-3.281	-2.842	-2.315	-1.788	-1.550	-1.088	-1.092	0.076
rms		0.054	0.085	0.092	0.050	0.040	0.057	0.042	0.101	0.058	0.065

Fairing Polynomial

$$YX_{B}5 = -3.63 - 1160x\gamma' - 807bx\gamma'^3 + 1190x\gamma'\delta^2 - 3.82x\delta^2 - 276.5x\delta^3 + 277.9x\delta$$

e = experimental points
f = faired points
rms = root mean square of differences

γ' = non-dim. sway velocity
δ = rudder angle in radians

Non-dimensional Moment, $NX_{B}3$

Drift Angle deg		Rudder Angle in deg.									rms
		-40.0	-30.0	-20.0	-10.0	0.0	10.0	20.0	30.0	40.0	
9.5	e	0.983	1.015	0.846	0.614	0.363	0.125	-0.099	-0.129	-0.164	
	f	0.976	0.984	0.860	0.647	0.390	0.151	-0.086	-0.216	-0.217	0.041
7.0	e	0.842	0.852	0.744	0.532	0.298	0.064	-0.137	-0.201	-0.217	
	f	0.867	0.884	0.770	0.567	0.320	0.072	-0.134	-0.253	-0.242	0.030
4.5	e	0.751	0.715	0.649	0.452	0.233	0.006	-0.200	-0.314	-0.274	
	f	0.747	0.771	0.663	0.467	0.227	-0.013	-0.211	-0.322	-0.302	0.025
2.0	e	0.654	0.609	0.539	0.348	0.146	-0.076	-0.289	-0.409	-0.395	
	f	0.625	0.652	0.547	0.355	0.120	-0.117	-0.309	-0.415	-0.390	0.026
1.0	e	0.605	0.586	0.497	0.311	0.103	-0.124	-0.335	-0.463	-0.414	
	f	0.578	0.605	0.501	0.309	0.074	-0.161	-0.353	-0.458	-0.432	0.022
0.5	e	0.581	0.553	0.485	0.273	0.073	-0.140	-0.363	-0.506	-0.444	
	f	0.555	0.582	0.478	0.286	0.051	-0.184	-0.375	-0.480	-0.453	0.025
0.0	e	0.541	0.515	0.443	0.249	0.037	-0.177	-0.398	-0.543	-0.465	
	f	0.532	0.559	0.455	0.263	0.028	-0.207	-0.398	-0.502	-0.475	0.025
-0.5	e	0.525	0.505	0.432	0.235	0.029	-0.199	-0.426	-0.579	-0.512	
	f	0.510	0.536	0.432	0.240	0.005	-0.230	-0.421	-0.525	-0.498	0.027
-1.0	e	0.483	0.489	0.396	0.198	-0.004	-0.231	-0.449	-0.593	-0.519	
	f	0.488	0.514	0.409	0.218	-0.018	-0.253	-0.444	-0.548	-0.521	0.022
-2.0	e	0.453	0.449	0.345	0.134	-0.074	-0.299	-0.528	-0.651	-0.586	
	f	0.447	0.472	0.366	0.173	-0.065	-0.299	-0.491	-0.595	-0.569	0.030
-4.5	e	0.379	0.407	0.306	0.059	-0.170	-0.415	-0.637	-0.757	-0.667	
	f	0.359	0.378	0.267	0.070	-0.171	-0.411	-0.606	-0.714	-0.691	0.028
-7.0	e	0.344	0.353	0.268	-0.011	-0.268	-0.524	-0.749	-0.864	-0.773	
	f	0.299	0.309	0.190	-0.015	-0.265	-0.510	-0.713	-0.828	-0.810	0.042
-9.5	e	0.303	0.288	0.215	-0.088	-0.345	-0.620	-0.859	-0.979	-0.871	
	f	0.274	0.273	0.142	-0.074	-0.333	-0.591	-0.803	-0.928	-0.920	0.044
rms		0.024	0.035	0.035	0.021	0.019	0.027	0.026	0.047	0.028	0.029

Fairing Polynomial

$$NX_{B}5 = +2.83 - 265.5x\gamma' + 1636x\gamma'^3 - 489.0x\gamma'\delta^2 + 12.54x\delta^2 + 136.7x\delta^3 - 138.8x\delta$$

e = experimental points
f = faired points
rms = root mean square of differences

γ' = non-dim. sway velocity
δ = rudder angle in radians

Table 3

Example of Analysis of Static-Drift-Angle Test. Fairing of Measured Side Force and Turning Moment.

Similar principles are applied in the analysis of results from tests made in the dynamic mode of operation. Figure 24 and Table 4 show, for example, the analysis of forces measured in the "pure-yaw" test.

The OUT-of-phase forces are in this case faired by the expressions:

$$X = (X_{rr}-mx_G) \; r^2$$

$$Y = (Y_r-mu) \; r + \frac{2}{3} \; Y_{rrr}r^3$$

$$N = (N_r-mx_Gu) \; r + \frac{2}{3} \; N_{rrr}r^3$$

and the IN-phase forces by expressions of the form:

$$Y = (Y_{\dot{r}}-mx_G) \; \dot{r}$$

$$N = (N_{\dot{r}}-I_z) \; \dot{r}$$

The hydrodynamic coefficients are determined after corrections for differences in mass and moment of inertia for model and ship.

Calculation of Coefficients in X-Equation

When the ship is sailing straight ahead with constant velocity, u_1, the propeller thrust, modified by the thrust-deduction effect, exactly equals the resistance of the ship:

$$X = T(1-t) - R_T = 0$$

This equilibrium condition defines the initial propeller thrust and the corresponding propeller torque and revolutions.

As soon as a manoeuvre is initiated, the equilibrium condition is disturbed, and the X-force, which represents the difference between the propeller thrust and the ship resistance, will then vary as a function of speed, u, and propeller revolutions. Approximating the X-force by a third-order polynomial:

$$X(u) = a_0 + a_1 \; \Delta u + a_2 \; \Delta u^2 + a_3 \; \Delta u^3$$

where $\Delta u = \dfrac{u-u_1}{U}$, the dimensionless hydrodynamic coefficients X_*, X_u, X_{uu} and X_{uuu} can be obtained directly as the coefficients of the approximating polynomial, as follows:

$$X_* = a_0 \sim 0; \quad X_u = a_1; \quad X_{uu} = a_2; \quad X_{uuu} = a_3;$$
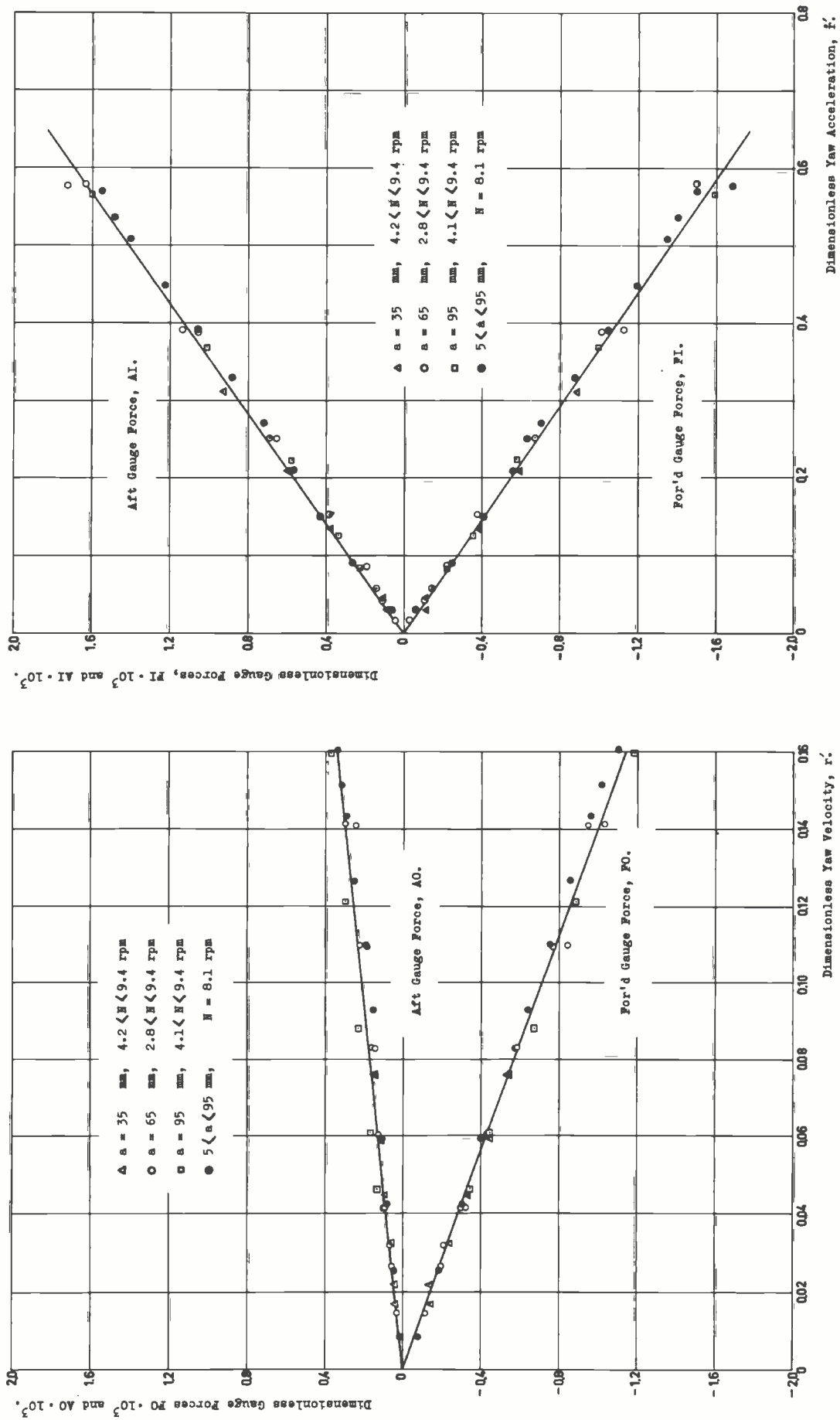
Figure 24

Example of Results from Pure-Yaw Test. Transverse IN-phase and
OUT-of-phase Forces as Function of Yaw Velocity and Acceleration.

Table 4

Example of Analysis of Pure-Yaw Test.
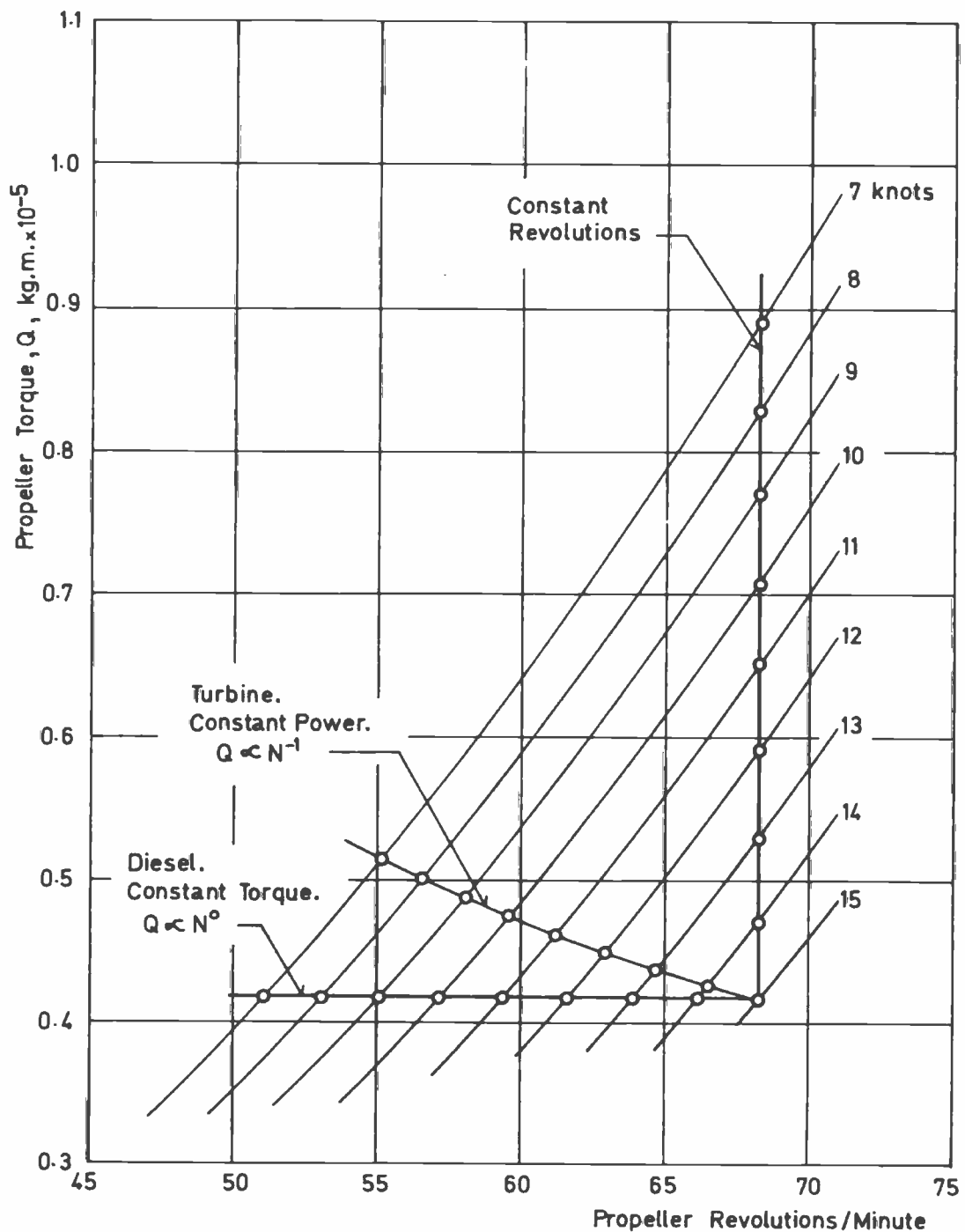
Figure 25

Relationship between Propeller Revolutions and Propeller Torque
as Function of Speed Reduction Encountered while Manoeuvring.

It has been found that the X-force and corresponding coeffi-
cients are computed most accurately on the basis of the results from
the open-water, resistance and self-propulsion tests. Table 5 shows
examples of such calculations. The thrust deduction coefficient,
t = 0.136, and wake coefficient, w = 0.160, used in the computation,

**CALCULATION OF NON-DIM. COEFFS. Xu, Xuu and Xuuu
on the basis of Ship EHP and Propeller Open-Water Curves.**

Order No.6295
Prop. Thrust Calculated for CONST. PROP. REVS.
Equilibrium Speed (Approach Speed) 15.00 knots

J	KT input	KT fair	g·KQ input	g·KQ fair
0.0000		0.4734		0.7181
0.1000		0.4354		0.6576
0.2000		0.3927		0.5983
0.3000		0.3515		0.5397
0.4000		0.3098		0.4819
0.4400	0.2930	0.2931	0.4590	0.4589
0.4900	0.2720	0.2720	0.4300	0.4303
0.5400	0.2510	0.2509	0.4020	0.4017
0.5900	0.2300	0.2297	0.3730	0.3732
0.6400	0.2060	0.2085	0.3450	0.3447
0.6900	0.1870	0.1872	0.3160	0.3163
0.7400	0.1660	0.1659	0.2890	0.2878
0.7900	0.1450	0.1446	0.2590	0.2593
0.8400	0.1250	0.1253	0.2310	0.2307
0.8900	0.1020	0.1020	0.2020	0.2021

Speed kn	EHP hp	Resist. xp5 kg	KT fair	Thrust xp5 kg	g·KQ input	Torque xp5 kg.m	g·KQ fair	J	PHP hp	Prop. Revs. rpm
7.00	286.0	0.0596	0.4734	0.8550	0.4590	0.8913	0.7181	0.396	8504.7	68.3
8.00	414.0	0.0755	0.4354	0.7899	0.4300	0.8314	0.6576	0.453	7933.8	68.3
9.00	582.0	0.0943	0.3927	0.7244	0.4020	0.7718	0.5983	0.509	7365.2	68.3
10.0	789.0	0.1150	0.3515	0.6587	0.3730	0.7124	0.5397	0.566	6790.1	68.3
11.0	1060	0.1405	0.3098	0.5928	0.3450	0.6531	0.4819	0.622	6252.1	68.3
12.0	1391	0.1690	0.2931	0.5268	0.3160	0.5938	0.4589	0.679	5666.6	68.3
13.0	1815	0.2036	0.2720	0.4607	0.2890	0.5346	0.4303	0.735	5104.9	68.3
14.0	2318	0.2414	0.2509	0.3945	0.2590	0.4752	0.4017	0.792	4534.4	68.3
15.0	2919	0.2857	0.2297	0.3284	0.2310	0.4157	0.3732	0.849	3966.7	68.3
15.0	2919	0.2857		0.3284		0.4157		0.849	3966.7	68.3

Speed kn	u 0-dim	X-force xp5 kg	Xnp5 0-dim	Xnp5 fair 0-dim
7.00	-1.14	0.679	386.7	386.7
8.00	-0.875	0.607	264.6	264.5
9.00	-0.667	0.532	183.1	181.2
10.0	-0.500	0.454	126.7	126.6
11.0	-0.364	0.372	85.7	85.7
12.0	-0.250	0.286	55.4	55.3
13.0	-0.154	0.194	32.1	32.2
14.0	-0.0714	0.095	14.2	14.2
15.0	0.00000	-0.0002	0.0	0.0

non-dim Xunp5 = -190.4
non-dim Xuunp5 = 122.8
non-dim Xuuunp5 = -5.8

**CALCULATION OF NON-DIM. COEFFS. Xu, Xuu and Xuuu
on the basis of Ship EHP and Propeller Open-Water Curves.**

Order No.6295
Prop. Thrust Calculated for CONSTANT POWER 15.00 knots
Equilibrium Speed (Approach Speed) 15.00 knots

J	KT input	KT fair	g·KQ input	g·KQ fair
0.0000		0.4734		0.7181
0.1000		0.4354		0.6576
0.2000		0.3927		0.5983
0.3000		0.3515		0.5397
0.4000		0.3098		0.4819
0.4400	0.2930	0.2931	0.4590	0.4589
0.4900	0.2720	0.2720	0.4300	0.4303
0.5400	0.2510	0.2509	0.4020	0.4017
0.5900	0.2300	0.2297	0.3730	0.3732
0.6400	0.2060	0.2085	0.3450	0.3447
0.6900	0.1870	0.1872	0.3160	0.3163
0.7400	0.1660	0.1659	0.2890	0.2878
0.7900	0.1450	0.1446	0.2590	0.2593
0.8400	0.1250	0.1253	0.2310	0.2307
0.8900	0.1020	0.1020	0.2020	0.2021

Speed kn	EHP hp	Resist. xp5 kg	KT fair	Thrust xp5 kg	g·KQ input	Torque xp5 kg.m	J	PHP hp	Prop. Revs. rpm
7.00	286.0	0.0596	0.4734	0.4855	0.4590	0.5152	0.491	3966.8	55.1
8.00	414.0	0.0755	0.4354	0.4667	0.4300	0.5021	0.547	3966.8	56.6
9.00	582.0	0.0943	0.3927	0.4476	0.4020	0.4892	0.599	3966.7	58.1
10.0	789.0	0.1150	0.3515	0.4282	0.3730	0.4764	0.648	3966.8	59.6
11.0	1060	0.1405	0.3098	0.4085	0.3450	0.4639	0.694	3966.7	61.2
12.0	1391	0.1690	0.2931	0.3887	0.3160	0.4515	0.737	3966.8	62.9
13.0	1815	0.2036	0.2720	0.3687	0.2890	0.4393	0.777	3966.8	64.7
14.0	2318	0.2414	0.2509	0.3486	0.2590	0.4274	0.814	3966.8	66.5
15.0	2919	0.2857	0.2297	0.3284	0.2310	0.4157	0.849	3966.7	68.3
15.0	2919	0.2857		0.3284		0.4157	0.849	3966.7	68.3

Speed kn	u 0-dim	X-force xp5 kg	Xnp5 0-dim	Xnp5 fair 0-dim
7.00	-1.14	0.360	204.9	204.9
8.00	-0.875	0.328	142.9	142.8
9.00	-0.667	0.292	100.7	100.9
10.0	-0.500	0.255	71.1	71.0
11.0	-0.364	0.212	49.0	49.0
12.0	-0.250	0.167	32.3	32.2
13.0	-0.154	0.115	19.0	19.1
14.0	-0.0714	0.0598	8.5	8.5
15.0	0.00000	-0.0002	0.0	0.0

non-dim Xunp5 = -116.6
non-dim Xuunp5 = 48.3
non-dim Xuuunp5 = -5.8

Table 5

Derivation of Non-Dimensional Coefficients
X_u, X_{uu} and X_{uuu}, Calculation Examples
for Constant Power and Constant Propeller
Revolutions per Minute.

but not indicated in the table, are taken from the self-propulsion test. These values are assumed to be constant for all speeds. The corresponding propeller thrust values are computed from the open-water propeller curves assuming constant wake, and taking the type of engine and engine setting to be maintained during the manoeuvre into account. As shown in the example, the propeller thrust can be calculated assuming constant propeller revolutions, or assuming the propeller torque to vary proportionally to the revolutions to a certain power. If torque is assumed to vary inversely proportionally to propeller revolutions, the thrust corresponding to a turbine power-plant capable of maintaining constant power output would be obtained. If torque is assumed to be constant during the manoeuvre, the corresponding condition for a diesel engine would be obtained. Figure 25 illustrates the relationship between propeller revolutions, torque and speed for these various conditions.

The variation of propeller revolutions with speed as derived from this computation can conveniently be used to obtain the correct propeller revolutions, which have to be used when tests are executed at reduced speeds to obtain the Δu- and revolution-dependent coefficients, ("rudder-angle-and-speed" tests).

The three coefficients, X_u, X_{uu} and X_{uuu}, can also be obtained experimentally by fairing X-force measurements made for zero rudder angle in a "rudder-angle-and-speed" test. Such experimentally derived values have agreed well with the calculated coefficients.

Measurement of Model Polar Moment of Inertia

The term $(N_{\dot{r}}-I_z)$ measured in the "pure-yaw" test contains the effect of model moment of inertia, I_z. For prediction of ship-scale manoeuvres, it is necessary, as mentioned above, to correct for the difference between model and ship inertias.

The inertia of the model, including instrumentation and equipment, is found by oscillating the model in air on a torsional pendulum. The torsion rod is of 6 mm. piano-wire, 2 m. long, clamped at the top to a stiff beam and at the bottom to a fitting which can be rigidly fastened to the yoke normally used for lifting models. Four wooden struts are used to prevent movement of the model relative to the yoke (see Figure 26).
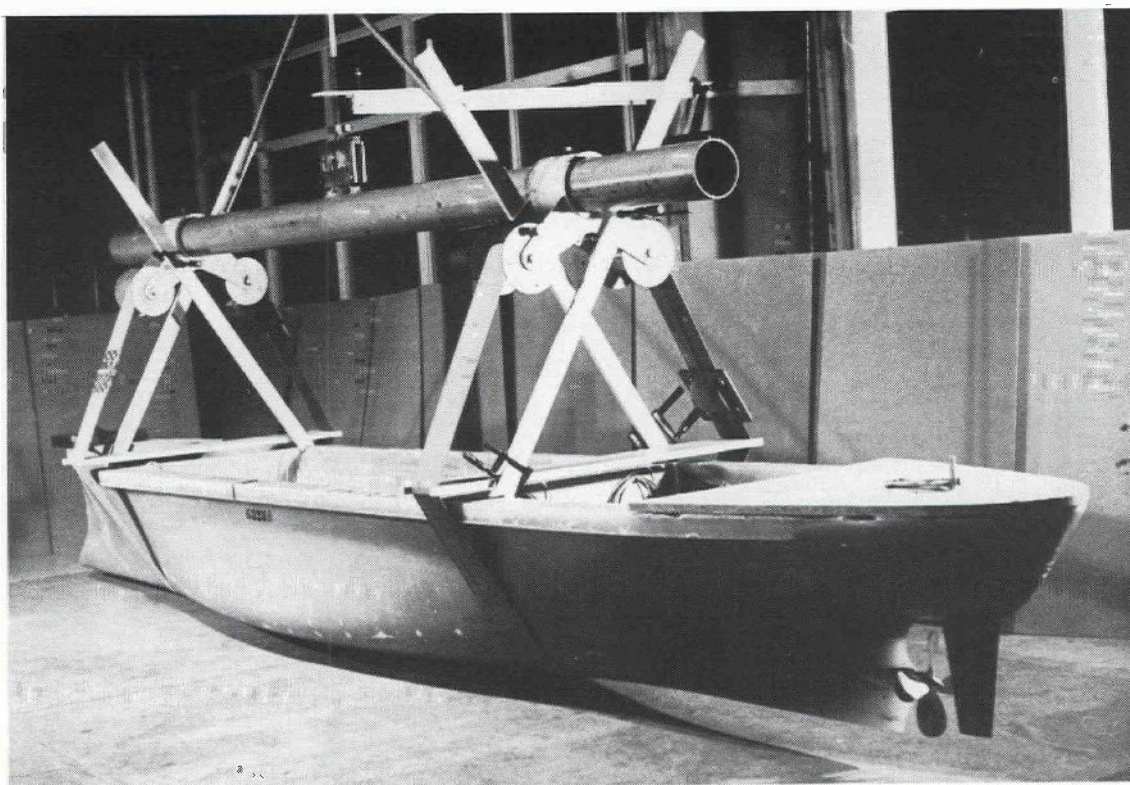
Figure 26

Model Suspended on Torsional Pendulum for
Measurement of Polar Moment of Inertia.

The torsion rod is enclosed, as a safety precaution, by a
brass tube which will restrain the rod if it should break. A steady-
ing support is used to prevent the model from swinging.

The inertia of the model is found by first measuring the
period of oscillation of the model and yoke, and then the period of
the yoke without the model. The period of oscillation can be measured
with sufficient accuracy using a stop-watch, as the time for one com-
plete oscillation is of the order of 2 minutes. The very slow move-
ment of the model precludes the possibility of significant aerodynamic
damping.

The inertia of the full-scale ship is normally computed on
the basis of longitudinal weight distribution and main dimensions.

The ability to account for differences in inertia between
model and ship is convenient as it permits the model to be constructed
without paying any regard to its inertia. Model testing can be exe-
cuted for any value of model inertia, and the appropriate ship value
introduced in the analysis of the force measurements.

Scale Effects

Most of the hydrodynamic coefficients are obtained from model tests, hence it is reasonable to give some consideration to correlation between model and full-scale results before applying the coefficients to the prediction of full-scale manoeuvres.

The model tests are conducted according to Froude's law, consequently Reynolds' number is not satisfied, and the possibility of scale effects due to differences in Reynolds' number must be considered.

Results from airfoil testing are relevant in a discussion of scale effects. Such tests, covering a wide range of Reynolds' numbers, indicate that change of Reynolds' number has no systematic effect on the lift-curve slope, whereas the variation of maximum lift might be appreciable because separation or flow-breakdown occurs earlier for the relatively thicker boundary layer around a model body. As most of the hydrodynamic coefficients are due to related circulation and viscous drag effects, scale effects should not be expected for any of the first-order coefficients, e.g. Y_v, Y_r, Y_δ, N_v, N_r, N_δ etc. In the case of the non-linear coefficients, however, scale effects could be more serious, as these coefficients are more likely to be influenced by separation or flow-breakdown. Normally, non-linear coefficients of the motion parameters v and r, for instance: Y_{vvv}, Y_{rrr} etc., are determined for relatively small values of v and r corresponding to angles of attack below that at which separation takes place. For this reason, scale effects are probably also negligible for these coefficients. This is not true for the rudder, as rudder deflection for which rudder characteristics are measured will generally cover the range of rudder-lift breakdown. For the coefficients $Y_{\delta\delta\delta}$ and $N_{\delta\delta\delta}$, in particular, it has sometimes been found desirable to make corrections for this scale effect.

Résumé of Experimental Programme

A summary of a typical experimental programme is given in Table 6. This programme is used as a standard when testing cargo ships for which complete predictions of extreme manoeuvres are required.

The table refers to the series of Planar-Motion Mechanism experiments which are necessary for the prediction of manoeuvres made

Table 2 – Standard Programme for Manoeuvring Tests carried out by means of the Planar Motion Mechanism

Type and Description of Test	Range of Variables	Number of runs	Derivatives obtained from Test — one variable	Derivatives obtained from Test — cross-coupling	Remarks
1. STATIC RUDDER AND DRIFT ANGLE TEST. In each run the model is travelling with a constant angle between path of origin and centerline, i.e. constant drift angle and rudder angle, δ, is varied.	$\delta = 0$ to ± 40 deg in steps of 10. $\beta = 0, \pm 1, \pm 2, \pm 4.5, \pm 7, \pm 9, \pm 12$, ± 14 and for unstable ships ± 17 and ± 20 deg. $r = 0$, $U = U_0 = $ m/sec.		X_{vv}, $X_{\delta\delta}$, Y_v, Y_{vvv}, Y_δ, $Y_{\delta\delta\delta}$, Y_δ, N_v, N_{vvv}, N_δ, $N_{\delta\delta\delta}$, N_δ	$X_{v\delta}$, $Y_{v\delta}$, $Y_{\delta vv}$, $N_{v\delta}$, $N_{\delta vv}$	In case of a partial test, is should consist of one of the following combinations: $\beta = 0$, all δ; $\delta = 0$, all β; ...
2. PURE SWAY TEST. The bow and stern are oscillated in phase and a pure sway motion is produced. The side velocity and acceleration are varied by changing the amplitude of oscillation in between each run. Frequency of oscillation is kept const. Phase angle is zero.	$\delta = 0$ $v_{max} = a \, 2\pi n$; $r = 0$ $\dot v_{max} = a(2\pi n)^2$ where $a = 35, 50, 65, 80$ and 95 mm. $n = N/60$ $N = $ rpm. $\psi_B = 0$ deg		$(m-Y_{\dot v})$, $(xm_G - N_{\dot v})$		
3. YAW AND DRIFT ANGLE TEST. During the runs the bow and stern of the model are oscillated out of phase in such a way that the center line stays tangent or at a constant angle with the tangent to the path travelled by origin.	Pure yaw / Yaw & drift $1/\cos\beta$		$(x_{rr} + m x_G)$, $(Y_r - mU)$, Y_{rrr}, $(xm_G - N)$, $(N - xx_G U)$, $N_{rrr}/(I - Y)$	Y_{rvv}, Y_{vrr}, N_{rvv}, N_{vrr}	$(X_{rv} + m) = m$; $(X_{rr} + m X_G) = m X_G$; X_{rr} is negligible since it has not been detected at max. obtainable Yaw velocity
4. STATIC SPEED AND RUDDER ANGLE TEST. For different speeds. Rudder angle, δ, is varied. Propeller revs. are normally kept constant.	$\delta = 0$ to ± 40 deg in steps of 10. $\beta = 0$ deg $r = 0$ $U = $ and m/s		X_u, X_{uu}, X_{uuu}	$X_{\delta\delta u}$, $Y_{\delta u}$, $Y_{\delta\delta\delta u}$, $N_{\delta u}$, $N_{\delta\delta\delta u}$	X_u, X_{uu} and X_{uuu} may also be calculated from resistance, self. propulsion and open water tests.
5. YAW AND RUDDER ANGLE TEST. During the runs the bow and stern are oscillated out of phase in such a way that the center line stays tangent to the path travelled by origin. This is done for different rudder angle.	$\delta = $ $\beta = $ $N = $ $U_o = U_o$			$X_{r\delta}$, $Y_{r\delta}$, $Y_{\delta rr}$, $N_{r\delta}$, $N_{\delta rr}$	This test is only made occasionally

δ = rudder angle in deg.
β = drift angle in deg.
r = yaw velocity radians/sec
U = model speed in m/sec
ψ_o = phase angle between bow and stern supports
$2d$ = distance between supports (≈ 2.100 m)
a = half PMM – amplitude
N = PMM-revolutions rpm. $n = N/60$

$r = -\sin\beta$
$v_{max} = a\,2\pi n$
$\dot v_{max} = a(2\pi n)^2$
$n = \tan\frac{\psi_o}{2}$
$r_{max} = 2v_{ma}\sin\frac{\psi_o}{2}\frac{1}{d\cos\beta}$
$\dot r_{max} = (2\pi n)^2 a \sin\frac{\psi_o}{2}\frac{1}{d\cos\beta}$

Table 6

Standard Test Programme.

for one given initial, or approach-speed. If other approach-speeds
are wanted, additional tests are necessary.

Short descriptions of each test are given in the table, to-
gether with suggested settings of the Planar-Motion Mechanism and the
hydrodynamic coefficients obtained from each of the tests are also
indicated.

Typical values for the different coefficients and examples
of predicted full-scale turning circles, zig-zag and spiral manoeuvres
are to be found in [4] and [5] .

INFLUENCE OF SPEED ON DIMENSIONLESS FORCE AND MOMENT COEFFICIENTS

The mathematical model (Equations 5) is composed of coeffi-
cients expressing relationships between orientations, velocities and
accelerations, and the resulting inertial and hydrodynamic forces and
moments, which act on a given hull-rudder-propeller combination.
These coefficients are non-dimensionalised, according to the consistent
system described in [2], by dividing mass by $\frac{1}{2}\rho L_{pp}^{3}$, length by L_{pp}
and time by $\frac{L_{pp}}{U}$, where U is the instantaneous velocity of the origin
of the body-axes relative to the fluid. The resulting non-dimensio-
nalising factors used are thus:

Table 7

Non-Dimensionalising Factors		
Quantity	Dimensions	Non-dim. Factor
Mass	kg.sec.^{2}/m.	$\frac{1}{2}\rho L_{pp}^{3}$
Inertia	kg.sec.^{2} m.	$\frac{1}{2}\rho L_{pp}^{5}$
X and Y forces	kg.	$\frac{1}{2}\rho L_{pp}^{2} U^{2}$
N moment	kg.m.	$\frac{1}{2}\rho L_{pp}^{3} U^{2}$
u and v	m./sec.	U
r	radians/sec.	U/L_{pp}
δ	radians	-
$\dot{u}$ and $\dot{v}$	m./sec.^{2}	U^{2}/L_{pp}
$\dot{r}$	radians/sec.^{2}	U^{2}/L_{pp}^{2}

Forces and moments resulting from surge, sway and yaw acceler-
ations, $\dot{u}$, $\dot{v}$ and $\dot{r}$, have been found, in general, to be independent
of the velocity of the origin, U. Non-dimensional coefficients ex-
pressing such data are then also independent of speed, since U^2 occurs
in the non-dimensionalising factors for both force (or moment) and
acceleration. This is supported by numerous experimental results.
For example, Figure 22 of Reference [11] shows complete agreement
between side forces and turning moments measured as functions of yaw
acceleration at ship speeds of 4, 6, 8 and 10 knots, for a 53 m. L_{pp}
trawler form.

Forces and moments resulting from drift angle, rudder angle
and yaw velocity are largely due to circulation and viscous cross-
flow drag. Drift-angle and rudder-angle forces may be likened to lift
forces acting on an airfoil having an angle of attack, and yaw-velo-
city is analogous to camber. It is thus reasonable to expect the re-
sulting hydrodynamic forces to vary proportionally with the square
of the flow-velocity as long as the flows have the same geometry, i.e.
as long as sinkage, trim, wave-making, flow-separation etc. do not
vary appreciably with speed.

Forces and moments due to drift angle and to yaw velocity
are principally dependent on the flow patterns around the hull, and
the speed of the origin is therefore a good representative velocity.
Non-dimensionalisation with this velocity results in dimensionless
values which only change with flow-geometry variations.

Figure 27 shows measurements of side force and turning moment
due to drift angle, made in "static-drift-angle" tests at speeds of
5, 10, 15, 20 and 25 knots ship speed, with the 20 ft. MARINER model
described in [5]. The same measured values are plotted in dimensional
and non-dimensional form and the faired lines are polynomials of the
form:

$$Y(v) = Y_* + Y_v v + Y_{vvv} v^3$$
$$N(v) = N_* + N_v v + N_{vvv} v^3$$

which have been fitted to the points by a least-square procedure. The
numerical values and coefficients of the polynomials are given in Appen-
dix A. The coefficients are plotted against speed in Figure 28.

It is seen that the non-dimensional values are almost in-
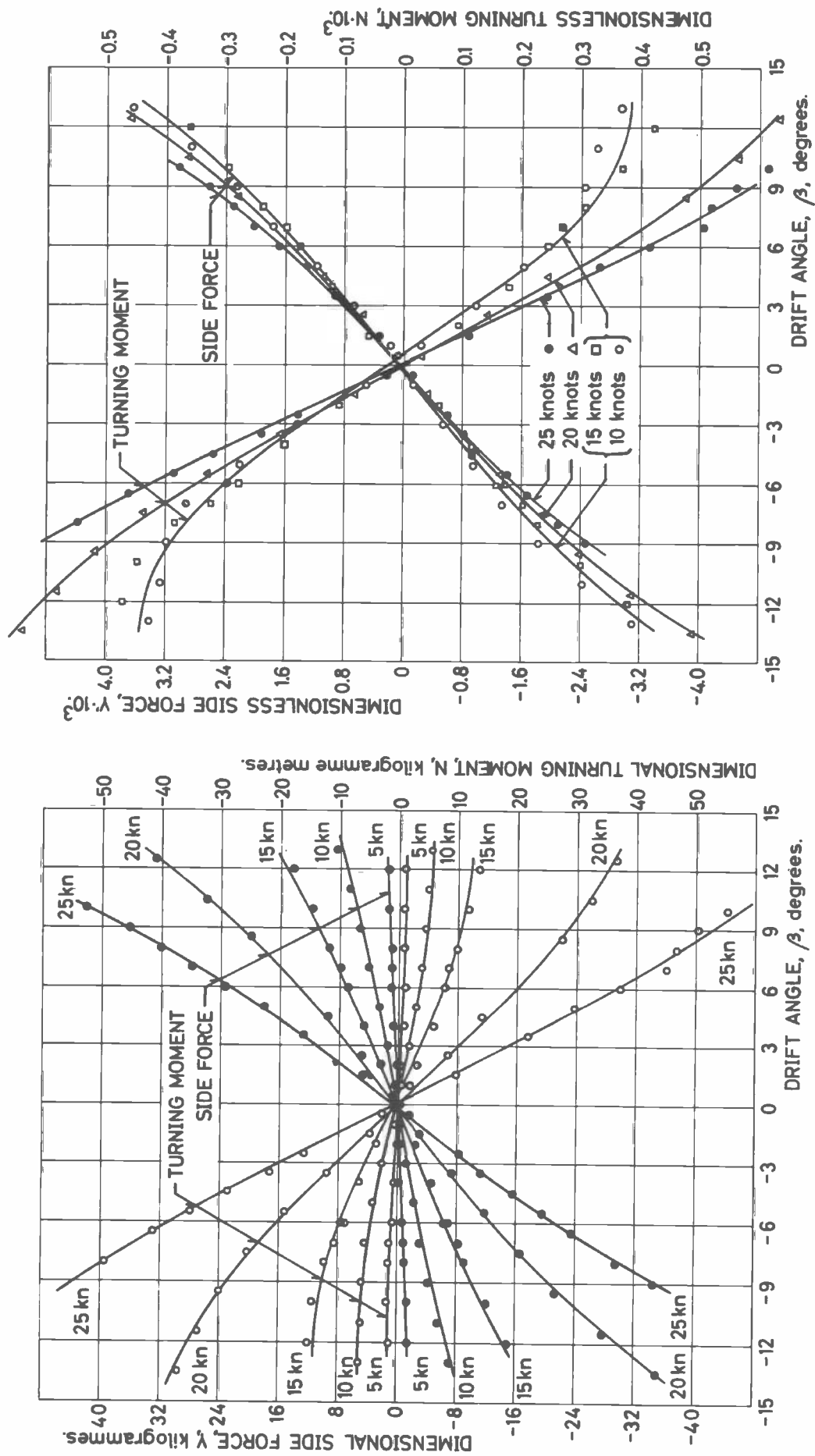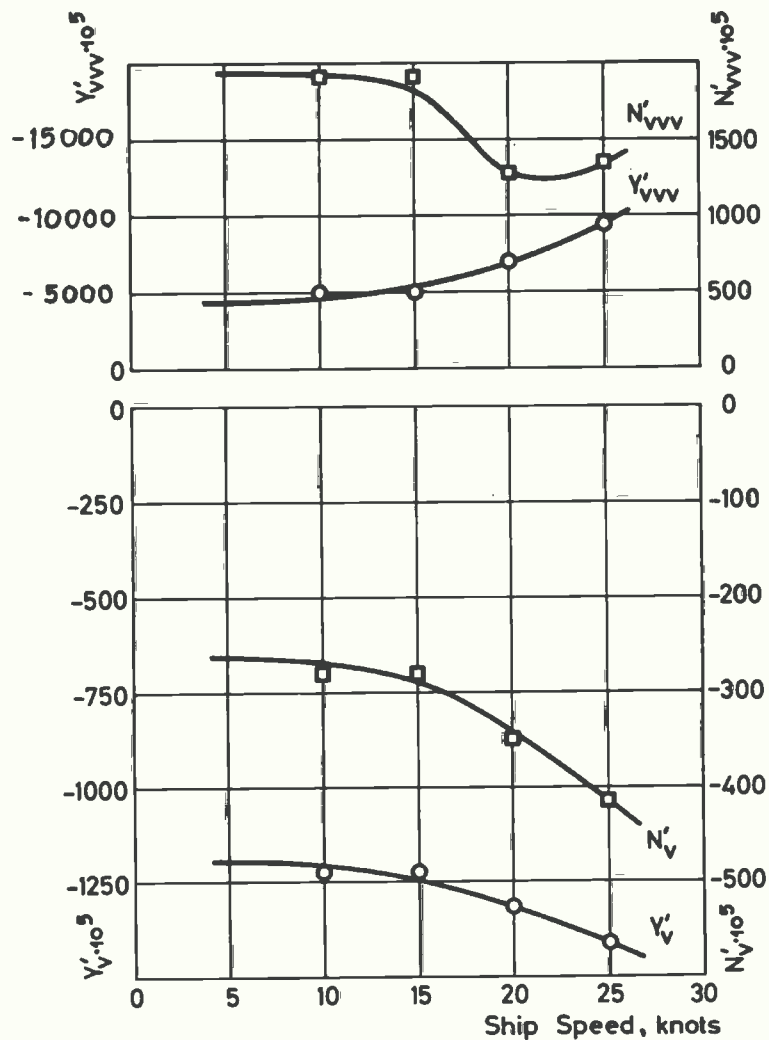dependent of speed up to 20 knots. Above about 20 knots, the non-

Figure 27

Results of Static-Drift-Angle Tests made at Different
Speeds - Dimensional and Dimensionless Plots.

Figure 28

Variation of
Dimensionless
Drift-Angle
Coefficients
with Speed

dimensional forces acting on the hull increase in size. This was due
to sinkage of the model both forward and aft. Two effects were appa-
rent. The model sank more as the speed increased, increasing the la-
teral area and hence the linear coefficients and, for a given speed,
sinkage increased with drift angle, causing the cubic terms to become
more pronounced. Sinkage, both with speed and drift angle, was greatest
at the bow, probably because the cross-flow under the forebody in-
creased the local velocity and reduced the hydrostatic pressure more
than was the case in the afterbody, where the flow had become straight-
ened somewhat.

On the basis of similar results obtained for angular velocities,
it can be concluded that Y'_v, Y'_r, N'_v and N'_r are largely independent of
speed over the speed ranges commonly covered by merchant ships. It
has consequently not been found necessary to include tests in the Stan-
dard Programme (Table 6) for measurement of the coefficients Y'_{vu}, Y'_{vuu},

Y'_{ru}, Y'_{ruu}, N'_{vu}, N'_{vuu}, N'_{ru} and N'_{ruu}.

Forces and moments due to rudder angle are dependent on the flow-velocity around the rudder. This is influenced by ship speed, and, for a rudder situated in a propeller slip-stream, by propeller revolutions. The speed of the origin is then, not a representative velocity, since the flow-velocity can vary markedly with propeller revolutions for constant ship speed.

Figures 29 to 31 inclusive show measurements of side force, turning moment and longitudinal force due to rudder angle, made in "static-rudder-angle" tests at 7 to 15 knots in steps of one knot, with the MARINER model described in [5]. The tests were made with constant propeller revolutions corresponding to the ship self-propulsion point at 15 knots. The numerical values and coefficients of the polynomials are given in Appendix B.

In contrast to the results of the "static-drift-angle" tests described above, the non-dimensional forces and moments vary markedly with speed, becoming infinite at zero ship speed. The coefficients of the fairing polynomials are plotted against non-dimensional speed, $\Delta u' = \dfrac{u-u_1}{U}$, in Figure 32.

The cross-coupling terms $Y_{\delta u}$, $Y_{\delta\delta\delta u}$, $N_{\delta u}$, $N_{\delta\delta\delta u}$ and $X_{\delta\delta u}$ obtained from these data are of importance in the prediction of radical manoeuvres when speed loss is appreciable. Since the propeller slip-stream has a strong influence on the forces generated by a rudder situated within it, it can be seen that these cross-coupling terms will vary with engine characteristics and control settings. Values corresponding to a particular type of engine or control arrangement can conveniently be obtained however, by carrying out model tests at pre-determined revolution and speed values which have been obtained from calculations of the type described in the foregoing chapter.

The experimental results presented in the foregoing Figures 27 to 32 were measured with the model free to sink and trim but restrained in roll.

A distinction should be drawn between "speed-reduction" tests of the type described above, and tests at different speeds in which the propeller revolutions correspond to the propulsion point for the speed in question. The non-dimensional results of such tests vary very little with speed, which may be explained in a rough way by considering the flow-geometry at different speeds to be similar in such tests, as the revolutions increase uniformly with ship speed.

Figure 29

Results of Static-Rudder-Angle Tests made at Different Speeds –
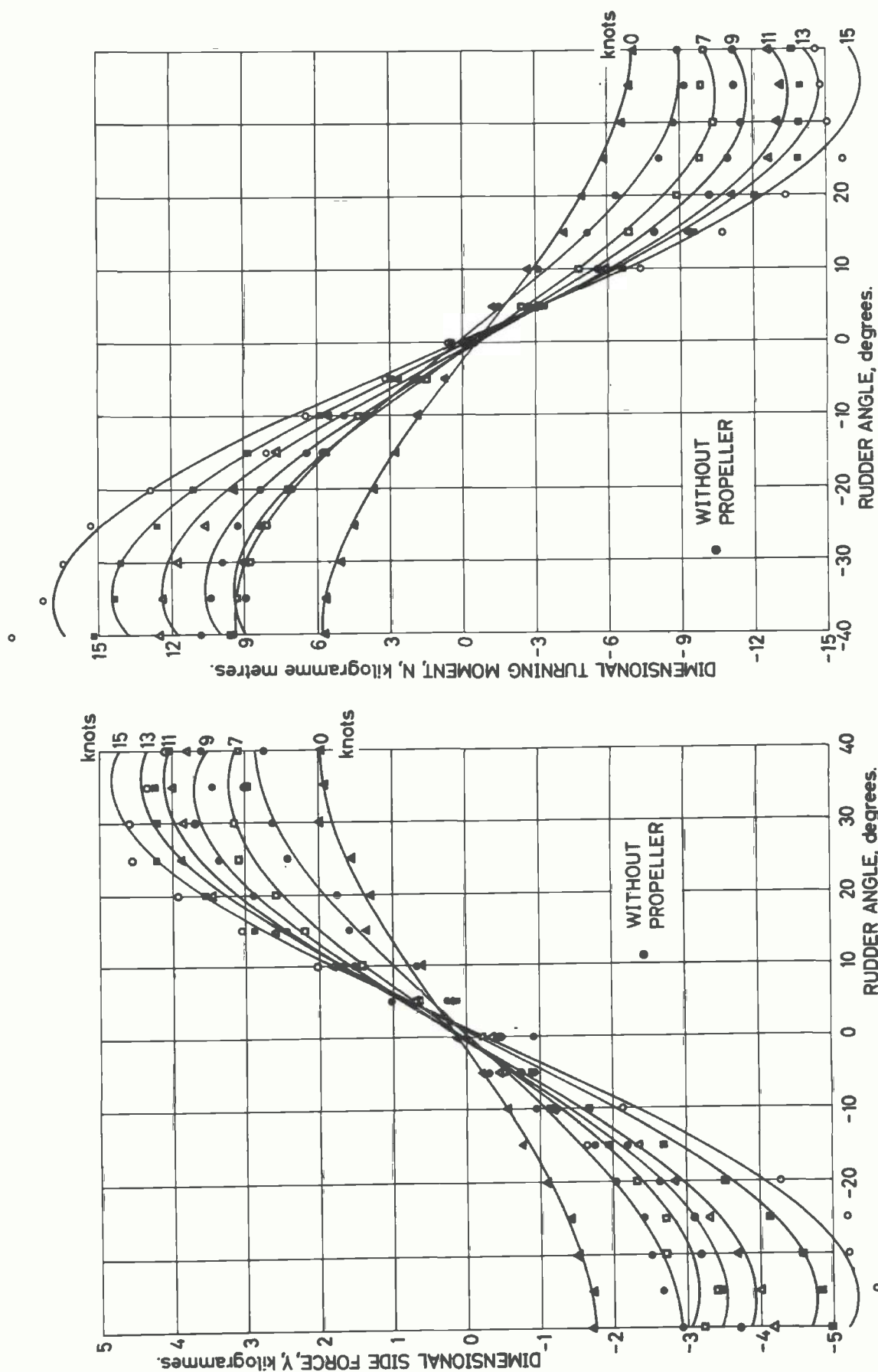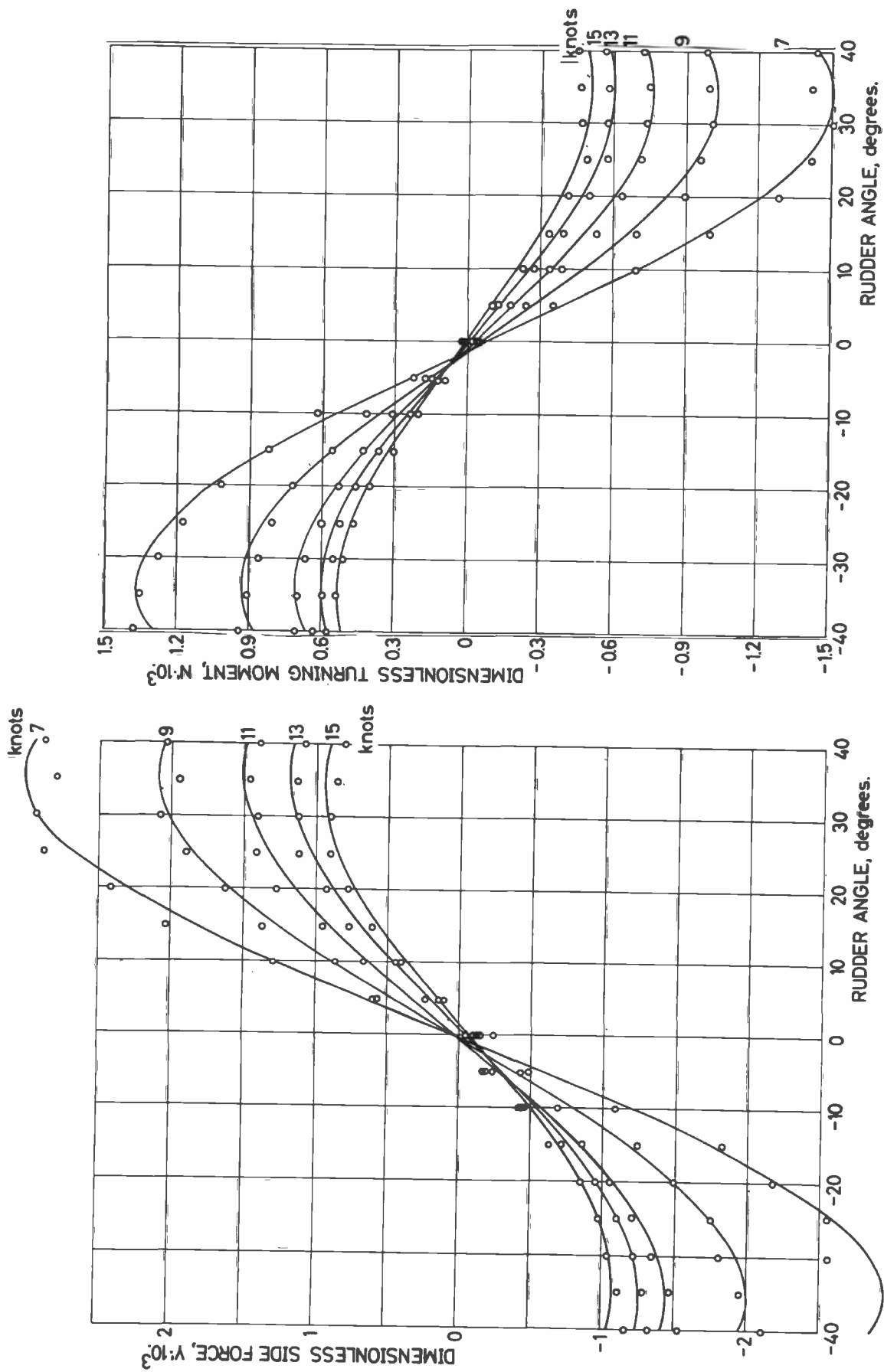Dimensional Plots of Side Force, Y, and Turning Moment, N.

Figure 30

Results of Static-Rudder-Angle Tests made at Different Speeds -
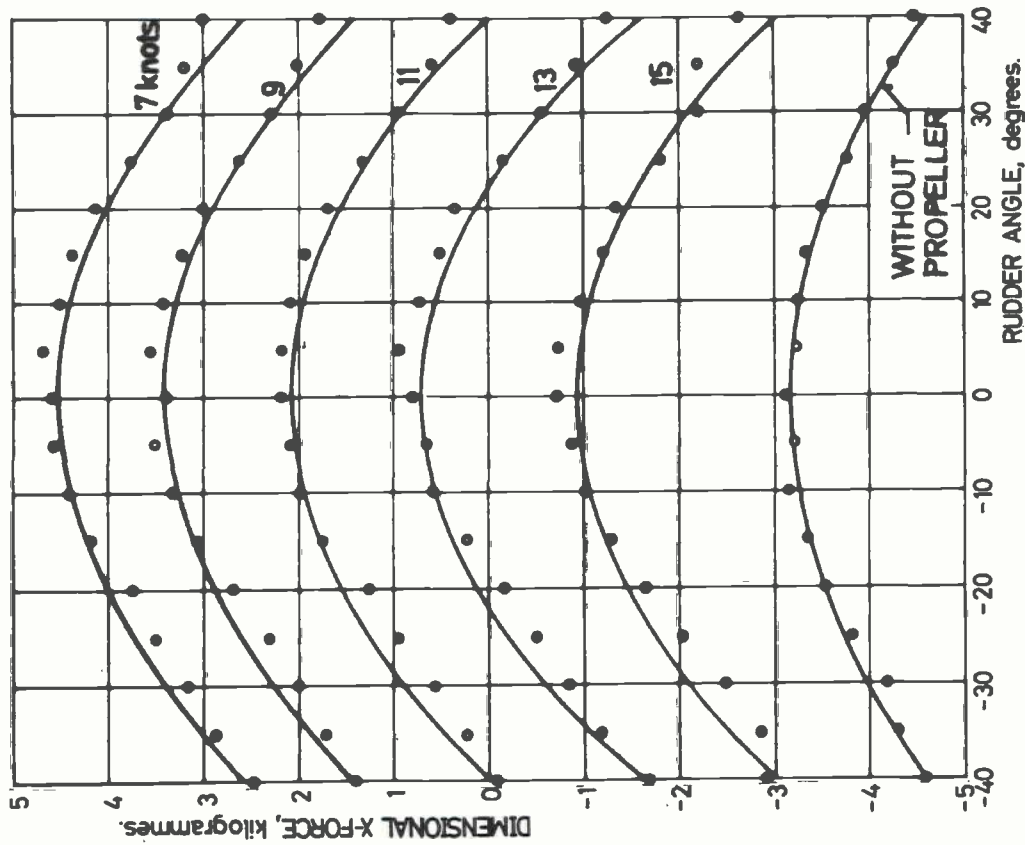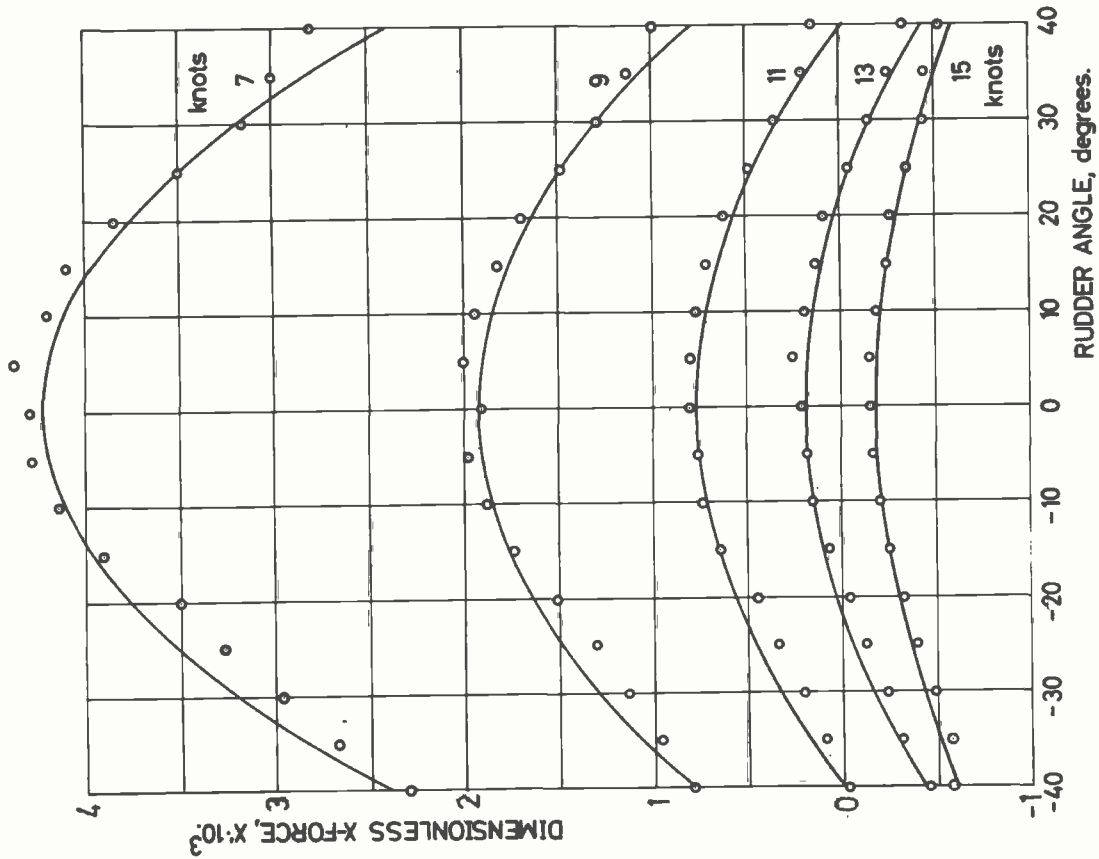Dimensionless Plots of Side Force, Y', and Turning Moment, N'.

Figure 31

Results of Static-Rudder-Angle Tests made at Different Speeds –
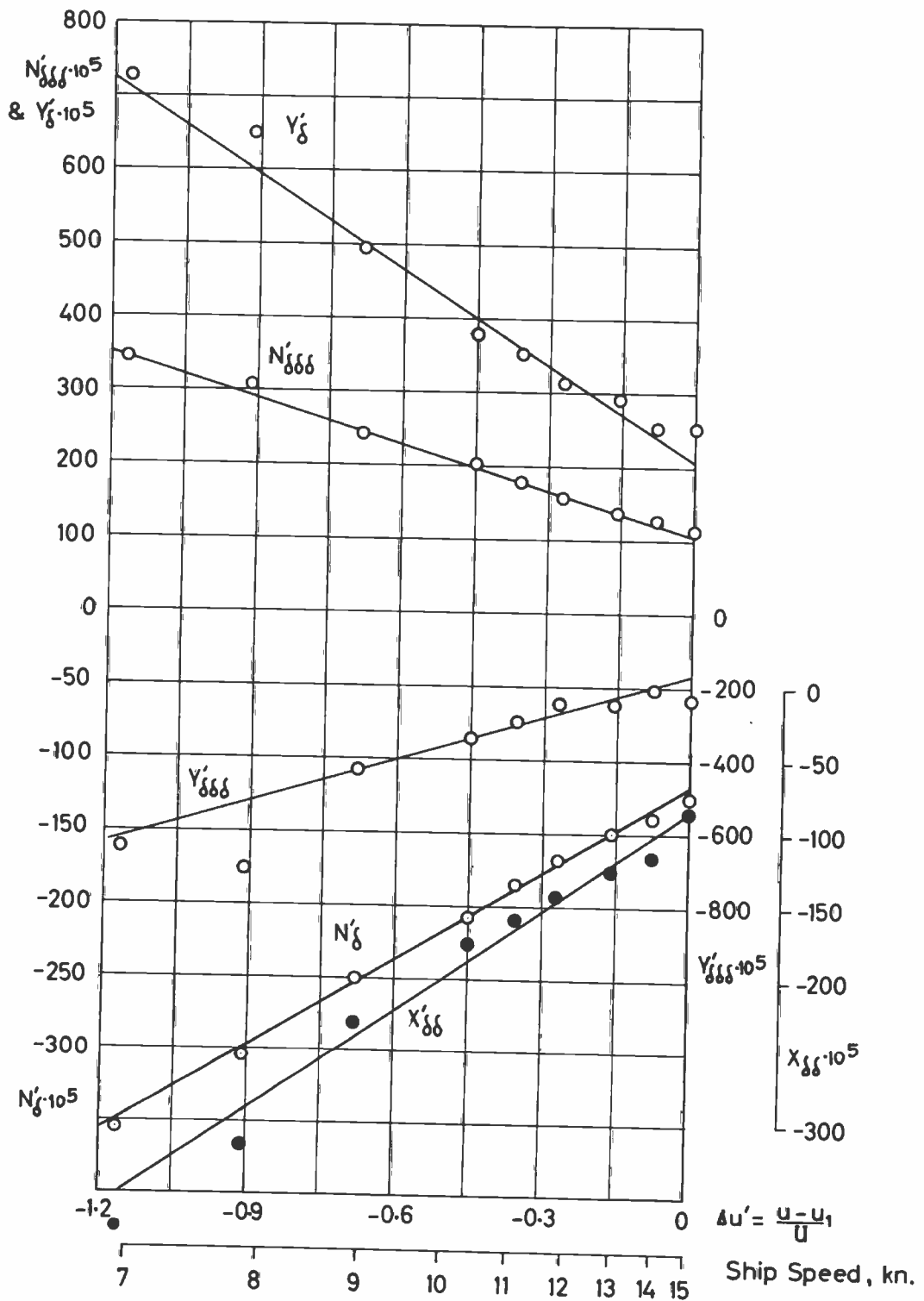Dimensional and Dimensionless Plots of Longitudinal Force, X.

Figure 32

Variation of Dimensionless Rudder-Angle
Coefficients with Speed.

FREQUENCY AND TANK-INTERFERENCE EFFECTS

Resonant Standing-Waves

The following consists of a brief description of some aspects of the influence of frequency-dependent surface-waves on force measurements made with the HyA Planar-Motion Mechanism used in the dynamic mode. Not much information is available, as the policy adopted has been that of avoiding these effects, but, in order to be able to do this, two series of exploratory tests were made soon after the mechanism was completed, and it is felt that the results of these tests are of sufficient interest to warrant description.

It is not unnatural that oscillation of a body in a free-surface should give rise to waves which are dependent on frequency and amplitude of oscillation, as well as on the speed of the body through the water. When the frequency of such waves corresponds to the natural frequency of the water in the towing tank, then tank resonance may be expected. Such resonance can result in the build up of significant standing-waves which completely preclude the possibility of making useful measurements.

The frequencies at which tank resonance occurs are solely dependant on tank dimensions [12] and governed by the relation:

$$\text{Period} = \frac{2\pi}{\sigma}$$

where

$$\sigma^2 = gk \tanh kh$$

$$\frac{2\pi}{k} = \text{wave length} = 2b, b, \frac{2}{3} b, \frac{2}{4} b, \text{ etc..}$$

h = depth of tank water

b = breadth of tank

g = acceleration due to gravity

For the HyA towing tank, when $b = 2h$, the first four resonant standing-wave systems, according to these relationships, have periods of 4.07, 2.78, 2.26 and 1.98 seconds. The corresponding revolutions of the HyA Planar-Motion Mechanism at which tank resonance may be expected are then 14.8, 20.5, 26.5 and 30.3 revolutions per minute.

"Pure-sway" tests and "pure-yaw" tests were made with a 6 m. model of the MARINER class of vessels, for revolution of the Planar-Motion Mechanism covering the range from zero to 35 r.p.m.. The object
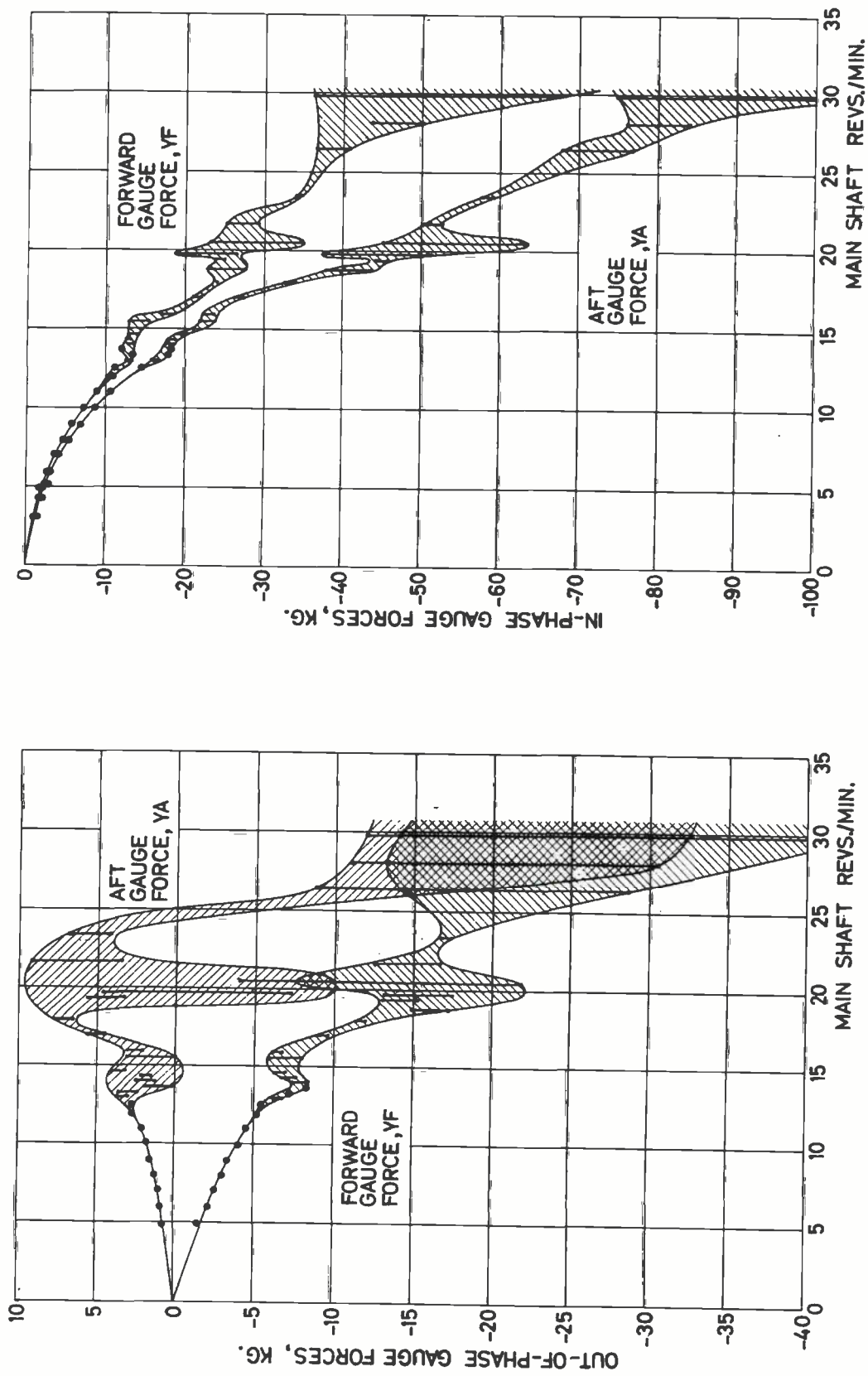
Figure 33

Results of Pure Sway Tests — Dimensional Gauge Forces as
Functions of Planar-Motion Mechanism Revolutions per Minute.

of the tests was to find the low frequency area in which the measured forces ceased to be frequency dependent. The model used in the tests was the same as that described in [5], and the tests were made predominantly at 15 knots ship-speed and with 65 mm. amplitude at the scotch-yokes. The raw forces measured at the Y-gauges in the "pure-sway" tests are shown plotted in Figure 33. Above about 12 r.p.m. the forces measured during a run down the tank varied in a manner akin to the "beating" phenomenon resulting from the interference of two wave-trains having nearly equal frequencies. The ranges of variation of forces measured during a run down the tank are shown by heavy lines, and when the forces were repeatable, the values are indicated by single points in the usual manner.

It is evident that resonant standing-waves occurred at about 15, 20 and 30 r.p.m. exactly as predicted by theory.

At the higher frequencies, standing-waves were clearly visible, and in an additional test at zero speed, they built up to alarming proportions, the whole water surface in the portion of the tank adjacent to the model being set into violent motion.

Below 12 r.p.m. however, no standing-waves were observable and it can be said that, if they did exist, then the wave height was less than 1 mm.. This was ascertained by close examination of the water level on the tank side while oscillating.

In the "pure-yaw" tests, results similar to those shown in Figure 33 were obtained, the resonant ranges occurring at about the same frequencies, but the variation of the measured forces in the resonant areas being less marked. This is explained by the fact that the model was a more effective wave-maker when oscillating with sway motions than when oscillating with yaw motions.

To sum up, it may be said that, for the model and speed tested, undesirable effects due to tank resonance were found to be negligible below about 12 r.p.m..

While tests have only been made with one model, at zero and 15 knots, it is considered improbable that differences in speed or model proportions such as block-coefficient, length to draught, and length to breadth ratios, would precipitate the onset of resonant waves. Based on these considerations, oscillatory tests made with the HyA Planar-Motion Mechanism used in the dynamic mode, are normally carried out at about 8 r.p.m., thus allowing a reasonable safety-margin.

Frequency-Effects

A more insidious source of differences between measurements
made using a steady-state technique such as a rotating arm, and mea-
surements made with a Planar-Motion Mechanism, stems from unsteady
flow effects (independent of the free-surface) which invalidate the
assumption of quasi-steady conditions. This is a similar phonomenon
to the well-known unsteady lift-forces which act on an air-foil having
an oscillatory angle of attack. Waves generated as a result of the
oscillatory motions of the model (independent of the tank boundaries),
and reflections of such waves from the tank walls, are two other
sources of differences.

Since such effects, while repeatable, are frequency dependent,
they can be assessed by comparing force-measurements made at differ-
ent frequencies, the agreement of which may safely be assumed to pre-
clude the possibility of significant unsteady-flow effects.

The results of "pure-sway" tests and "pure-yaw" tests pre-
viously reported (Figures 4 and 5, and Tables 7 and 8 of [5]), showed
that forces resulting from yaw velocity, yaw acceleration, and sway
acceleration are quite independent of frequency of oscillation, with-
in the low-frequency range used during the tests. Forces resulting
from sway velocity, i.e. drift angle, were found to vary with fre-
quency, but to approach the steady-state results of the "static drift-
angle" test as frequency tended to zero.

Higher Order Frequencies

The periodic motions generated by the HyA Planar-Motion
Mechanism are of almost perfect sine and cosine character, and so,
during a given run, the resulting hydrodynamic forces at the Y-gauges
must necessarily be of the same frequency as the motions. There are
no grounds to expect periodic forces having frequencies which are
integer multiples of the frequency of oscillation, as opposed, e.g.,
to analyses of fluctuating thrust and torque in a propeller shaft,
when integer multiples of the basic shaft-frequency would depend on
number of blades, deadwood, etc.. It is not therefore considered a
disadvantage of the synchronous-switch technique for integration of
periodic forces, that the OSCIL programme is sensitive to uneven
integer multiples of the frequency of the motion and insensitive to
even multiples, and vice versa for the CONST programme. Neither is

it thought helpful to consider an alternative method of integration, in which the force signals are multiplied by sin ωt and cos ωt, as yielding the first harmonics of a Fourier analysis [13] .

No difficulties have been encountered due to vibration of the HyA towing carriage and Planar-Motion Mechanism, presumably because of their stiff construction, which ensures that any small vibrations are of such low amplitude and high frequency that the resulting high frequency forces acting at the Y-gauges are negligible in comparison with the forces under investigation.

CONCLUSIONS

The method adopted at HyA for investigating steering and manoeuvring qualities of surface ships has been described. A Planar-Motion Mechanism system is utilized for the experimental measurement of hydrodynamic coefficients, and predictions of manoeuvres are obtained from solutions of the equations of motion using a digital computer.

The mathematical model at present in use at HyA for simulation of steering and manoeuvring of surface ships is based on a third-order Taylor expansion of forces and moments in the equations of motion. The mathematical model has been reduced to a manageable form by retaining only those hydrodynamic coefficients which experimental experience has shown not to be negligible. Roll and heel have also been neglected in the mathematical model since they are felt to have little influence on prediction of manoeuvres, with the possible exception of fast warships.

The Planar-Motion Mechanism system designed and built at HyA is used in a conventional towing tank and designed to oscilllate the same large 6 to 7 metre wax models also used for resistance and propulsion tests. The mechanism is designed as a low-frequency, high-amplitude oscillator in order to reduce possible frequency problems and to cover adequately the various velocity and acceleration parameters encountered in ship manoeuvres.

The various tests which can be executed by the mechanism in its static and dynamic modes of operation (outlined in Figures 2 to 4) make the Planar-Motion Mechanism a versatile instrument for measurement of all of the hydrodynamic coefficients, both linear and non-

linear, which appear in the mathematical model.

The periodic acceleration- and velocity-dependent forces measured by the force gauges in the dynamic mode of operation of the Planar-Motion Mechanism are separated and recorded by integration using a synchronous-switch technique. The integration is controlled by programming circuits in a processing unit, and the principles of the measuring technique have been described in detail.

Considerations in the design of the different Planar-Motion Mechanism tests and the analysis of force measurements to determine the hydrodynamic coefficients have been discussed. Results from resistance, self-propulsion and open-water tests are used to compute coefficients in the X-equation and to obtain the important relationship between propeller r.p.m. and speed reduction encountered in manoeuvres, for different types of engines and engine settings. An experimental programme used as standard at HyA for testing cargo ships is shown in Table 6.

The influence of speed on the non-dimensional coefficients has been discussed, and the results which supplement those previously reported by HyA for the MARINER form (Reference [5]) have been presented as examples. It is found that the non-dimensional coefficients Y'_v, Y'_r, N'_v and N'_r are almost independent of speed over the speed range covered by normal merchant ships and measurement of the coefficients Y'_{vu}, Y'_{ru}, N'_{vu} and N'_{ru} has not been recommended as standard in the experimental programme. The coefficients Y'_δ, $Y'_{\delta\delta\delta}$, N'_δ and $N'_{\delta\delta\delta}$ are shown to vary considerably with speed, forces on the rudder being strongly influenced by the propeller slip-stream. The cross-coupling terms $Y'_{\delta u}$, $Y'_{\delta\delta\delta u}$, $N'_{\delta u}$ and $N'_{\delta\delta\delta u}$ are consequently of importance in prediction of radical manoeuvres where speed loss is appreciable, and they should be measured as standard.

It has been found that resonance with a system of standing waves built up in the towing tank precludes the possibility of oscillating models above a certain critical frequency. The resonance is easily avoided, however, at the low frequency of oscillation recommended for experiments, but the range of yaw velocities which can be generated by the present HyA Planar-Motion Mechanism, is consequently limited. Whereas an acceptable coverage can be obtained for the 6 to 7 metre cargo ship models, the range of yaw velocities which can be obtained for the smaller naval-ship models is more limited than desirable, except at lower speed-values.

Forces measured in the low-frequency range have been found either independent of frequency, or to vary with frequency but approach steady-state results as frequency tends to zero.

It is finally concluded that the semi-theoretical technique combining Planar-Motion Mechanism model-testing and computer-prediction of manoeuvres allows scaling problems to be treated satisfactorily. Large models can be utilized in the testing, whereby scale effects in general are reduced. Tests can be carried out at the ship propulsion point by applying a towing force via the rigid connection to the mechanism, the correct propeller r.p.m. being obtained by taking the particular engine type and control arrangement into account. The individual measurement of the various coefficients gives an insight into the hydrodynamic phenomena involved and consequently allows corrections to coefficients for difference in Reynolds' number for model and ship to be considered.

ACKNOWLEDGMENTS

REFERENCES

[1]   "Nomenclature for Treating the Motion of a Submerged Body through a Fluid", The Society of Naval Architects and Marine Engineers, Technical and Research Bulletin No. 1-5, Apr. 1952.

[2]   Imlay, F.H.: "A Nomenclature for Stability and Control", David Taylor Model Basin Report 1319, May 1959.

[3]   Abkowitz, M.A.: "Lectures on Ship Hydrodynamics - Steering and Manoeuvrability", Hydro- and Aerodynamics Laboratory Report Hy-5, May 1964.

[4]   Strøm-Tejsen, J.: "A Digital Computer Technique for Prediction of Standard Maneuvers of Surface Ships", David Taylor Model Basin Report 2130, in print.

[5]   Chislett, M.S. and Strøm-Tejsen, J.: "Planar Motion Mechanism Tests and Full-Scale Steering and Manoeuvring Predictions for a MARINER Class Vessel", Hydro- and Aerodynamics Laboratory, Report Hy-6, April 1965.

[6]   Gertler, M.: "The DTMB Planar-Motion-Mechanism System", Symposium on the Towing Tank Facilities, Zagreb, Sept. 1959.

[7]   Goodman, A.: "Experimental Techniques and Methods of Analysis used in Submerged Body Research", Third Symposium on Naval Hydrodynamics, Scheveningen, Sept. 1960.

[8]   Prohaska, C.W.: "Preliminary Description of the Lay-out and Instrumentation of the Danish Towing Tank", Paper presented at the Symposium on the Towing Tank Facilities and Measuring Technique, Zagreb, Sept. 1959.

[9]   Paulling, J.R. and Wood, L.W.: "The Dynamic Problem of Two Ships Operating on Parallel Courses in Close Proximity", University of California, Series 189, Issue 1, July 18, 1962.

[10]   Zunderdorp, H.J. and Buitenhek, M.: "Oscillatory Techniques at the Shipbuilding Laboratory", Report No. 111 of the Shipbuilding Laboratory of the Technological University, Delft, 1963.

[11]   Bárdarson, H.R., Wagner Smitt, L. and Chislett, M.S.: "Conversion of Trawlers to Purse-Seiners - A Turning Ability Study including Full-Scale Trials and Captive Model Tests with Alternative Rudder Arrangements", Hydro- and Aerodynamics Laboratory, Report No. Hy-9, (in print).

[12]   Lamb, H.: "Hydrodynamics", Dover Publications, New York, page 364.

[13]   Van Leeuwen, G.: "The Lateral Damping and Added Mass of a Horizontally Oscillating Shipmodel", Netherlands Research Centre T.N.O. for Shipbuilding and Navitation, Report No. 65 S, Dec. 1964.

APPENDIX A

Experimental Results of Static Drift Angle and Speed Tests

β deg	Y' $\times_{10}3$	N' $\times_{10}3$	β deg	Y' $\times_{10}3$	N' $\times_{10}3$
Nominal Ship Speed = 10 knots Exact Model Speed = 1.048 m./sec.			**Nominal Ship Seed = 20 knots** Exact Model Speed = 2.06 m./sec.		
1	0.170	0.031	0.5	0.090	0.031
3	0.668	0.121	2.5	0.562	0.143
5	1.179	0.203	4.5	1.080	0.244
7	1.767	0.258	8.5	2.243	0.477
9	2.257	0.306	10.5	2.914	0.565
11	2.885	0.328	12.5	3.676	0.634
13	3.659	0.368	-1.5	-0.329	-0.082
-1	-0.142	-0.062	-3.5	-0.817	-0.206
-3	-0.539	-0.178	-5.5	-1.312	-0.330
-5	-0.962	-0.276	-7.5	-1.872	-0.438
-7	-1.337	-0.366	-9.5	-2.388	-0.520
-9	-1.840	-0.398	-11.5	-3.100	-0.583
-11	-2.432	-0.409	-13.5	-3.908	-0.641
-13	-3.110	-0.427			

(Faired together with 15 knot data, see below.)

Fairing Expressions:

$$Y\times_{10}5 = 4.1 - 1323v - 6967v^3$$
$$N\times_{10}5 = 0.0 - 348.7v + 1293v^3$$

β deg	Y' $\times_{10}3$	N' $\times_{10}3$	β deg	Y' $\times_{10}3$	N' $\times_{10}3$
Nominal Ship Speed = 15 knots Exact Model Speed = 1.534 m./sec.			**Nominal Ship Speed = 25 knots** Exact Model Speed = 2.57 m./se.		
0	-0.034	-0.006	1.5	0.346	0.108
2	0.481	0.093	3.5	0.916	0.243
4	0.958	0.178	5	1.308	0.332
6	1.395	0.244	6	1.676	0.415
7	1.578	0.262	7	2.016	0.505
8	1.914	0.306	8	2.303	0.520
10	2.380	0.370	9	2.619	0.561
12	2.889	0.424	10	3.032	0.615
-2	-0.492	-0.112	-0.5	-0.109	-0.028
-4	-0.940	-0.200	-2.5	-0.588	-0.177
-6	-1.390	-0.279	-4.5	-1.116	-0.321
-7	-1.645	-0.325	-3.5	-0.812	-0.241
-12	-3.043	-0.473	-5.5	-1.405	-0.388
-10	-2.411	-0.447	-6.5	-1.688	-0.462
-8	-1.823	-0.386	-8	-2.108	-0.549
-6	-1.260	-0.297	-9	-2.484	-0.659

Fairing Expressions: (10 and 15 knots)

$$Y'\times_{10}5 = 7.1 - 1225v' - 5049v^3$$
$$N'\times_{10}5 = -2.9 - 280.0v' + 1905v^3$$

Fairing Expressions:

$$Y'\times_{10}5 = 5.5 - 1413v' - 9535v^3$$
$$N'\times_{10}5 = -1.0 - 414.5v' + 1357v^3$$

APPENDIX B

Experimental Results of Static Rudder Angle and Speed Tests

The following experimental measurements were made with constant propeller revolutions. 345 revs./min. model scale, corresponding to the ship self-propulsion point at 15 knots.

Y- and X-forces have been non-dimensionalised with $1/2 \cdot \rho \cdot Lpp^2 U^2$, N-moments with $1/2 \cdot \rho \cdot Lpp^3 U^2$, where U is exact model speed, given in the last table.

δ	$Y' \times 10^3$	$N' \times 10^3$	$X' \times 10^3$	δ	$Y' \times 10^3$	$N' \times 10^3$	$X' \times 10^3$
15 knots (without propeller)				**14 knots**			
-40	-0.590	0.292	-0.910	-40	-1.218	0.588	-0.549
-30	-0.508	0.279	-0.837	-30	-1.103	0.535	-0.371
-20	-0.409	0.219	-0.705	-20	-0.864	0.440	-0.187
-10	-0.192	0.122	-0.630	-10	-0.442	0.228	-0.014
0	0.000	0.000	-0.624	0	-0.124	0.007	0.053
10	0.133	-0.097	-0.649	10	0.387	-0.238	0.011
20	0.350	-0.198	-0.702	20	0.815	-0.461	-0.082
30	0.526	-0.270	-0.794	30	0.944	-0.524	-0.291
40	0.549	-0.276	-0.897	40	0.965	-0.531	-0.465
-35	-0.537	0.278	-0.860	-35	-1.212	0.570	-0.473
-25	-0.484	0.260	-0.745	-25	-1.021	0.511	-0.285
-15	-0.350	0.178	-0.672	-15	-0.646	0.344	-0.079
-5	-0.064	0.056	-0.644	-5	-0.183	0.117	0.000
5	0.052	-0.046	-0.648	5	0.135	-0.118	0.053
15	0.315	-0.159	-0.669	15	0.597	-0.370	-0.032
25	0.485	-0.252	-0.753	25	0.945	-0.522	-0.192
35	0.602	-0.284	-0.853	35	0.979	-0.535	-0.388
15 knots.				**13 knots.**			
-40	-1.171	0.576	-0.587	-40	-1.331	0.629	-0.448
-30	-1.043	0.510	-0.493	-30	-1.222	0.553	-0.228
-20	-0.857	0.400	-0.331	-20	-0.947	0.461	-0.043
-10	-0.426	0.201	-0.207	-10	-0.445	0.242	0.155
0	-0.094	0.017	-0.147	0	-0.118	0.021	0.208
10	0.407	-0.227	-0.193	10	0.445	-0.274	0.189
20	0.786	-0.413	-0.269	20	0.938	-0.499	0.091
30	0.914	-0.468	-0.440	30	1.126	-0.573	-0.153
40	0.814	-0.452	-0.525	40	1.087	-0.563	-0.336
-35	-1.119	0.537	-0.571	-35	-1.292	0.597	-0.317
-25	-0.979	0.465	-0.405	-25	-1.104	0.523	-0.133
-15	-0.629	0.303	-0.259	-15	-0.719	0.366	0.060
-5	-0.186	0.098	-0.176	-5	-0.235	0.122	0.171
5	0.139	-0.100	-0.148	5	0.116	-0.135	0.247
15	0.611	-0.332	-0.243	15	0.766	-0.394	0.132
25	0.907	-0.486	-0.363	25	1.126	-0.573	-0.044
35	0.867	-0.460	-0.439	35	1.134	-0.577	-0.247

δ	$Y' \times 10^3$	$N' \times 10^3$	$X' \times 10^3$	δ	$Y' \times 10^3$	$N' \times 10^3$	$X' \times 10^3$
12 knots.				**9 knots.**			
-40	-1.422	0.664	-0.208	-40	-2.117	0.940	0.795
-30	-1.280	0.611	0.019	-30	-1.803	0.866	1.133
-20	-0.997	0.505	0.266	-20	-1.491	0.726	1.515
-10	-0.479	0.265	0.447	-10	-0.685	0.424	1.879
0	-0.076	0.003	0.533	0	-0.051	-0.039	1.913
10	0.516	-0.313	0.490	10	0.866	-0.487	1.939
20	1.062	-0.586	0.350	20	1.635	-0.890	1.688
30	1.307	-0.664	0.090	30	2.081	-1.006	1.286
40	1.327	-0.654	-0.082	40	2.032	-0.979	0.994
-35	-1.384	0.657	-0.112	-35	-1.968	0.908	0.971
-25	-1.138	0.562	0.122	-25	-1.755	0.809	1.305
-15	-0.733	0.406	0.374	-15	-1.247	0.561	1.733
-5	-0.264	0.109	0.492	-5	-0.427	0.173	1.977
5	0.186	-0.161	0.511	5	0.575	-0.242	2.003
15	0.846	-0.451	0.457	15	1.375	-0.693	1.823
25	1.241	-0.656	0.230	25	1.900	-0.955	1.481
35	1.269	-0.668	0.000	35	1.949	-0.982	1.133
11 knots.				**8 knots.**			
-40	-1.536	0.710	-0.029	-40	-2.234	1.101	1.484
-30	-1.354	0.666	0.208	-30	-2.022	0.970	1.979
-20	-1.047	0.536	0.455	-20	-1.615	0.858	2.425
-10	-0.440	0.314	0.729	-10	-0.871	0.475	2.968
0	-0.131	-0.016	0.800	0	-0.023	-0.050	3.133
10	0.666	-0.335	0.764	10	1.428	-0.606	3.036
20	1.270	-0.631	0.619	20	2.514	-1.105	2.706
30	1.416	-0.736	0.345	30	2.469	-1.182	2.124
40	1.395	-0.716	0.149	40	2.361	-1.171	1.789
-35	-1.472	0.699	0.088	-35	-2.127	1.059	1.707
-25	-1.217	0.602	0.345	-25	-1.958	0.919	2.207
-15	-0.867	0.434	0.639	-15	-1.576	0.703	2.725
-5	-0.177	0.149	0.768	-5	-0.448	0.181	3.046
5	0.230	-0.171	0.800	5	0.509	-0.309	3.094
15	0.949	-0.531	0.706	15	1.959	-0.912	2.915
25	1.417	-0.716	0.482	25	2.447	-1.194	2.415
35	1.459	-0.743	0.215	35	2.318	-1.171	1.920

δ	Y' $\times 10^3$	N' $\times 10^3$	X' $\times 10^3$	δ	Y' $\times 10^3$	N' $\times 10^3$	X' $\times 10^3$
10 knots.				7 knots.			
-40	-1.639	0.814	0.183	-40	-3.013	1.378	2.294
-30	-1.541	0.751	0.514	-30	-2.548	1.275	2.953
-20	-1.211	0.602	0.759	-20	-2.171	1.018	3.500
-10	-0.585	0.360	1.034	-10	-1.081	0.623	4.116
0	-0.199	0.000	1.112	0	-0.222	-0.040	4.283
10	0.684	-0.378	1.062	10	1.299	-0.692	4.196
20	1.158	-0.700	0.923	20	2.409	-1.280	3.842
30	1.452	-0.834	0.581	30	2.926	-1.502	3.158
40	1.404	-0.771	0.372	40	2.873	-1.433	2.798
-35	-1.552	0.798	0.334	-35	-3.207	1.353	2.673
-25	-1.407	0.678	0.595	-25	-2.551	1.176	3.258
-15	-0.990	0.500	0.884	-15	-1.819	0.825	3.898
-5	-0.343	0.151	1.079	-5	-0.488	0.227	4.277
5	0.180	-0.189	1.131	5	0.594	-0.346	4.371
15	0.989	-0.558	1.029	15	2.034	-0.993	4.091
25	1.354	-0.803	0.767	25	2.874	-1.413	3.500
35	1.392	-0.778	0.495	35	2.791	-1.418	2.997

Non-dimensional Coefficients obtained from fairing the above experimental measurements are:

Nominal Ship Speed. knots	Exact Model Speed. m./sec.	Y'_* $\times 10^5$	Y'_δ $\times 10^5$	$Y'_{\delta\delta\delta}$ $\times 10^5$	N'_* $\times 10^5$	N'_δ $\times 10^5$	$N'_{\delta\delta\delta}$ $\times 10^5$	$X'_{\delta\delta}$ $\times 10^5$
15[+)]	1.54	-0.7	120.5	-77.0	0.6	-67.3	54.9	-58.5
15	1.54	-6.2	254.5	-234.7	1.0	-127.6	114.7	-85.4
14	1.43	-6.1	256.3	-205.1	0.2	-140.9	129.0	-171.1
13	1.334	-4.0	294.0	-248.6	-0.3	-150.1	137.9	-127.1
12	1.214	-0.1	315.3	-247.5	-2.2	-169.9	159.3	-143.5
11	1.138	3.3	353.6	-298.3	-2.8	-186.8	178.7	-159.3
10	1.064	-5.0	379.7	-342.9	-2.1	-209.1	202.6	-176.4
9	0.917	5.1	496.5	-429.9	-5.1	-251.6	244.2	-231.7
8	0.807	18.4	650.4	-703.7	-8.4	-305.2	309.4	-316.2
7	0.713	4.1	729.5	-642.9	-7.3	-364.4	346.4	-374.4

[+)] without propeller.